AFCRL - 70-0493

A PILOT STUDY ON THE APPLICATION OF GEOSYNCHRONOUS METEOROLOGICAL SATELLITE DATA TO VERY SHORT RANGE TERMINAL FORECASTING

Thomas H. VonderHaar and Richard S. Cram

Space Science and Engineering Center
The University of Wisconsin
1225 West Dayton Street
Madison, Wisconsin 53706

1970

Contract No. F19628-70-C-0207

Project No. 8628

Task No. 862811

Unit No. 86281101

FINAL REPORT

Period Covered: 1 April 1970 through 31 August 1970

30 September 1970

Contract Monitor: John H. Conover, Meteorology Laboratory

Prepared
for

AIR FORCE CAMBRIDGE RESEARCH LABORATORIES
UNITED STATES AIR FORCE
BEDFORD, MASSACHUSETTS 01730

AFCRL - 70-0493

A PILOT STUDY ON THE APPLICATION OF GEOSYNCHRONOUS METEOROLOGICAL SATELLITE DATA TO VERY SHORT RANGE TERMINAL FORECASTING

Thomas H. VonderHaar and Richard S. Cram

Space Science and Engineering Center
The University of Wisconsin
1225 West Dayton Street
Madison, Wisconsin 53706

Contract No. F19628-70-C-0207

Project No. 8628

Task No. 862811

Unit No. 86281101

FINAL REPORT

Period Covered: 1 April 1970 through 31 August 1970

30 September 1970

Contract Monitor: John H. Conover, Meteorology Laboratory

Prepared
for

AIR FORCE CAMBRIDGE RESEARCH LABORATORIES
UNITED STATES AIR FORCE
BEDFORD, MASSACHUSETTS 01730

ABSTRACT

The study assembles a unified body of data consisting of very high space and time resolution reflected radiance measurements from a geosynchronous satellite (ATS-III) along with concurrent meteorological radar, ceiling, visibility and surface pressure reports at selected air terminals in the central United States. This data set allows familiarization with the meteorological potential of nearly continuous observation of cloud conditions from a geosynchronous platform. It may also serve as initial input to quantitative techniques for evaluating the satellite data and/or for testing its usefulness in very short range weather forecasting. In this regard, a second portion of the study presents arrays of statistical descriptors of the satellite data.

CONTENTS

This page is blank

1.0 Introduction

The purpose of this pilot study is twofold:

(a) to assemble a unified body of data from both geosynchronous satellite measurements and conventional meteorological observations in order to allow a test of the usefulness of the new type of satellite data for improving terminal ceiling and visibility forecasts;

and (b) to experiment with the construction of arrays of quantitative descriptors of the satellite radiance measurements in anticipation of the potential use of such parameters as predictors in a statistical relation designed to allow the test of forecasting improvement mentioned above.

Thus the pilot study is aimed as a first, new look at an existing problem of weather forecasting. Results of the study will aid decisions on both the course and the magnitude of subsequent work, if any. This new work may extend to other meteorological applications, in addition to terminal forecasting. A new look is possible because of the availability of the measurements from a geosynchronous satellite, ATS-III.

Only in recent years have the data from NASA's Applications Technology Satellites I and III allowed nearly continuous views of changing cloud patterns related to the real-time weather. This is possible, because the satellites are in geostationary orbit, at altitudes near 22,000 miles, and thus orbit the earth's equator with a period of 24 hours, the same rotation as a point on the earth's surface. In addition, the experiments on these satellites were designed to obtain high precision measurements of reflected solar radiation from spots on the earth as small as 2 miles (1, 2, 3).

From the existing archive of ATS satellite data stored on tape, three days were chosen for the pilot study. On these days successive satellite measurements and weather station observations were collected over and around three terminals of interest. Analyses were prepared

of the satellite radiance fields, radar observations, ceiling and visibility reports, and surface pressure measurements. A sampling of these analyses as well as special time-distance cross-sections of the same parameters are presented in this report. The remainder of the nine cases studied is available for future use, as required. In like manner, only selected examples of the satellite data statistics are presented for illustration of their potential.

Results of the pilot study are encouraging and suggest several possible new areas of application of the geosynchronous satellite measurements. Furthermore, they indicate that it should be profitable to proceed to the actual test of a significant sample of cases like those in this study in order to evaluate the use of such satellite data for improving air terminal forecasts. Such very short range predictions are a form of quantitative "now-casting" (i.e., forecasting from a continuously up-dated set of initial values).

2.0 Preparation of the Data Set

The pacing item for case selection was the few number of days during 1968 and 1969 when the ATS satellite data were available on tape in a nearly unbroken time sequence. Together with the requirement to view active weather patterns over the United States, this fact focused our selection of case days to those when a "severe weather alert," a period of special data acquisition, occurred.

2.1 Use of geosynchronous satellite data

During the spring of 1968 and 1969, NASA's geosynchronous satellite ATS-III was positioned at longitudes giving the spinscan camera experiment on board a good view of the United States during all the daylight hours. This experiment, a set of photomultiplier tubes behind a small telescope (1, 2), obtained reflected solar radiance measurements as it scanned the earth's disc. West-to-east scans resulted from spacecraft rotation, and a north-to-south scan was forced by mechanical stepping. After transmission and digitization, one frame (one picture of the illuminated earth disc) is composed of 2408 scan lines with 8192 samples (elements) per line. Each sample has 8 bit precision (levels from 0-255 digital counts). These digital counts are directly proportional to the voltage output of the "camera" and, in turn, to the reflected radiance (3) arising from the camera's field-of-view (0.1 milliradians). Near subpoint of the spacecraft this field-of-view is equivalent to a ground resolution of about 2 nautical miles from spacecraft altitude.

After processing at NASA's ground station at Rosman, N. C., the tapes containing the satellite experiment signal were sent to the University of Wisconsin for use and archiving. Because of some difficulty with the analog recorded during the period of interest to this study, only those tapes digitized at the ground station were chosen for use.[1] Following checks of tape quality, three days were selected

---

[1] Since May 1969, a new analog recorder has removed this limitation on the use of precision ATS data.

for this study: April 19 and 23, 1968, and April 4, 1969. The total number of tapes (pictures) and the time interval covered on each day were as follows:

April 19, 1968	2156-2318 Z	(1 1/2 hr; 4 tapes)
April 23, 1968	1701-1946 Z	(2 1/2 hr; 5 tapes)
April 4, 1969	1428-1948 Z	(5 1/2 hr; 8 tapes)

Although the time intervals to be studied were less (in two cases) than planned, the ATS data coverage is still much greater than that provided by a "snapshot" from a polar orbiting satellite.

In digital form, one frame of ATS-III data from the spinscan camera fills one reel of high-density tape. To minimize data handling, only a region enclosing most of the United States was chosen for further processing, data "navigation" and "normalization" to an earth-located reference. This was done according to a procedure designed by Smith, Phillips, and Vonder Haar.[2] The technique uses recognizable landmarks within the ATS data array to derive the orientation of the satellite's spin axis. Together with a knowledge of satellite ephemeris, the transformation from satellite coordinate system (line-element) to earth coordinate system (latitude-longitude) is a matter of geometry. The technique is very similar to one reported in (4). The resulting best-fit of landmarks gave all cases a relative alignment error of ± 10 nautical miles maximum over the region of interest. Actual construction of the normalized ATS data field requires a great deal of array interpolation and averaging within the computer (UNIVAC 1108 and CDC 3600).

Following normalization and selection of specific terminal areas (see 2.2), the reflected radiance values (in terms of digital counts) were objectively analyzed on an x-y plotter at nine contour levels (i.e., 15, 30, 45, 60, 75, 90, 105, 120, 130). These were chosen after view of the relative variation across the scene shown in the first picture of each daily sequence. Since reflected radiance from a cloud changes due to variations in the angular reflection characteristics as well as because of physical changes in the cloud itself,

---

[2]Unpublished report.

contour values of all frames after the first in the day were normalized according to a bi-directional reflectance method of Marshall and Vonder Haar.[3] It is based on work done as an aid to interpreting NIMBUS satellite data (5, 6). The normalization factors vary slightly with location during a particular day. However, for the frames and days used in this pilot study, the normalization ranged from 7 per cent at the minimum to a factor of two within a daily sequence.

It is important to note that the brightness normalization applies only to variations within a given day and allows intercomparison of reflected radiance measurements from clouds with high relative accuracy within that day. Additional factors must be considered in establishing relative accuracies from one day to another. These include: (a) location (subsatellite point) of the satellite (b) spacecraft camera gain settings (c) spacecraft/ground station telemetry link (d) gain setting of video processor and recorders on the ground.

Without a reference signal injected at the spacecraft instrument and carried throughout the downlink onto digital tape, day-to-day variation in (a) thru (d) above precludes day-to-day comparision of radiance values without additional checks.[4] During the time periods used in this pilot study, the experimental ATS-III satellite system and spinscan experiment were subject to several adjustments (not always completely recorded). In addition, a reference level was not available. Since the major emphasis of the pilot study is on variations at an air terminal within a given day, the after-the-fact relative calibration checks were not performed.

---

[3]Unpublished report. (see appendix A)

[4]The relative calibration checks are best done during the navigation and normalization phases of data reduction when selected portions of the image frame are used for earth location. They may include the following: significant samples of clear ocean and/or land surfaces (i.e., Sahara region, White Sands, or salt flats) under the same angular conditions; and/or limb radiance, lunar, space level, or integrated frame brightness values.

In addition to assembling an important part of the data set for this pilot study, work with the geosynchronous ATS data broadened the experience base and contributed a great deal to current techniques for landmark identification, use of navigation programs, and preparation of normalized data. It was very nearly a pioneer effort in ATS data application.

Figures 1, 2, and 3 (a, b, and c respectively) show reproductions of one selected frame of ATS data for each day of the pilot study, a closeup of the United States' area, and a view of the area for which normalized data were derived.

2.2 Selection of terminals

A display of the synoptic weather situation in the early morning hours on each of the three days of the pilot study is shown in Figures 4a, b, and c. Since we wished to acquire a good range of ceiling and visibility accurrences for the data set, three areas (of 100 mile radius) were picked for each day. These regions surround a "central" air terminal; two have significant weather with one relatively clear. Other factors influenced the choice of terminals in this pilot study. They were:

(a) areas were restricted to the normalized portion of the tapes (see Figures 1c, 2c, and 3c).

(b) good radar coverage was required for comparison purposes.

(c) The "central" terminal should be flanked by a sufficiently dense and well-distributed network of supporting stations that record visibility, ceiling, surface pressure, and other synoptic variables.

The following were chosen for use:

Date	Central Station	No. of Stations in Group	No. of Available Radars Covering Area
April 19, 1968	Omaha, Neb. OMA	13	2
"	Wichita Falls, Tex. SPS	12	3
"	Springfield, Mo. SGF	10	5
April 23, 1968	Columbia, Mo. CBI	8	2
"	Columbus, Ohio CMH	11	3
"	Meridian, Miss. MEI	10	1
April 4, 1969	Meridian, Miss. MEI	10	2
"	Ft. Wayne, Ind. FWA	16	3
"	Dodge City, Kan. DDC	6	2

Figure 5 shows the location of the selected stations.

2.3 Conventional meteorological data

The rationale for forming the present study over regions of the United States having a high density of weather reporting stations was to allow detailed comparison of the ATS satellite observations with more conventional meteorological reports. As mentioned in 2.1, there are no gaps in the satellite's areal coverage with ground resolution of 2-3 miles. Except in special cases we can expect synoptic weather reports to represent a region larger than this about the pertinent station. Allowing for some small uncertainty in location of the satellite data, it is apparent that comparison of a slightly smoothed field of satellite measurements at full camera resolution with concurrent meteorological observations should work very well.

Data were obtained on microfilm from the National Weather Records Center. These included the hourly and three-hourly surface weather reports as well as reproductions of the filmed weather radar scopes. In all cases, the conventional meteorological data were selected at

times closest to the time of the appropriate satellite measurement. The time differences did not exceed 10-15 minutes for the surface weather reports and were even less for the radar coverage.

Prints of radar images were made and the portion of the radar screen which covered each station group marked on the prints (Figure 6). The radar range was commonly 250 miles, thus allowing a station group to be completely depicted within a radar photo, provided the radar station was chosen close enough to the "central" terminal. On the occasions where multiple radar coverage was possible, all available radar pictures were used in the study. Despite the differences in both scale and coordinate systems, the radar data presentation allows relatively easy comparison among the satellite analyses and other arrays. An alternate approach, manual transformation of the apparent echoes to a latitude-longitude base, would introduce undue subjectiveness into the pilot study.

All other meteorological variables used were transformed to a map base identical with the satellite data contour maps. Analyses included ceiling height (or cloud height where no ceiling exists), visibility, and surface pressure. The ceiling analyses show the amount of cloud cover (C = clear, ϕ = scattered, $\oplus$ = broken, $\oplus$ = overcast, $\boxtimes$ = obscured). Visibility analyses also indicate significant weather at each station (see Appendix B). Examples of these analyses are given in the following sections. The choice of those noted occurred because both ceiling and visibility are special quantities of interest at air terminals; whereas, surface pressure, radar echoes, and satellite observations of cloudiness are considered to be potential predictors of the desired parameters.

3.0 Simultaneous Analysis

In this first part of the pilot study we present simultaneous analyses of the ATS-III spinscan camera measurements and specific conventional meteorological observations over the same regions about a central station. In order to depict the weather situation over a region of 100 mile radius the analyses are presented for rectangular latitude-longitude areas (4° x 5°); slightly larger areas than required. As mentioned earlier the central stations are not necessarily at the geometric center of the analyses.

3.0 Selected Displays

A total of 51 (17 picture times x 3 station cases/picture time) joint analyses of the satellite and conventional data have been completed. Only selected cases will be shown in this section; the remainder are available for study on special request. The three chosen examples differ only in small ways from the remaining 6 station cases.

The examples (see Appendix C) include (a) a single time sample with multiple radar coverage over a region of sharp cloud gradients and extensive thunderstorm activity on April 19, 1968; (b) a contrast between fair and severe weather conditions at a terminal over a short interval of time on April 23 1968; and (c) an extended time series of simultaneous observations from the satellite and the ground on April 4, 1969.

Detailed interpretation of the concurrent analyses is left to the reader who may have special objectives in examining the data set of this pilot study. A few comments are warranted of course, but the authors welcome post-publication discussion with all interested parties.

3.1.1 April 19, 1968; Witchita Falls, Texas (SPS)

Figures 7-12 depict the visibility, ceiling, radar and ATS satellite data analyses for the Witchita Falls, Texas area at 2318 GMT (1718 local time). Radar coverage is excellent from three sites: Oklahoma City, Fort Worth and Wichita. The ceiling and visibility reports comple-

ment the satellite view to show a wedge of clearing behind an active cold front. Radar echoes show strong squall line activity throughout eastern Oklahoma and south along the 97th meridian to below Ft. Worth. Consistent echo reports are also found in the vicinity of Hobart, Oklahoma. Reflected radiance measurements from the ATS-III show both the general cloud pattern as well as the very brightest regions and sharp gradients that indicate extensive cloud thickness. These latter agree very well with the simultaneous radar reports.

3.1.2 April 23, 1968; Columbus, Ohio (CMH)

The most important aspect of the geosynchronous satellite data is the ability to view a region (i.e., an air terminal) at high areal resolution nearly continuously in time. Between 1701 and 1946 GMT the Columbus, Ohio region experienced a high contrast in weather conditions with rapid development and advection of the active region seen just south of the vortex center in Figures 2a,b and c. The meteorological data in figures 13-18 show this sudden change very well. Satellite data analyses for the two time (figures 19a and 19b) also mark very well, perhaps even better, the movement and development of the bright triangular cloud mass and its neighboring regions of deep convection. Once again agreement between satellite and radar reports is quite good. How well was radar used as a forecast tool in this situation? In the absence of radar, could the nearly continuous satellite observations of reflected energy have been used in a prognostic technique? These questions suggest further study. It is evident, however, that the satellite measurements (giving total areal coverage over the region of interest) could improve the ceiling and visibility analyses derived from a few discrete points over the area. Despite the apparent complementary value of the satellite data, none of the conventional data analyses in this report were modified in this way.

3.1.3 April 4, 1969; Dodge City, Kansas (DDC)

At 8 a.m. local time a relatively weak surface low was centered in the region of the Dodge City terminal.

From about 8:30 a.m. until nearly 2 p.m. the ATS-III spinscan camera experiment acquired eight high-quality taped views of this region. Thus, the case gives us an opportunity to display a long time series of simultaneous satellite and conventional data. Figures 20-28 give the radiance fields and radar reports (from Wichita). Note that as the radar echoes subside during 1600-1800 GMT, the ATS radiation analyses show a temporary lack of very bright regions and a lessening of brightness gradients.

Surface pressure reports (figure 29-36) show smooth patterns of eastward movement and gradual weakening of the surface low. A glance at the following sequence of ceiling and visibility maps (Figures 37-52) shows that the smooth pressure field does not well depict the real-time weather over the area of study. Indeed the visibility and ceiling at Dodge City are generally decreasing as the pressure rises. Obviously the air flows now completely encircling the filling low are influencing the terminal weather.

3.2 Time Series

The Dodge City case from April 4, 1969 is an example of a relatively long viewing period from the geosynchronous satellite. Thus it provides the opportunity to study a time cross section of the parameters considered in this study (figure 53). The slow pressure rise already mentioned is apparent over the 6 hour interval. Ceiling and visibility reports were consistent for 5 hours at 15 miles and unlimited, no radar echoes were reported within 15 miles of the station.

Between 1900 and 2000 GMT station weather increases rapidly. A simultaneous 100% change of brightness occurs. Scanning the satellite data analyses we see that the gradient making the major cloud boundary was moving east-southeast at about 20 mph and could have been forecast for Dodge City.

But why the apparently anomolous brightness change of nearly equal magnitude that occurs nearly two hours earlier? Since this is near local noon a large specular reflection component not completely accounted for in the brightness normalization scheme is immediately suspect.

This problem can be treated further using results in the next section where other descriptions of the radiance pattern in addition to the simple field values, are considered.

Since Dodge City was quite free of significant weather during the time series (it had consistently high visibilities for the region studied) it serves as a good example of the advection monitoring capability of the geosynchronous satellite data. However, Hill City, Kansas, about 110 miles directly north, reported thunderstorms and rain showers, especially early in the day. A parameter cross section for this location is shown in figure 54. Here the situation is more chaotic with radar echoes near the station early in the day. Despite the probably heterogeneous cloud conditions (which might impair interpretation of the satellite data as well as make the surface observations difficult) we still note a relative agreement between the satellite observations and changing terminal weather (the brightness increase at 1130 local time is seen here also, but to a lesser magnitude).

To aid further study of a prime attribute of the ATS data, namely its frequent views of the same region, several additional time series are shown in figures 55-60. They were chosen to illustrate particularly low ceiling and visibility conditions. In these cases, it is especially interesting to compare surface pressure tendency, radar events and satellite measurements with sky cover and visibility reports.

4.0 Statistics of Reflected Radiance Fields

A second portion of the pilot study involved experimentation with the ordering of various statistical characteristics of the satellite data field onto a fixed grid (NMC). This was done for all the central station cases noted in the earlier section (thus 51 such arrays are available). Again, however, only some selected examples are included in this report.

The NMC (National Meteorological Center) grid is a regular square mesh overlaying a polar stereographic projection (true at 60°N). One NMC grid square over the central U.S. (35-40°N) is about 200 miles on a side. We ordered the radiance statistics into a 7 x 7 matrix of 1/16 NMC grids (approx. 50 x 50 miles), thus considering a region of about 350 miles square around the central stations.

Figures 61-71 depict eleven sample arrays of satellite data statistics. They include: a) mean brightness of the grid mesh $\overline{B}_{ij}$

b) standard deviation of brightness σ_B

c) relative dispersion $\sigma_B/\overline{B}_{ij}$

d) departure of mean grid brightness from the field mean $\overline{B}_T-\overline{B}_{ij}$ and

e) change of brightness from one grid time to the next grid time $\Delta\overline{B}_{ij}$

A typical grid mesh contained 30,400 measurements at full camera resolution;[5] all of these were used to derive the statistics.

No analysis of the statistical fields was attempted; the reader may scan the arrays or analyses as he wishes. Of course several other descriptions of the field could have been chosen, but the most simple were thought best for this first attempt. They show, collectively, that the ATS data present a wide dynamic range and regularly varing, yet discontinuous, field of observations. Such a quantitative repre-

---

[5] In the data processing for the arrays every two digital elements were averaged. (Since the sampling rate for digitization is about twice the frequency of contiguous scan spots, we retain geometrical resolution).

sentation of the cloud field offers many further research possibilities.

5.0 Summary of the Pilot Study

This study contains no conclusions; rather it poses questions and allows evaluation and planning of future work. It contains examples of the data set that has been assembled, the first extensive use of quantitative geosynchronous satellite measurements with concurrent conventional meteorological observation on a high resolution space and time scale.

In the opinion of the authors it shows that it should be profitable to proceed to a test of the use of quantitative radiance measurements from geosynchronous satellites in very short range terminal forecast techniques. This opinion is based on the apparently good representation of both homogeneous cloud masses and regions of intensive cloud development by the reflected radiance measurements from ATS-III. As can be seen from the time series, changes in radiance measured from a geosynchronous satellite are not always representative of changes in reported station ceiling and visibility. Thus, further study with the satellite data should emphasize other forecast parameters as well.

During the course of this study, lack of an internal relative calibration check in the ATS-III spinscan camera system prevented easy intercomparison of radiance measurements obtained on different days. While this problem can be overcome by extracting special information from the image scene (as is done for data mapping), future satellite systems should include an internal reference.

6.0 Acknowledgements

This study was directed by Dr. Thomas Vonder Haar, Principal investigator, with Richard Cram as project manager. Miss Sharon Nicholson assisted with the data analysis and Eric Smith and Ralph DeDecker coded the programs to use the geosynchronous satellite data. Professors Verner Suomi and Robert Parent were principal investigators for the mult-color spinscan camera experiment on NASA's ATS-III spacecraft. We thank all who aided with the design and data acquisition phases of the experiment.

7.0 References

1) Suomi, V., and R. Parent, A color view of planet earth. Bull. Amer. Meteorol. Soc., 49(2), 74, 1968.

2) Suomi, V., and T. Vonder Haar, Geosynchronous meteorological satellite. J. Spacecraft Rockets, 6, 3, 1969.

3) Vonder Haar, T.H., Meteorological applications of reflected radiance measurements from ATSI and ATSIII. J. Geophysical Research, 74, 23, Oct. 1969.

4) Doolittle, R.C., C.L. Bristor, and L. Lauritson, Mapping of geostationary satellite pictures, an operational experiment. ESSA technical Memorandum NESCTM 20, March 1970.

5) Brennan, B., and W.R. Bandeen, Anisotropic reflectance characteristics of natural earth surfaces. J. Applied Optics, 9, Feb. 1970.

6) Raschke, E., and W.R. Bandeen, The radiation balance of the planet earth from radiation measurements of the satellite nimbus II. J. Applied Meteorology, 9, 2, April 1970.

8.0 List of Figures

Appendix A

Bi-directional Radiance Normalization Method

(developed under separate contract)

The reflected solar radiance from clouds depends to a large extent on four variables: (a) drop size distribution and phase state (b) liquid water content (c) cloud thickness and (d) angular condition of the measurement scene (zenith angles of sun and sensor (ζ,θ) and their relative azimuth (ϕ). The first three variables depend on the physical characteristics of the cloud; the angular dependence is more related to the conditions of measurement and adds unwanted "noise".

If clouds, or other natural surfaces, were known to reflect solar energy according to Lamberts law (i.e., appeared as isotropic reflectors when viewed from different angles by an instrument of fixed field-of-view), then all angular dependence in the magnitude of a radiance measurement could be removed quite easily <u>if</u> one knew the magnitude of incident radiation on the surface of measurement. Given

$$N_r(\theta,\phi) = \int \rho(\zeta,\theta,\phi)\, N_i \cos\zeta \, d\Omega_i \qquad (1)$$

with N_i and N_r the incident and reflected radiance respectively, Ω_i the total solid angle subtended by the radiation source at the reflecting surface and ρ, the bi-directional reflectance (a property of the surface with units sr^{-1}). For a Lambert surface, the total directional reflectance r equals $\pi\ \rho$ since ρ = constant $\cdot$ cos θ. This follows from:

$$r(\zeta) = \int_0^{2\pi} \int_0^{\pi/2} [\rho(\zeta,\theta,\phi) \cos\theta] \sin\theta \, d\theta \, d\phi \qquad (2)$$

for a non-lambert reflector we must be able to specify the angular dependence of ρ in some similar manner in order to (numerically) integrate (2).

From special aircraft observation of cloud reflectives (Brennen and Bandeen (5) and others), as well as available theoretical calculations Raschke and Bandeen (6) have assembled information suitable to empirically represnet $\rho\ (\zeta,\theta,\phi)$. They do this in terms of a factor $\chi_{(\zeta,\theta,\phi)} = \frac{r(\zeta)}{\pi\rho}$ with $\chi > 1$ indicating reflected radiance greater than

that which would be received from a Lambert reflector when viewed under the same angular conditions (ζ,θ,ϕ); vice versa for $\chi(\zeta,\theta,\phi)<1$. (i.e., large χ values represent strong forward scattering properties that are unique to many atmosphere constituents including water droplets).

In practice, a time sequence of measurements of a given surface, cloud or land may be taken under different angular conditions because of:

(a) rapid movement of the instrument (i.e., on a satellite or aircraft) thus changing θ and/or ϕ while $\zeta=\zeta(t)$ x constant,

or

(b) relatively long elapsed time interval from beginning to end of the sequence (i.e., sensor mounted on a fixed platform) thus changing $\zeta(t)$ and ϕ with θ= constant.

For either case, the relative comparison of measurements within the sequence requires the ability to normalize for angular dependence of the reflected radiation.

Vonder Haar (3) discusses the proportionality between relative radiance measurements, D (called also, digital counts or brightness values) and the bi-directional reflectance, ρ (i.e., $D \sim V_c \sim N \sim \rho$). If the physical characteristics of a cloud remain absolutely constant, but it is viewed under different angular conditions, it will have different values of ρ and therefore D. However, if ρ is scaled by a proper factor (say $\chi_{(\zeta,\theta,\phi)}$) it can be effectively normalized to a common base (in this case to the total effective "diffuse" reflectance that would arise from a Lambert reflector). After further weighting by any change in magnitude of incident solar irradiance arising from the change in angular conditions we convert from diffuse reflectance to ρ using a new, appropriate χ value and thus to a new value of D. The new value is that which would be output from the ATS spinscan system if a cloud that did not change physical character was viewed at a different time (similar logic applies to views of identical clouds viewed at the same time but at widely separated geographical locations).

This bi-directional radiance normalization technique was used in the present report as indicated. It is the best available today but needs continuous revision as more data of the kind described in (5) become available.

Appendix B

Code for Ceiling & Visibility Analyses

Symbols

Clouds & Ceiling:

O or c = clear

◐ = scattered

◍ = broken

⊕ = overcast

⊗ = obscure

There is technically no ceiling if the sky is scattered or clear (i.e., less than .6 sky cover)

- before a symbol means thin; 1/2 or more of the sky is transparent

Cirriform cloud height is not estimated and is not called a ceiling.

/ = cirriform $\angle$ .6 sky cover

U = cirriform $\geq$ .6 sky cover

Ex: 12◐ = 1200 ft., broken; /— = thin, cirriform

Weather:

R = rain

L = drizzle

Z = freezing

D = dust

T = thunderstorm (with no rain associated)

W = shower

E = sleet

B = blowing

F = fog

H = haze

K = smoke

S = snow

A = hail

GF = ground fog

\+ = heavy

++ = very heavy

\- = light

-- = very light

Appendix C

DDC	-	Dodge City, Kan.	C	April 4, 1969
GAG		Gage, Okla.	C	
GCK		Garden City, Kan.	C	
GLD		Goodland, Kan.	M	
HLC		Hill City, Kan.	C	
LAA		Lamar, Colo.	M	
RSL		Russell, Kan.	C	
CMH	-	Columbus, Ohio	E	April 23, 1968
5G4		Lima, O.	E	
CV6		Cincinnati, O. (Greater Cin. Airport)	E	
DAY		Dayton, O.	E	
FDY		Findlay, O.	E	
FWA		Fort Wayne, Ind.	E	
HTS		Huntington, W. Va.	E	
IND		Indianapolis, Ind.	E	
LEX		Lexington, Ken.	E	
LUK		Cincinnati, O. (Luke's AFB)	E	
MFD		Mansfield, O.	E	
MIE		Mincie, Ind.	E	
OSU		Columbus O. (Ohio St. Univ. Airport)	E	
PMH		Portsmouth, O.	E	
ZZV		Zanesville, O.	E	
SPS	-	Witchita Falls, Tex.	C	April 19, 1968
ABI		Abilene, Tx.	C	
ADM		Ardmore, Okla.	C	
ADS		Dallas, Tex. (Addison)	C	

CDS	Childress, Tex.	C
DAL	Dallas, Tex. (Love Field)	C
DUC	Duncan, Okla.	C
FTW	Fort Worth, Tex. (Meacha)	C
GSW	Fort Worth, Tex. (Greater SW Intern)	C
HBR	Hobart, Okla.	C
LAW	Lawton, Okla.	C
MWL	Mineral Wells, Tex.	C
PWA	Okla. City, Okla. (Wiley Post)	C
OKC	Okla, City, Okla. (Will Rogers World)	C

C = Central Time = G.M.T. - 6 hrs.

E = Eastern Time = G.M.T. - 5 hrs.

M = Mountain Time = G.M.T. - 7 hrs.

Figure 1a

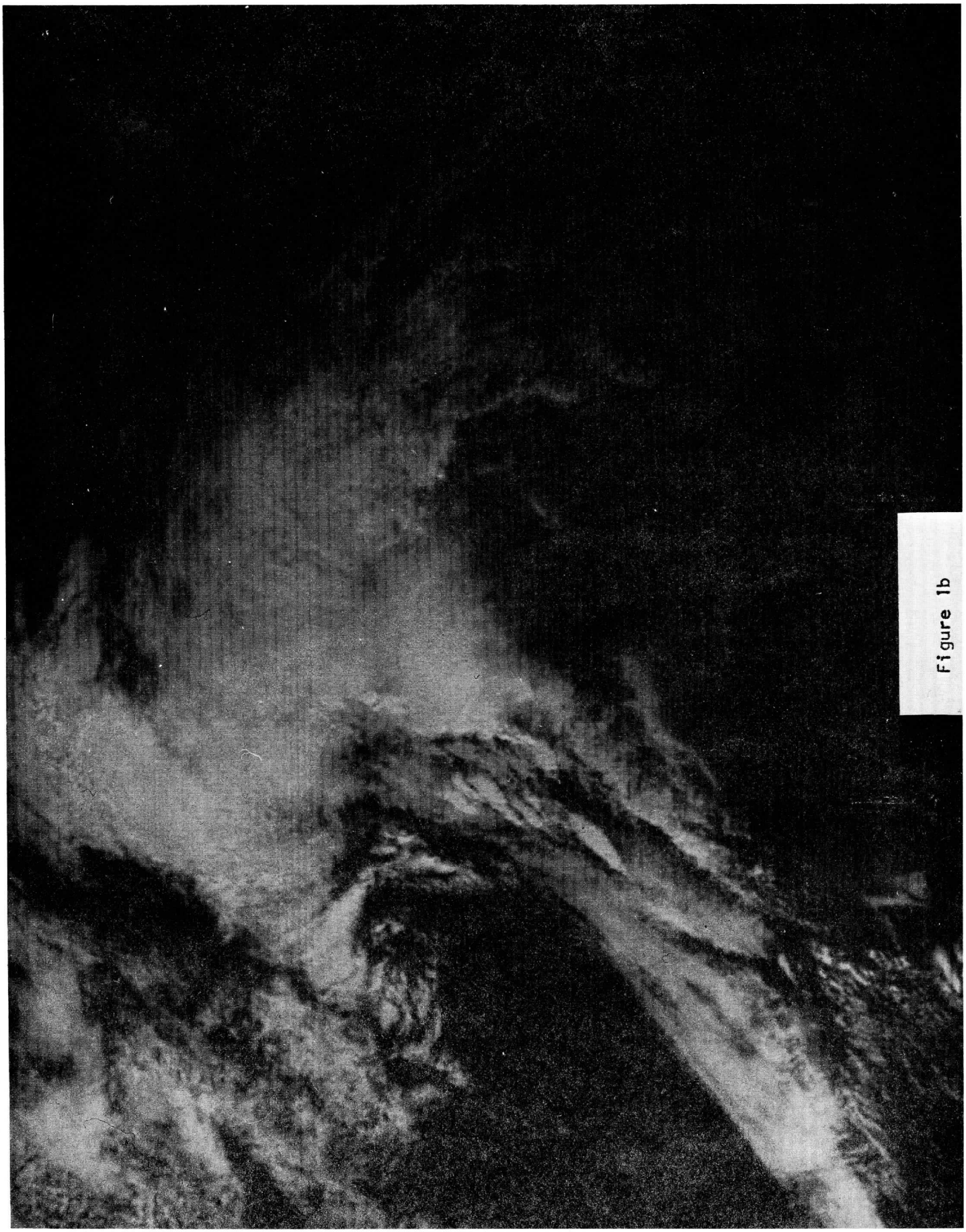

Figure 1b

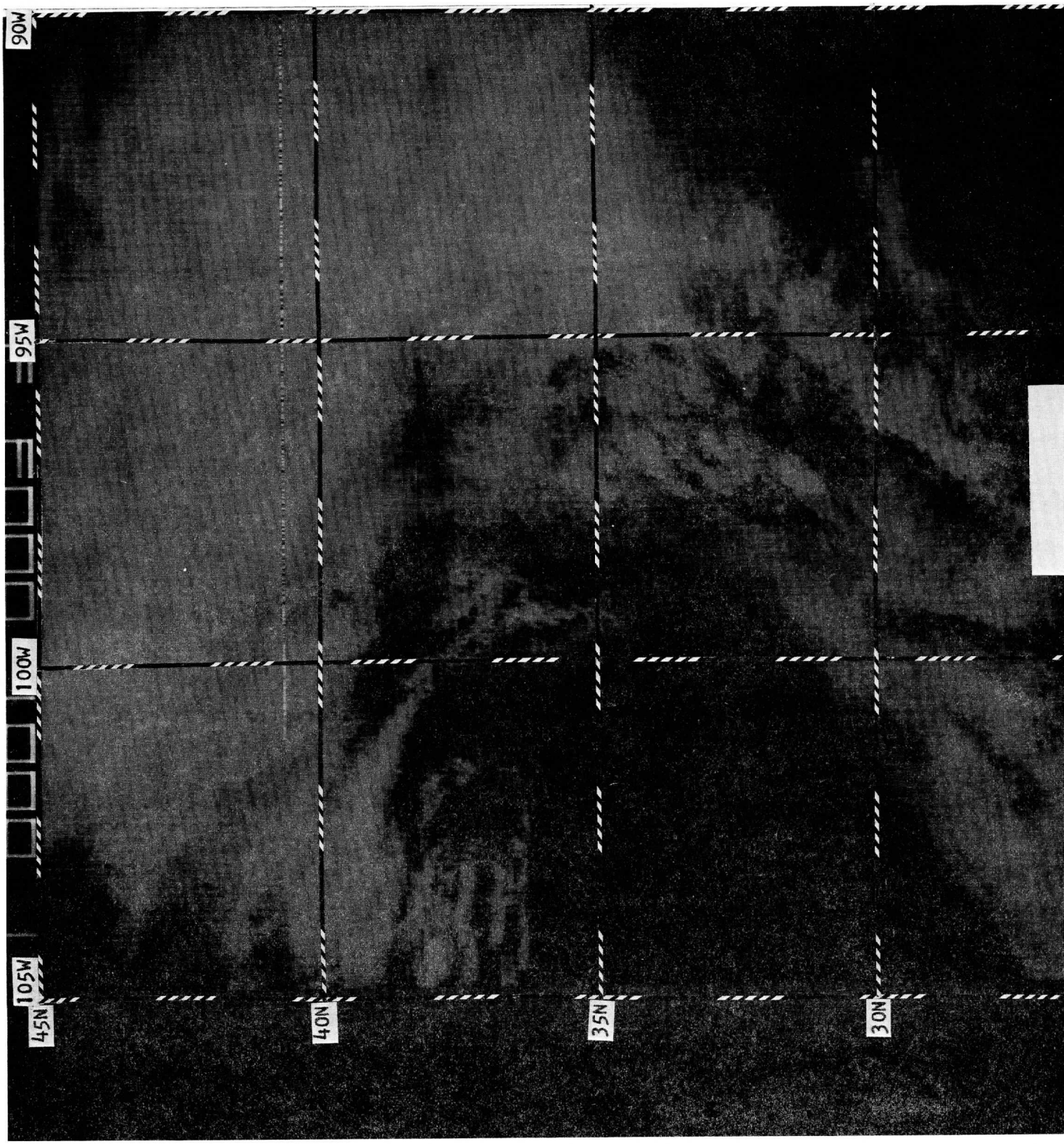
90W
95W
100W
105W
45N
40N
35N
30N

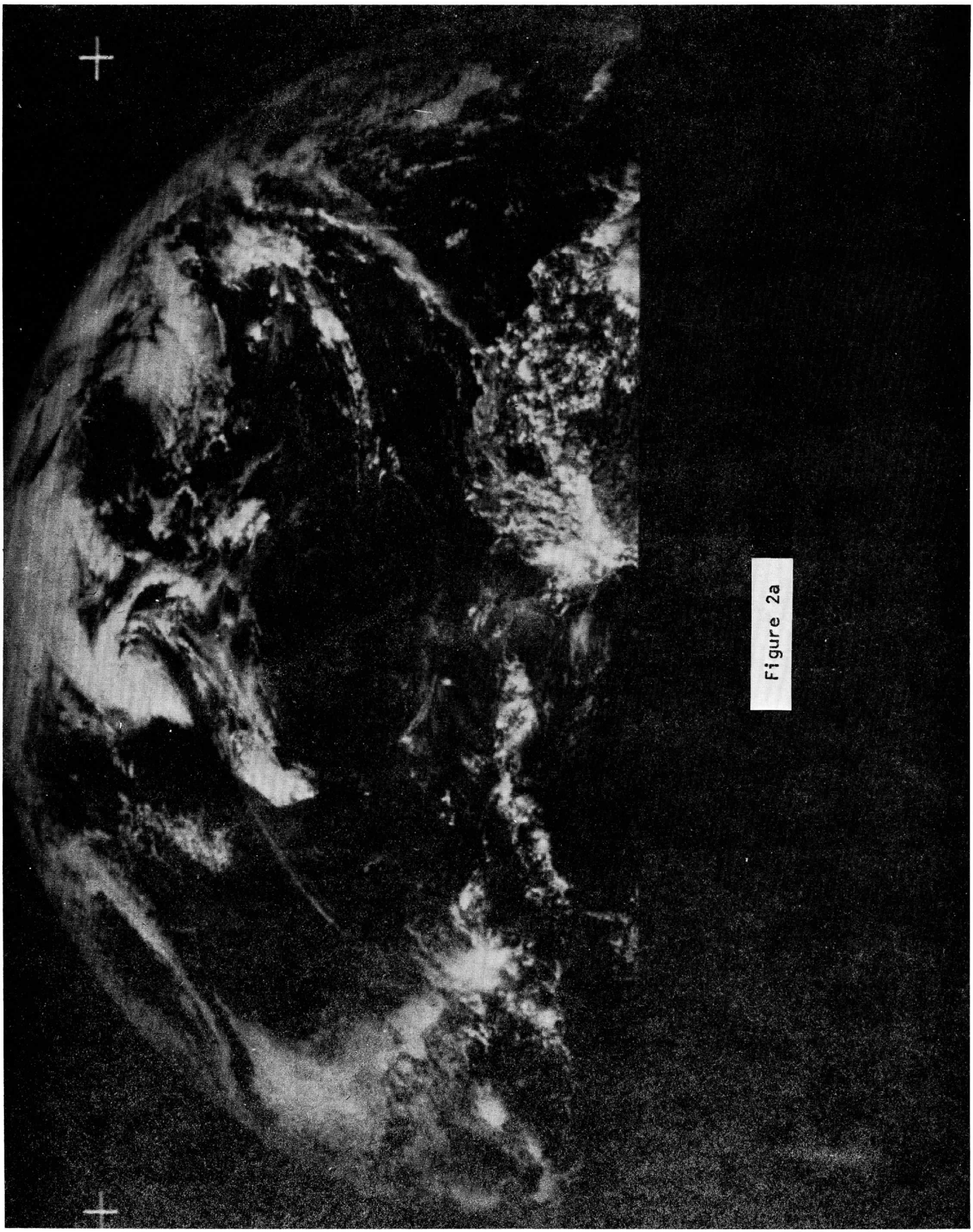

Figure 2a

Figure 2b

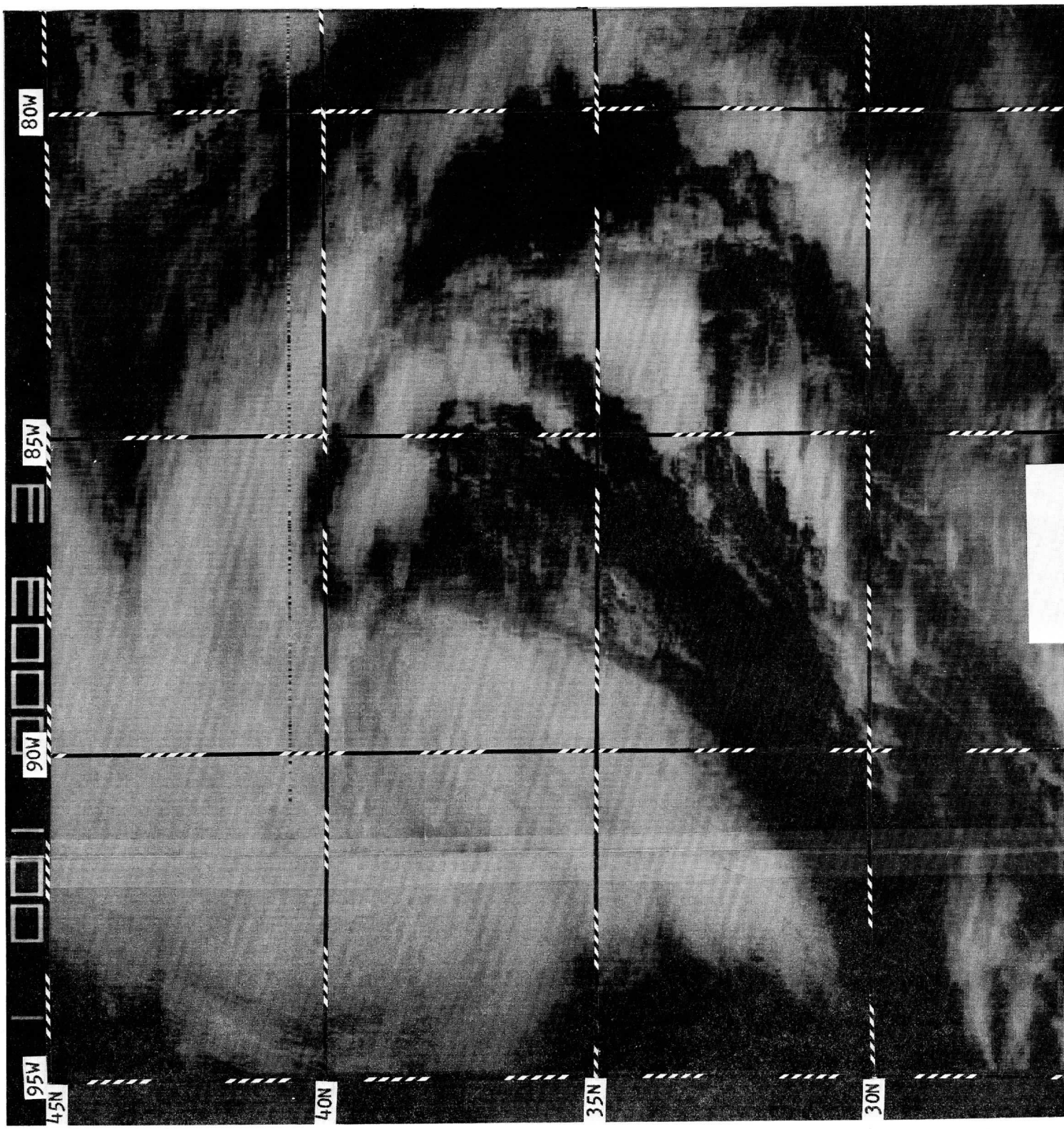
95W
90W
85W
80W
45N
40N
35N
30N

Figure 3a

Figure 3b

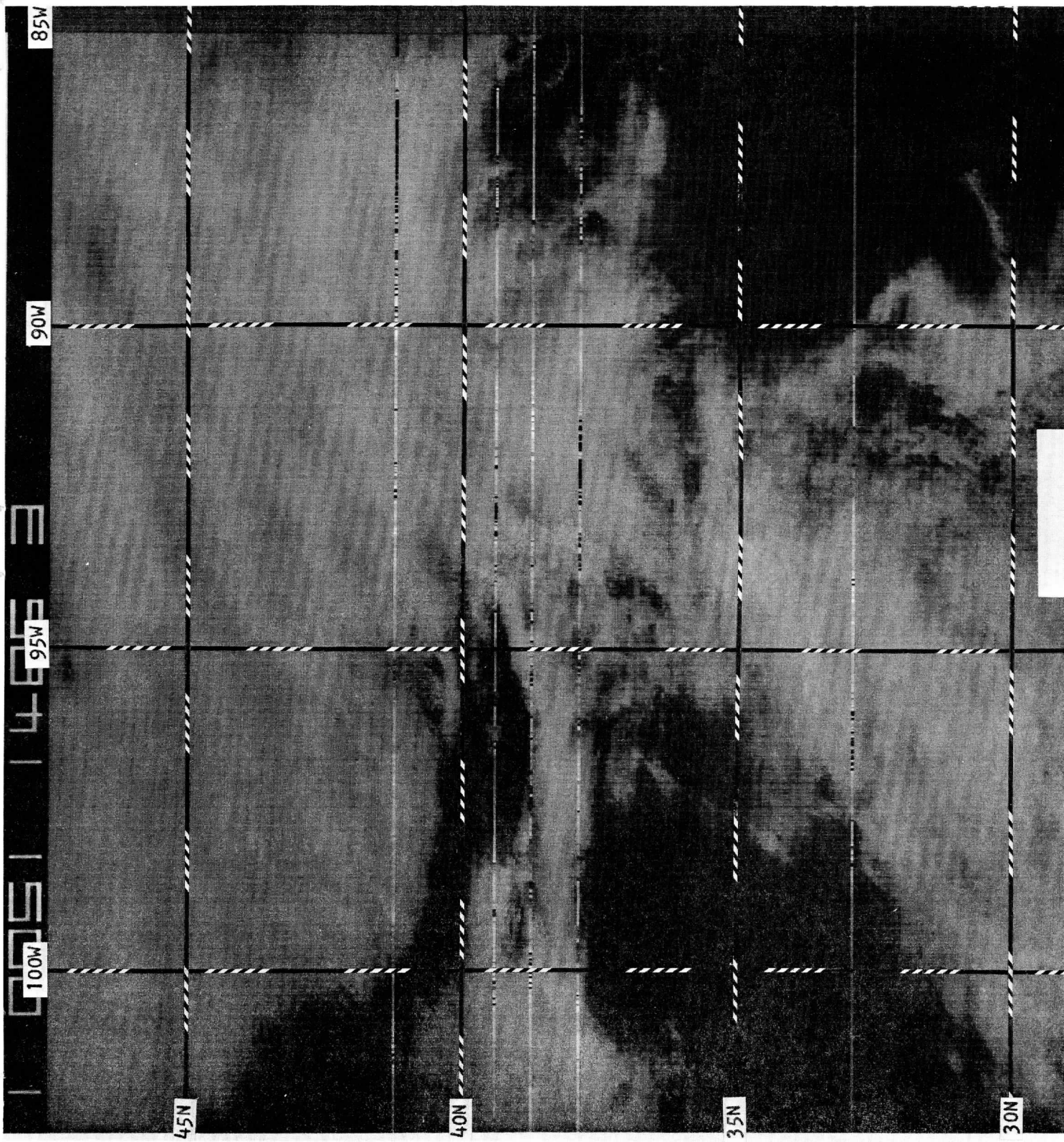
100W
95W
90W
85W
45N
40N
35N
30N

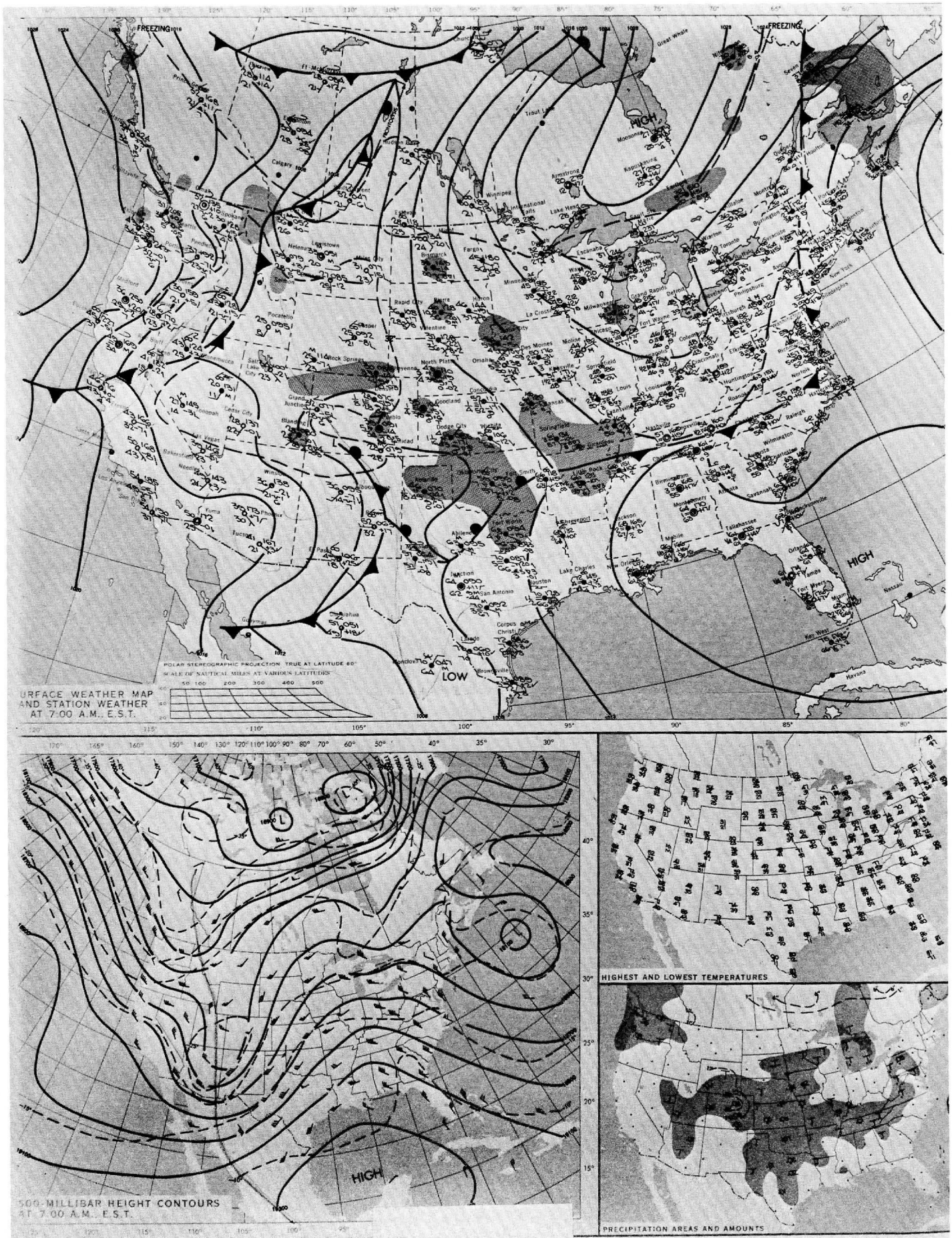
FREEZING
HIGH
LOW
POLAR STEREOGRAPHIC PROJECTION. TRUE AT LATITUDE 60°
SCALE OF NAUTICAL MILES AT VARIOUS LATITUDES
50 100 200 300 400 500
URFACE WEATHER MAP
AND STATION WEATHER
AT 7:00 A.M., E.S.T.
500-MILLIBAR HEIGHT CONTOURS
AT 7:00 A.M., E.S.T.
HIGHEST AND LOWEST TEMPERATURES
PRECIPITATION AREAS AND AMOUNTS

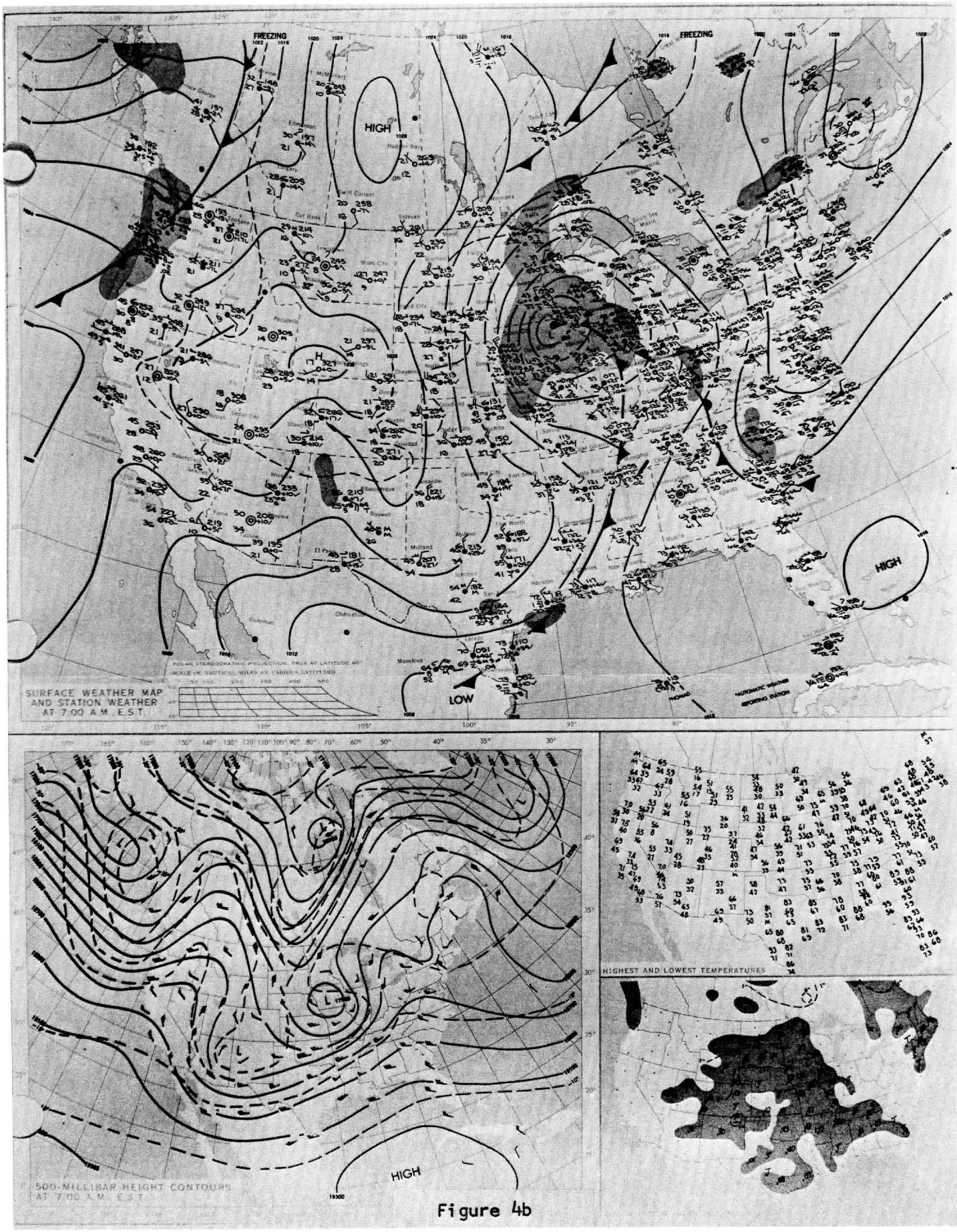
FREEZING
HIGH
LOW
SURFACE WEATHER MAP
AND STATION WEATHER
AT 7:00 A.M. E.S.T.
500-MILLIBAR HEIGHT CONTOURS
AT 7:00 A.M. E.S.T.
HIGHEST AND LOWEST TEMPERATURES

Figure 4b

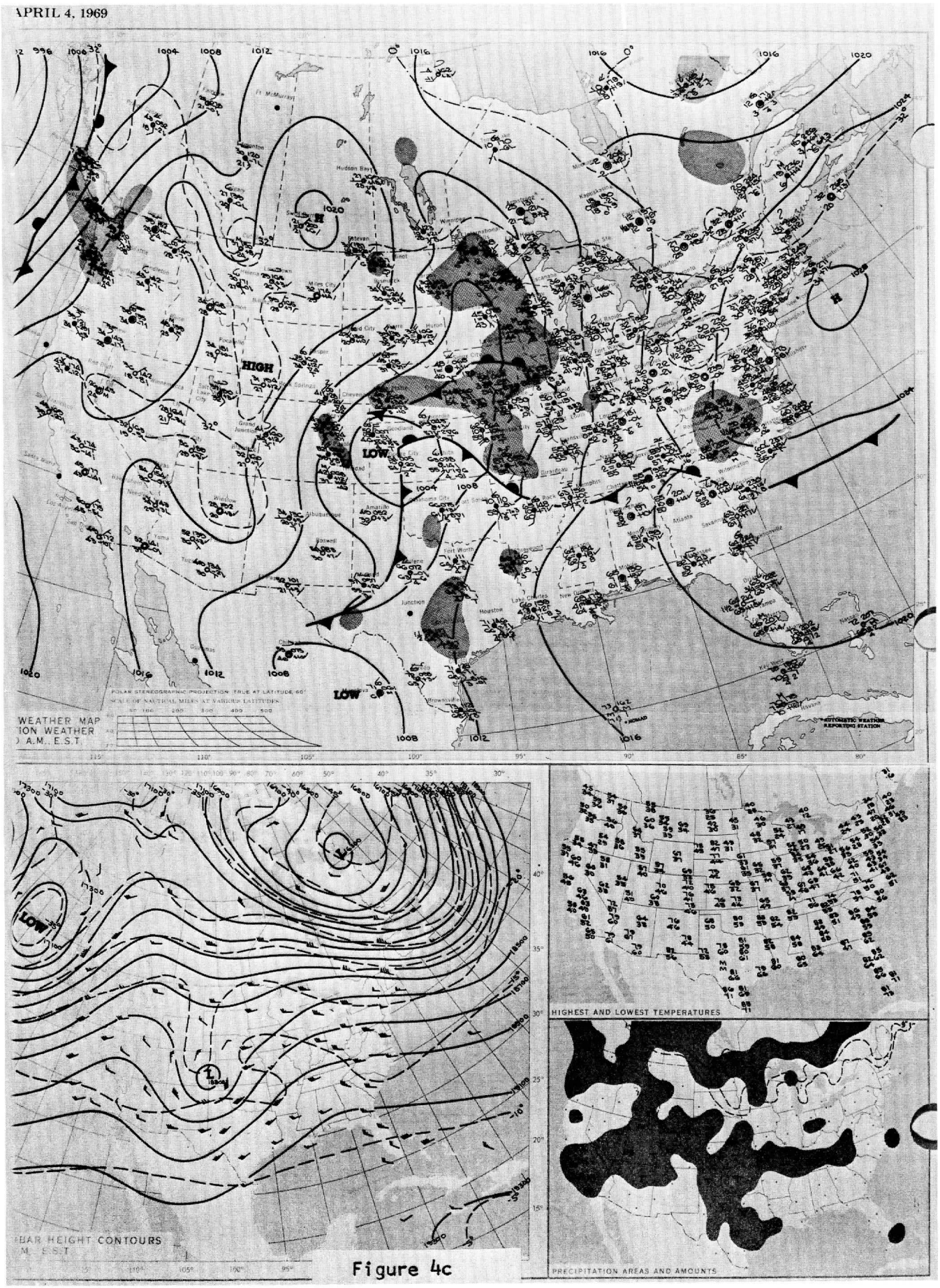
APRIL 4, 1969
HIGH
LOW
LOW
WEATHER MAP
ION WEATHER
) A.M. E.S.T.
HIGHEST AND LOWEST TEMPERATURES
PRECIPITATION AREAS AND AMOUNTS
BAR HEIGHT CONTOURS
M. E.S.T.

Figure 4c

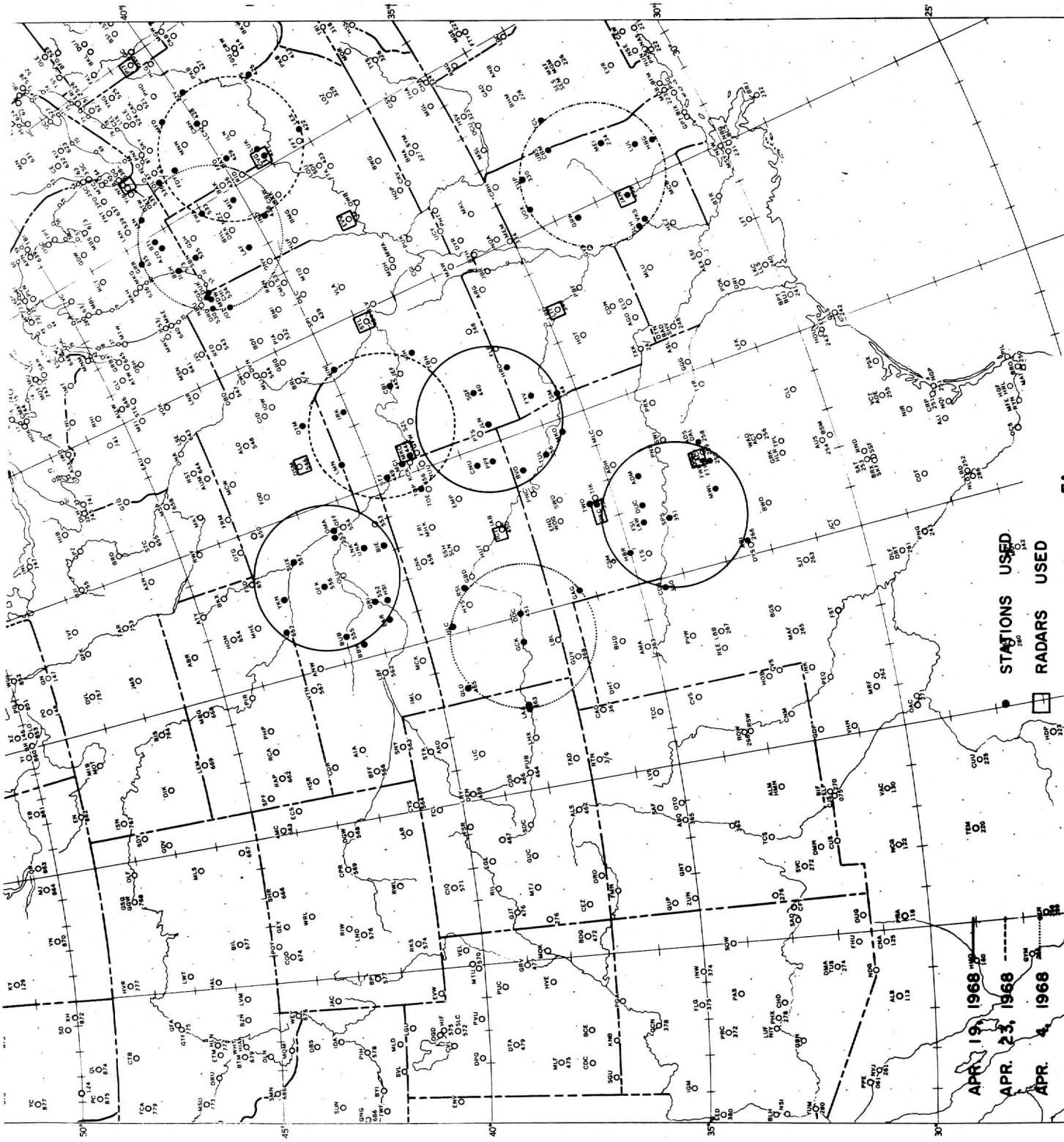
STATIONS USED
RADARS USED
APR. 19, 1968
APR. 23, 1968
APR. 4, 1968

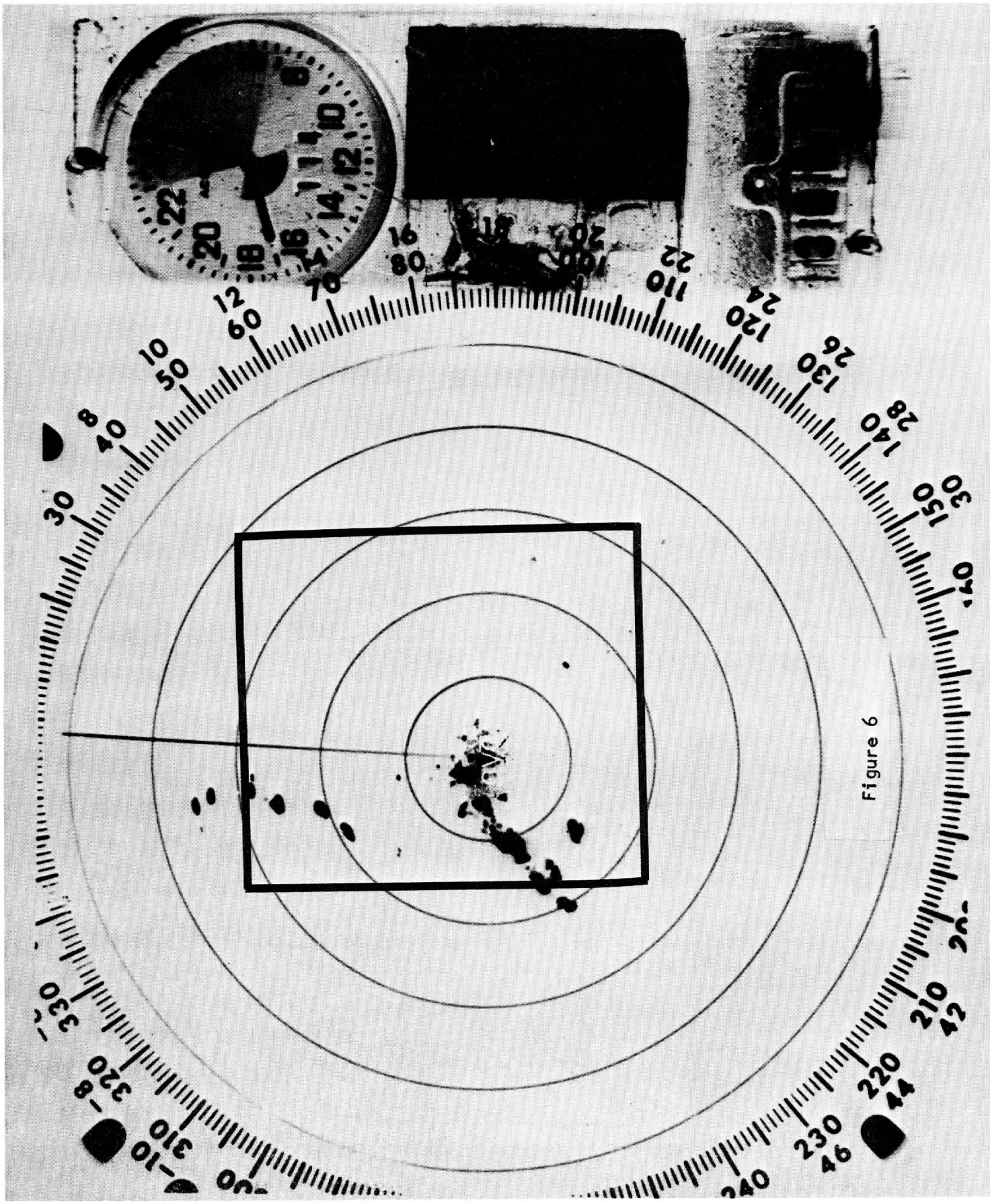

Figure 6

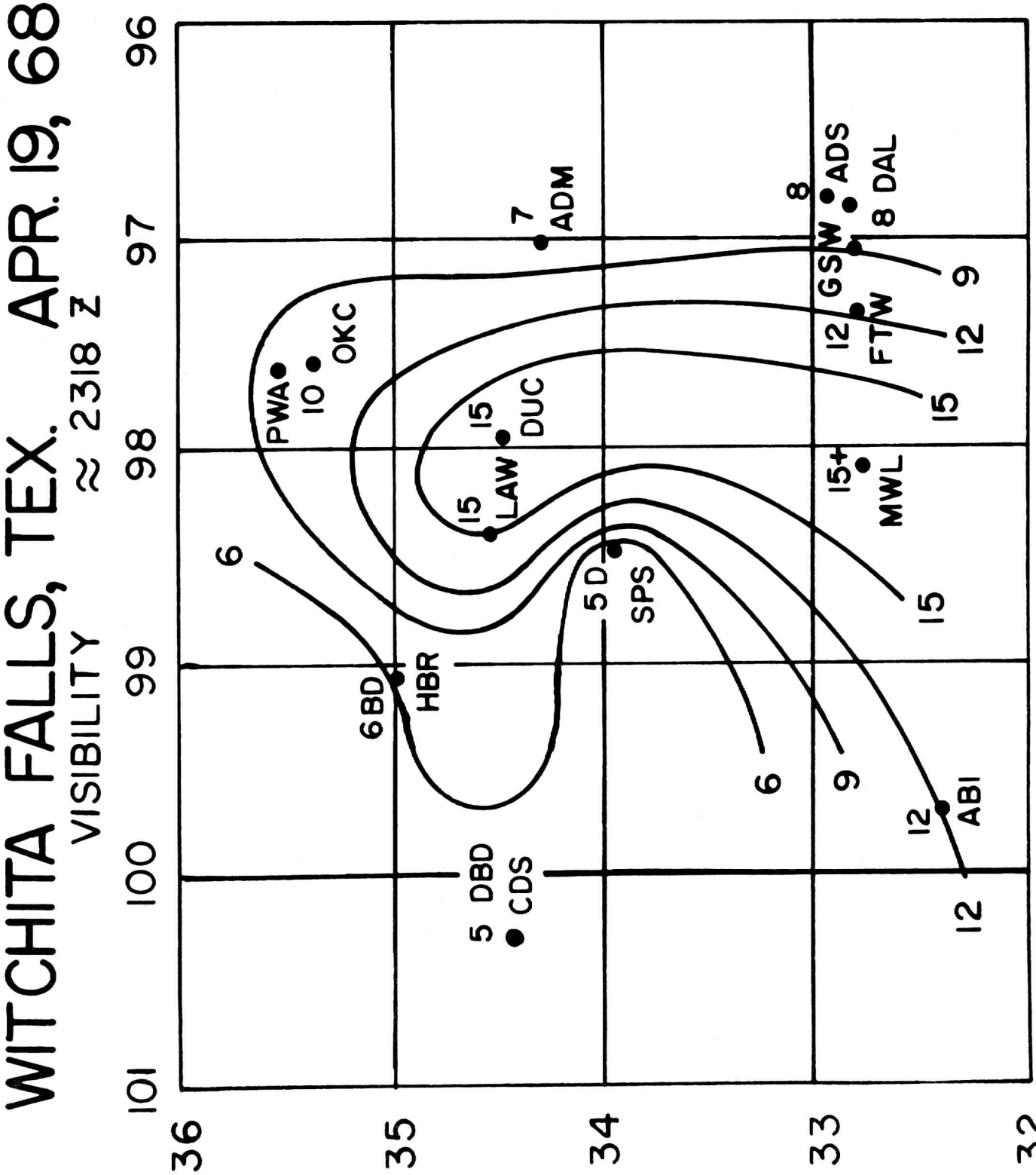
WITCHITA FALLS, TEX. APR. 19, 68
VISIBILITY
≈ 2318 Z
36
35
34
33
32
101
100
99
98
97
96
6
6BD
HBR
5 DBD
CDS
PWA
10
OKC
15
LAW
15
DUC
7
ADM
5D
SPS
15+
MWL
8
ADS
8 DAL
12
GSW
12
FTW
9
15
15
6
9
12
ABI
12

Figure 7

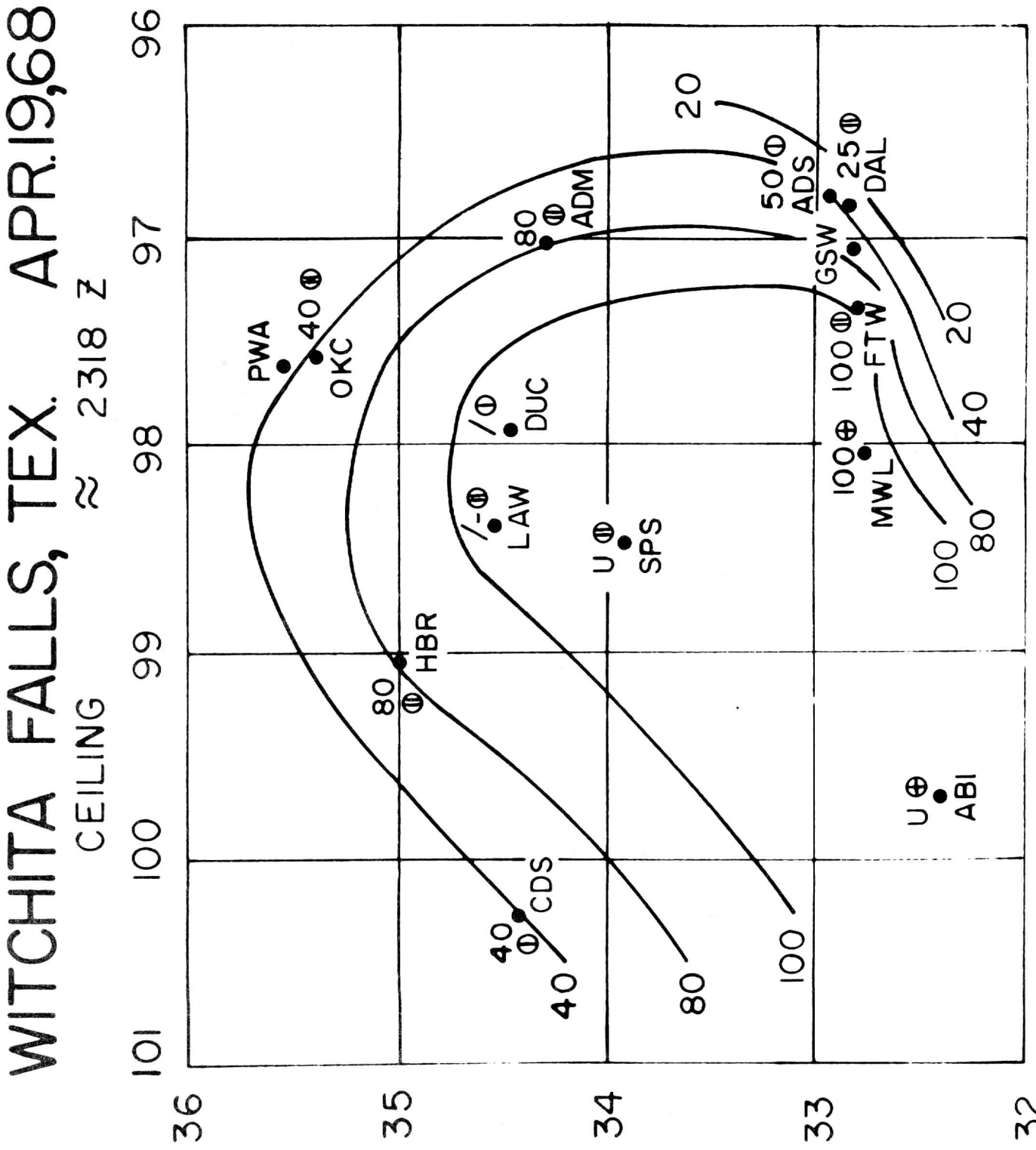
WITCHITA FALLS, TEX. APR.19,68
CEILING ≈ 2318 Z
101
100
99
98
97
96
36
35
34
33
32
PWA
40
OKC
80
ADM
50
ADS
25
DAL
20
GSW
100
FTW
20
40
80
100
MWL
100
/
DUC
/-
LAW
U
SPS
80
HBR
40
CDS
40
80
100
U
ABI

Figure 8

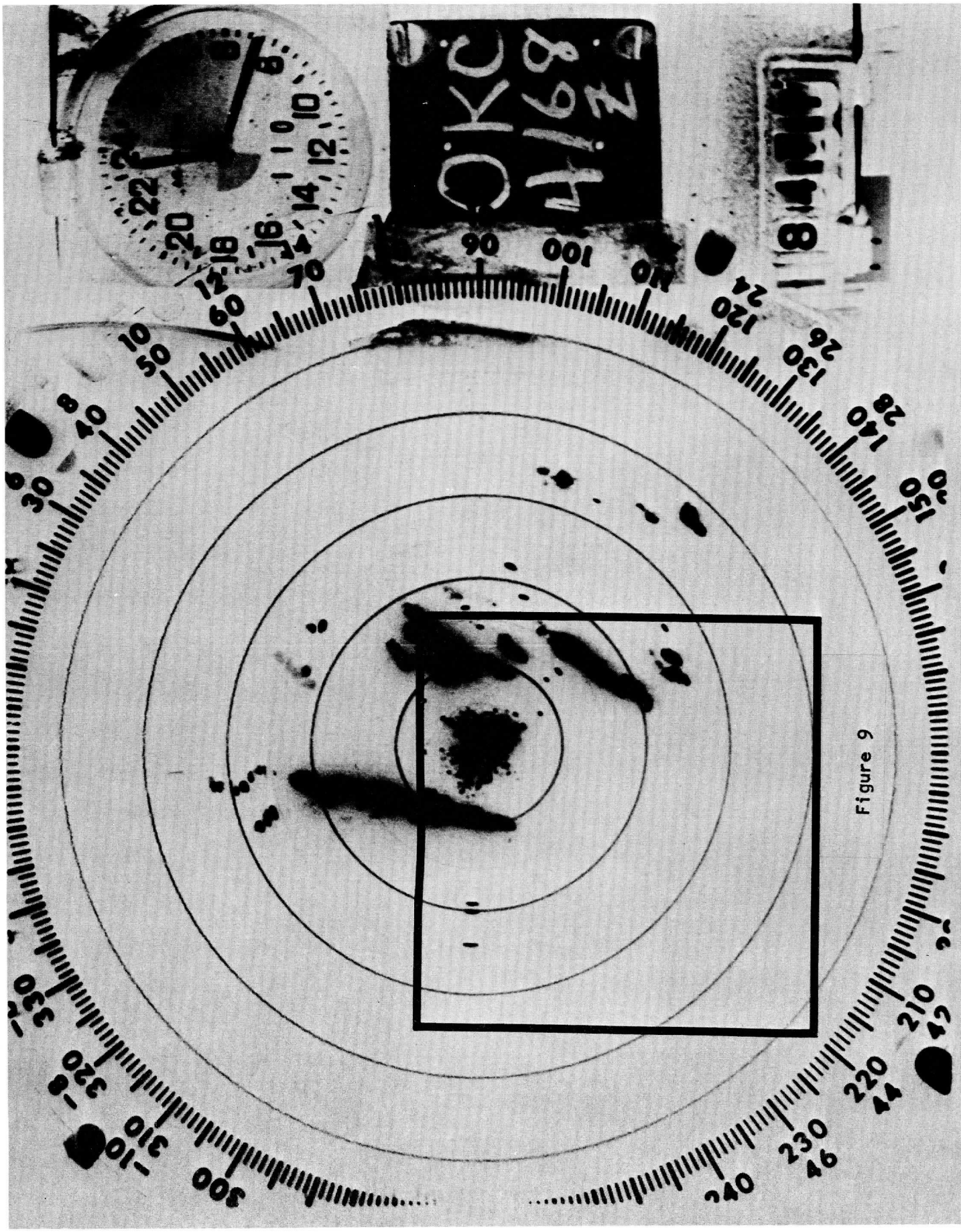

Figure 9

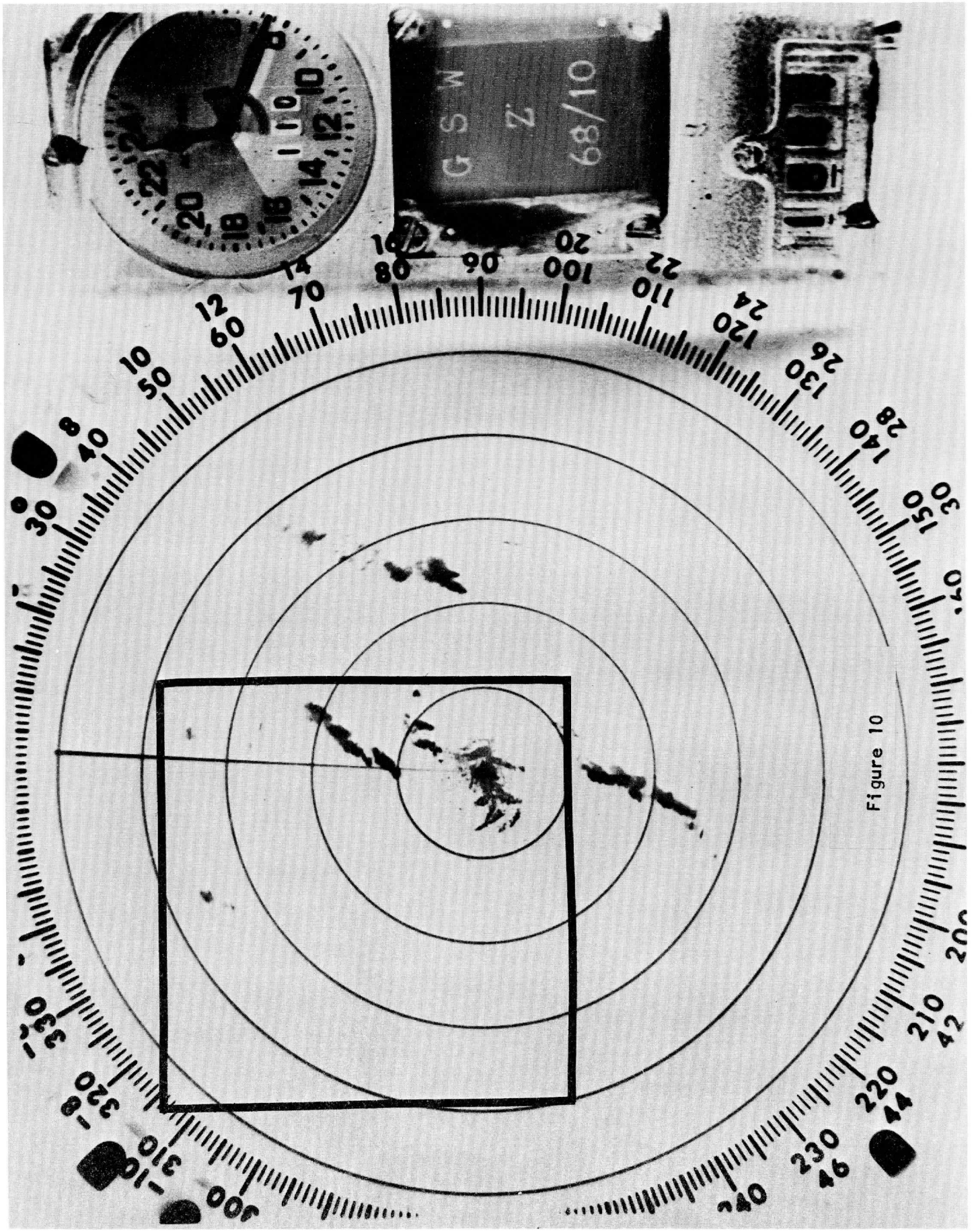

Figure 10

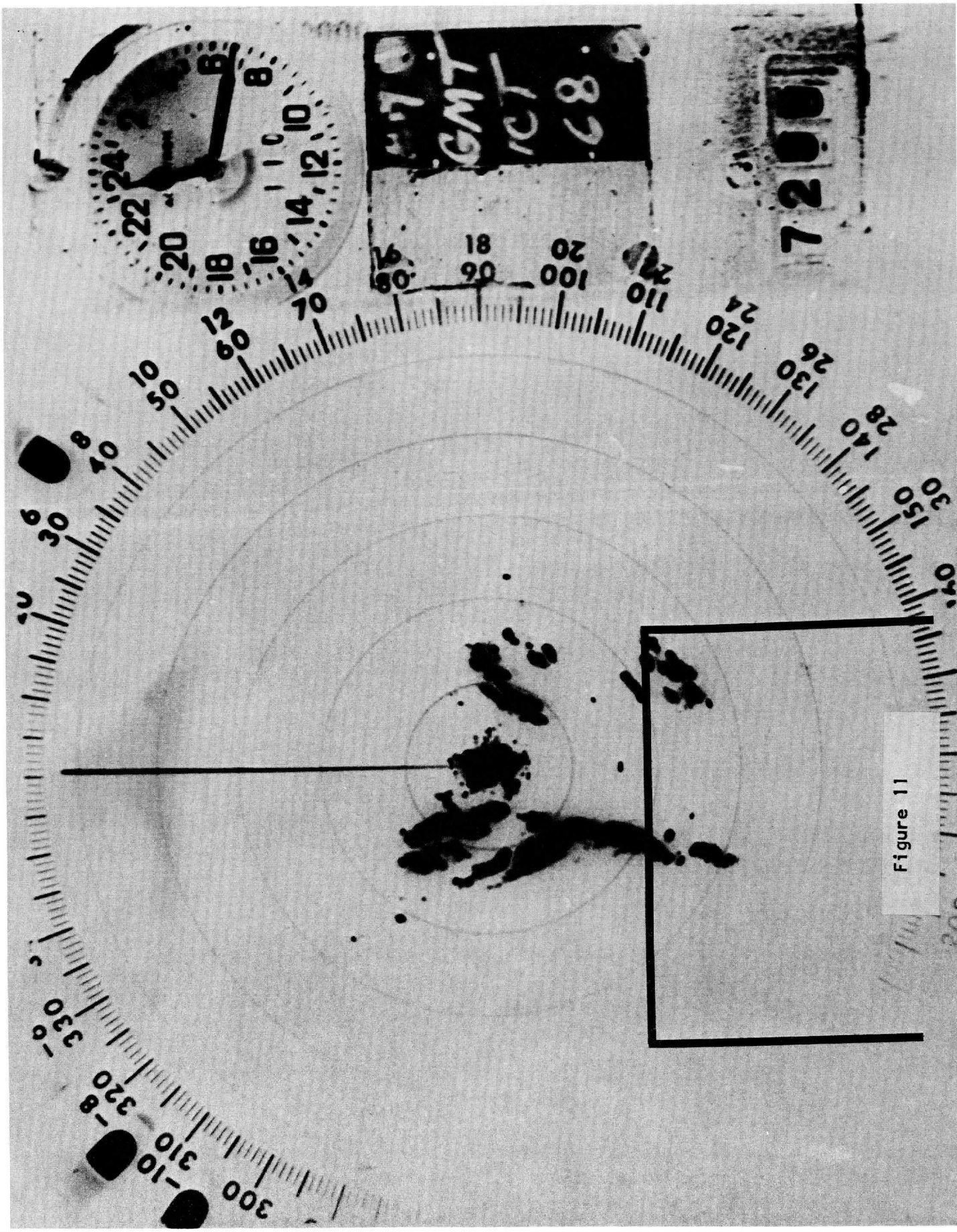

Figure 11

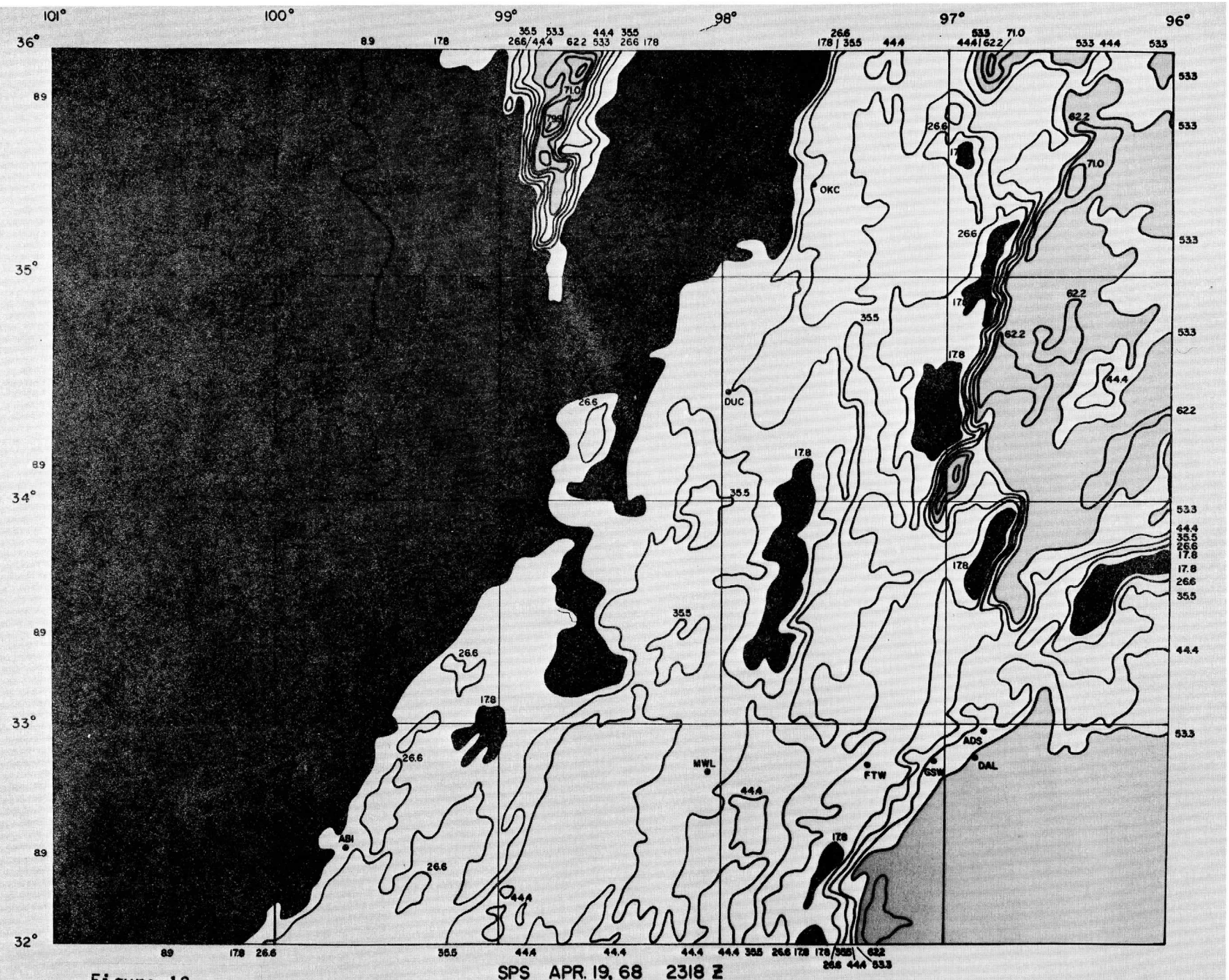
101°
100°
99°
98°
97°
96°
36°
35°
34°
33°
32°
OKC
DUC
MWL
FTW
GSW
ADS
DAL
ABI
SPS APR. 19, 68 2318 Z

Figure 12

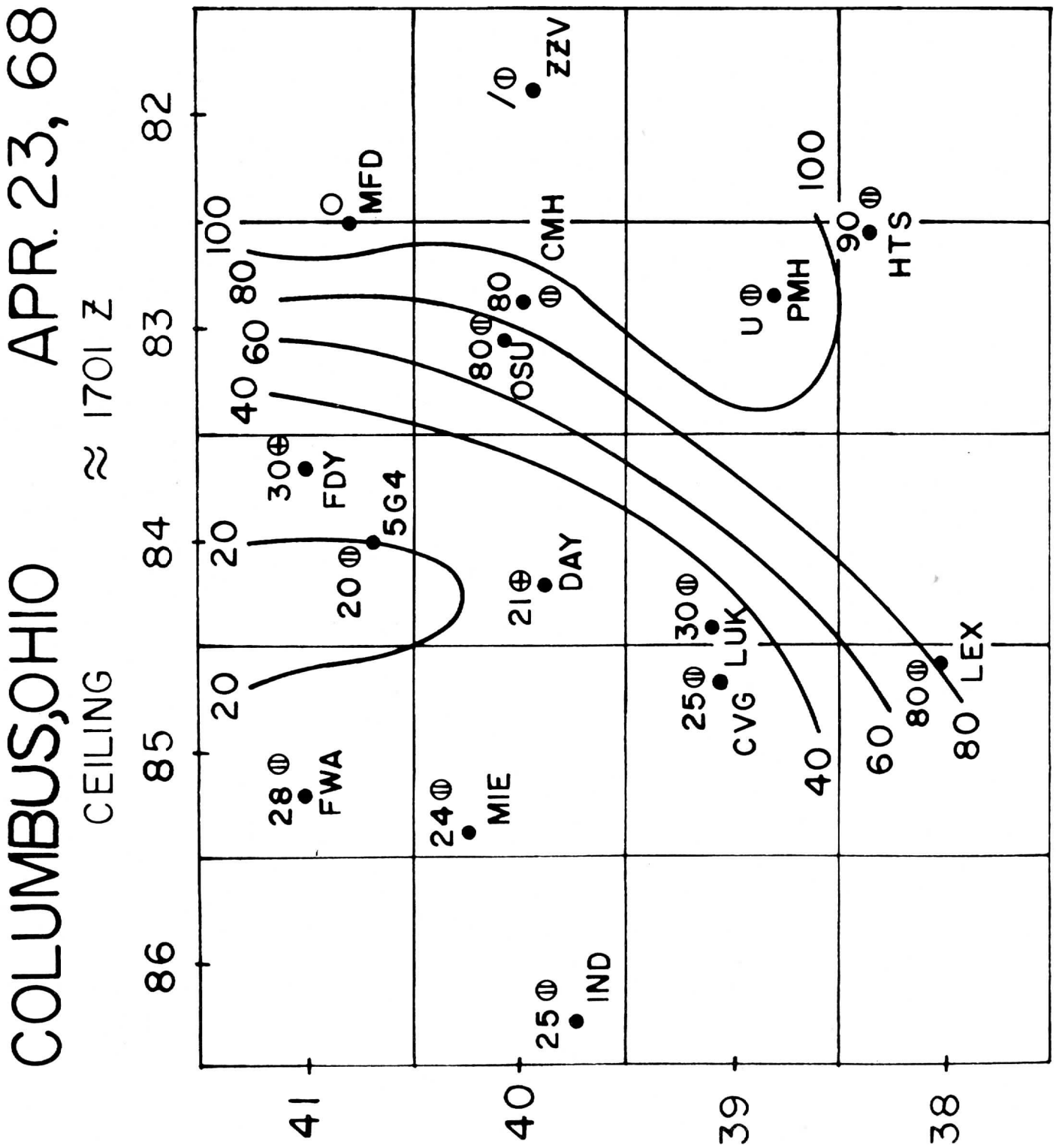
COLUMBUS,OHIO
APR. 23, 68
≈ 1701 Z
CEILING
86
85
84
83
82
41
40
39
38
MFD
ZZV
CMH
HTS
PMH
OSU
FDY
5G4
DAY
FWA
MIE
IND
LUK
CVG
LEX
100
80
60
40
20
30Φ
28Φ
24Φ
25Φ
21Φ
U Φ
90Φ

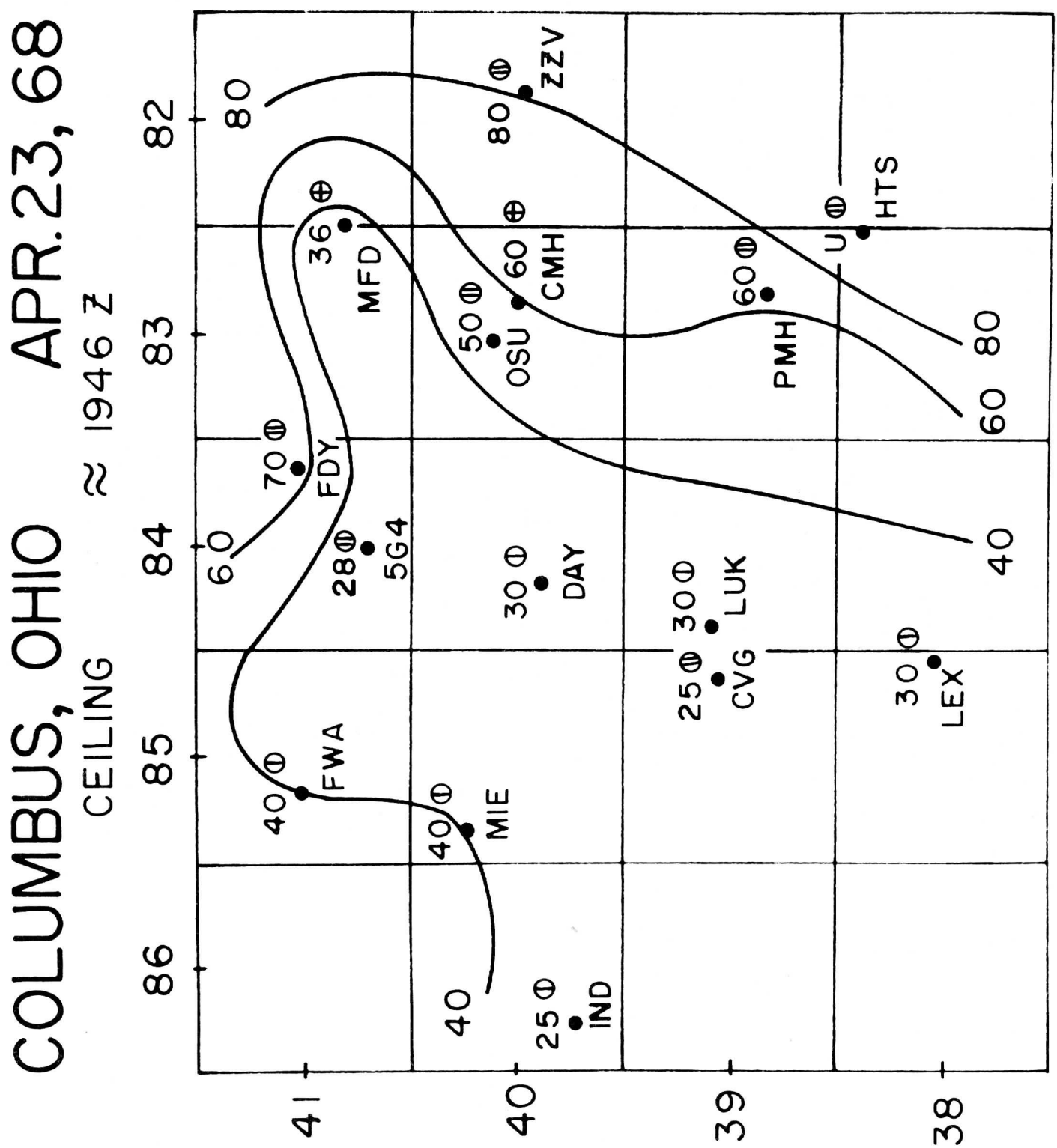
COLUMBUS, OHIO APR.23,68
CEILING ≈ 1946 Z
82
83
84
85
86
41
40
39
38
80
60
40
70 FDY
40 FWA
40 MIE
40
25 IND
28 5G4
36 MFD
30 DAY
50 OSU
60 CMH
80 ZZV
30 LUK
25 CVG
60 PMH
30 LEX
U HTS
60 80

Figure 14

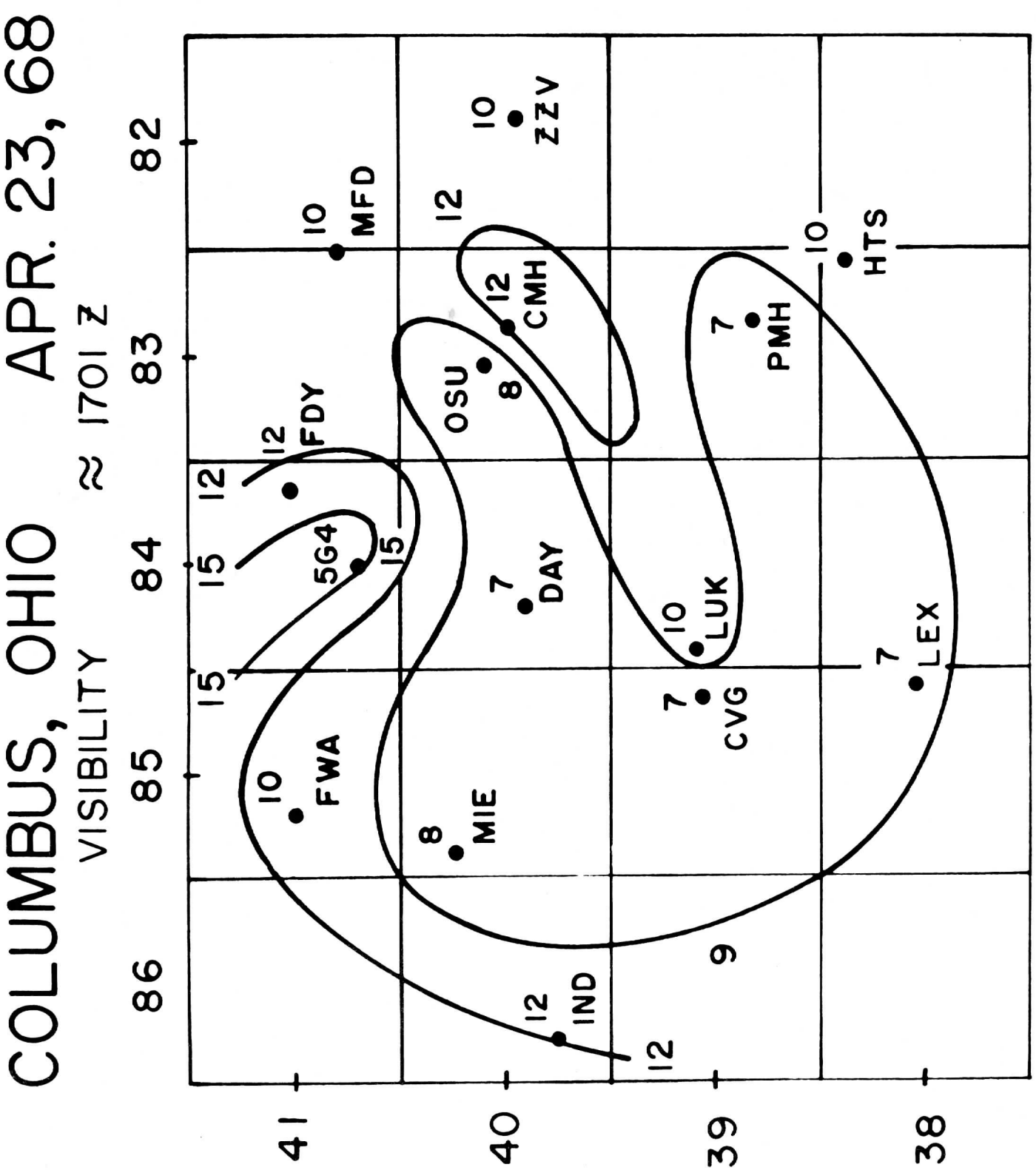
COLUMBUS, OHIO APR. 23, 68
VISIBILITY ≈ 1701 Z
86
85
84
83
82
41
40
39
38
10 FWA
12 IND
8 MIE
12 FDY
15 5G4
15
12
15
12
7 DAY
OSU
8
12 CMH
10 MFD
12
10 ZZV
10 LUK
7 CVG
9
7 PMH
10 HTS
7 LEX

Figure 15

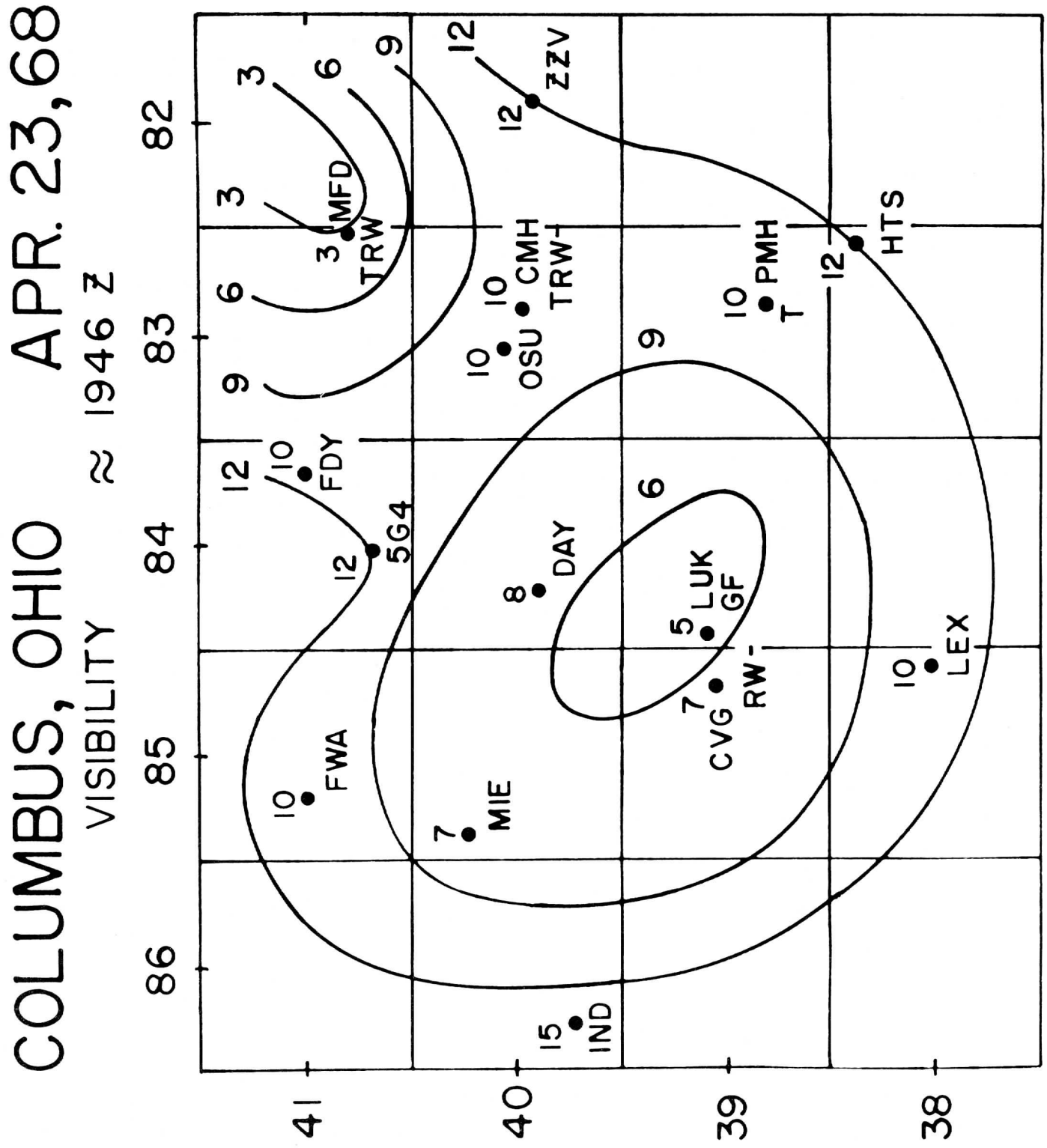
COLUMBUS, OHIO APR. 23,68
VISIBILITY ≈ 1946 Z
86
85
84
83
82
41
40
39
38
10 FWA
7 MIE
15 IND
12 10 FDY
12 5G4
8 DAY
5 LUK
7 CVG
GF
RW-
10 OSU
10 CMH
TRW
3 3 MFD
TRW
3 6 9
9 6
12 12 ZZV
10 PMH
T
12 HTS
10 LEX

Figure 16

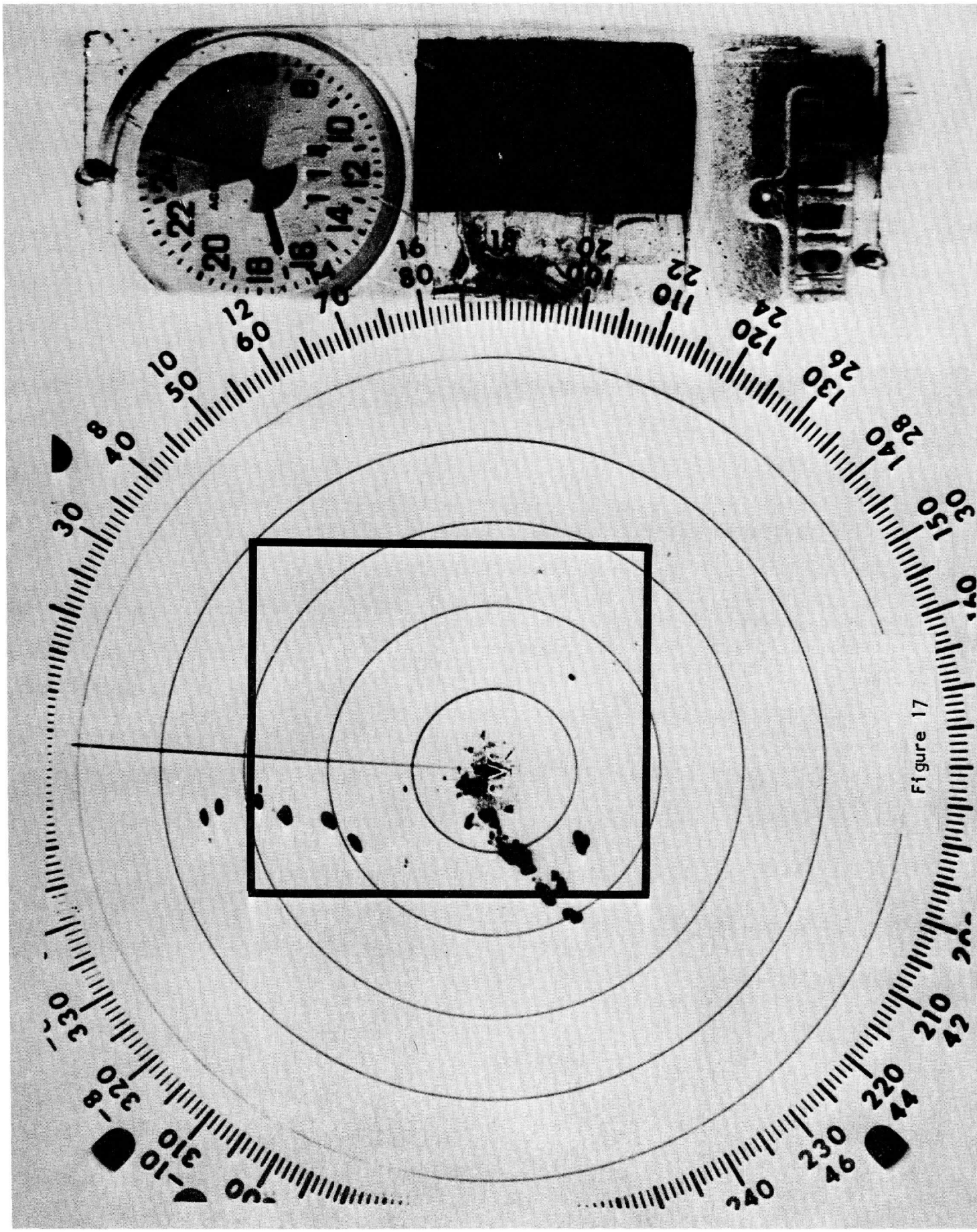

Figure 17

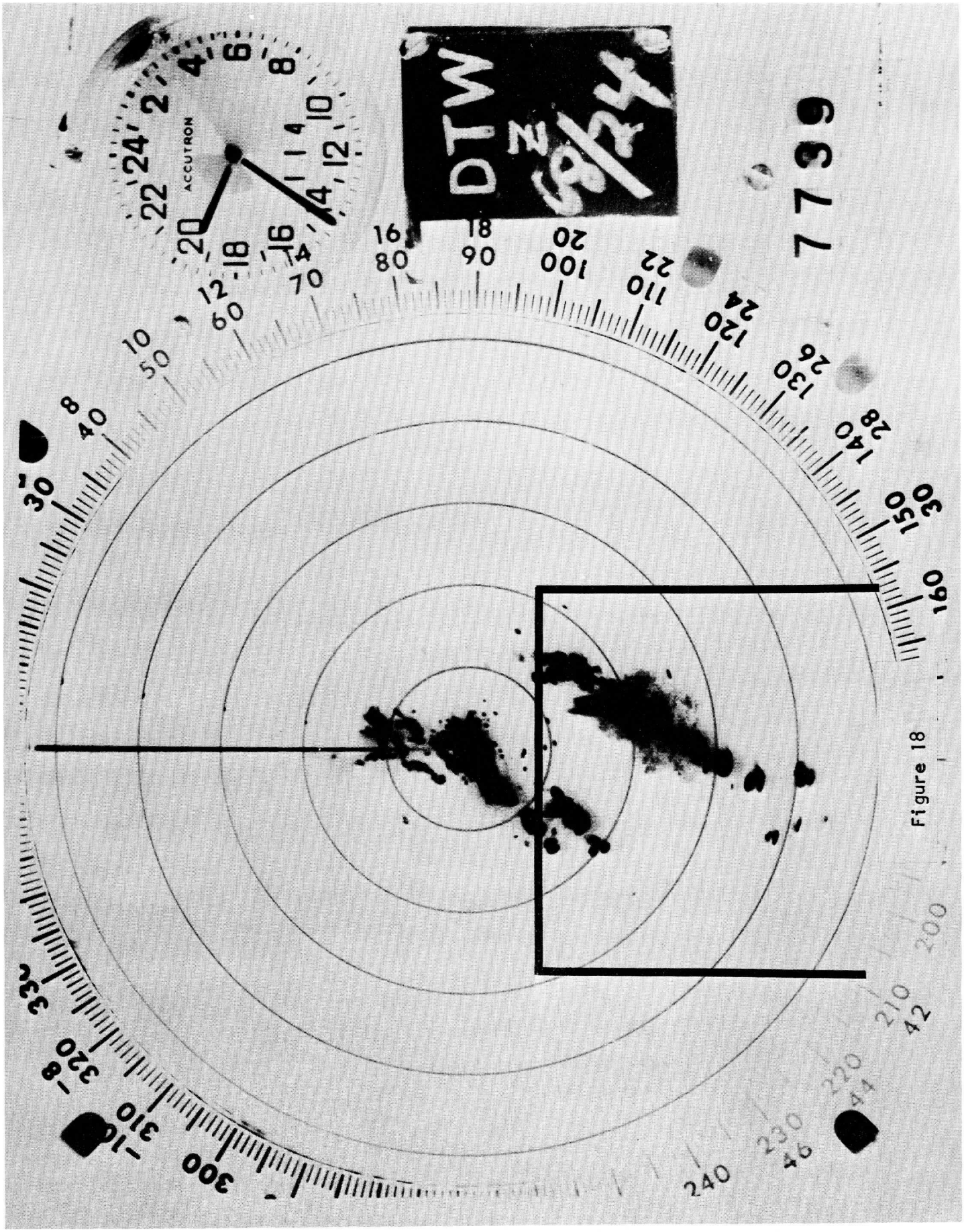

Figure 18

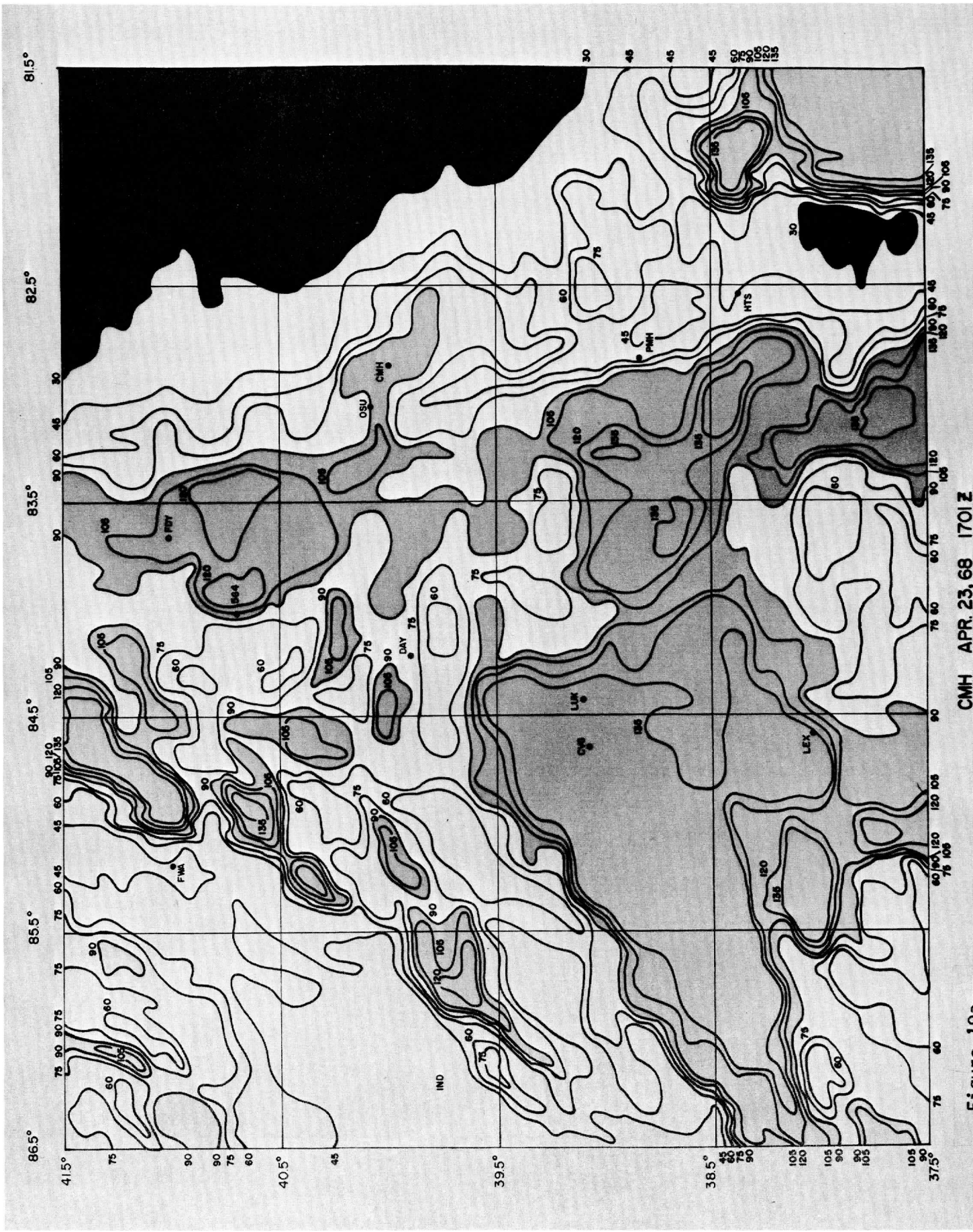
86.5°
85.5°
84.5°
83.5°
82.5°
81.5°
41.5°
40.5°
39.5°
38.5°
37.5°
FWA
FDY
OSU
CMH
PKH
HTS
DAY
IND
LUK
CVG
LEX
CMH APR. 23, 68 1701 Z


86.5°
85.5°
84.5°
83.5°
82.5°
81.5°
41.5°
40.5°
39.5°
38.5°
37.5°
FWA
IND
MIE
FOY
MFD
ZZV
OBU
CMH
PKH
HTS
CVG
LUK
LEX
CMH APR. 23, 68 1946 Z

Figure 19b

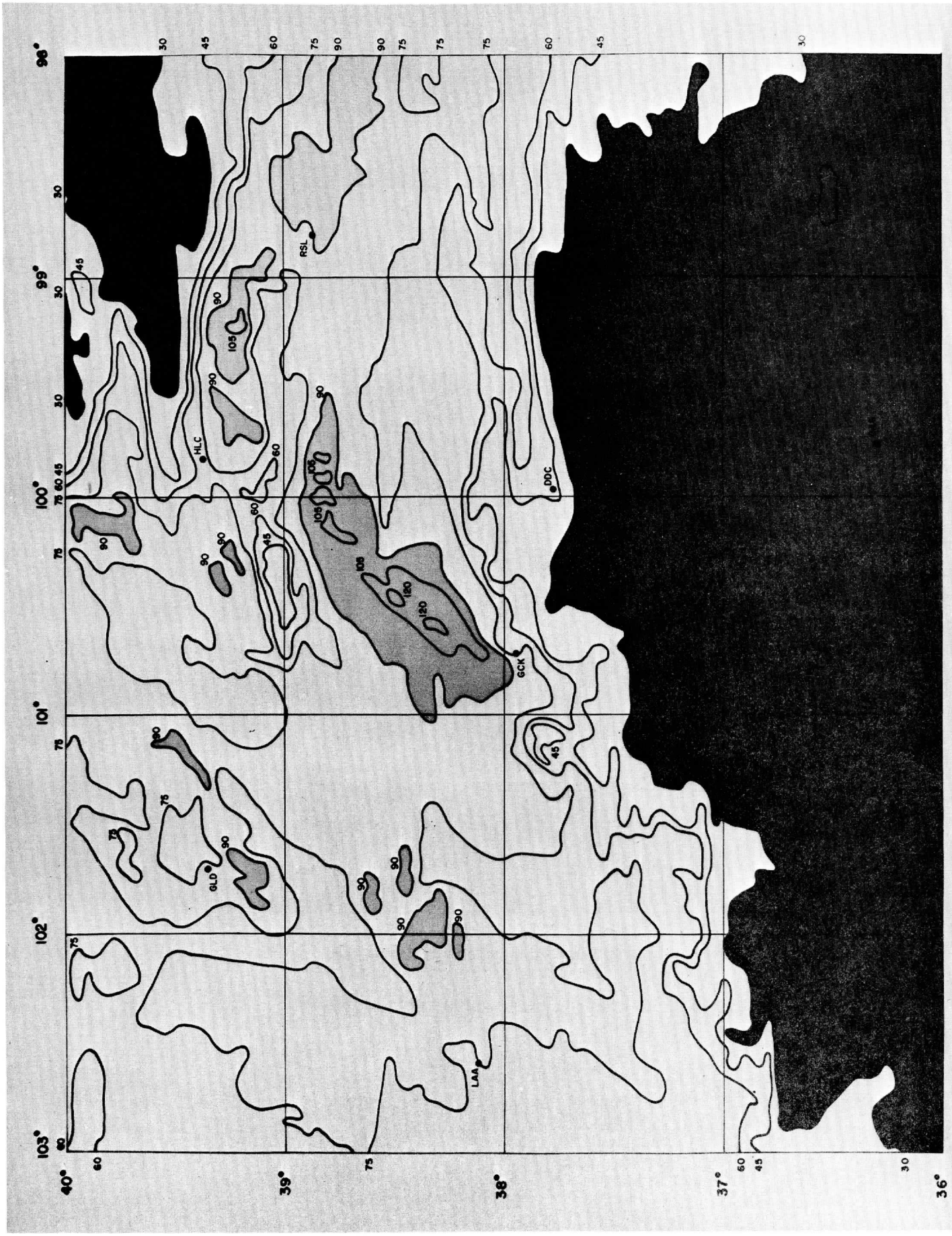
HLC
RSL
DDC
GCK
GLD
LAA
DDC APR. 4, 69 1428 Z

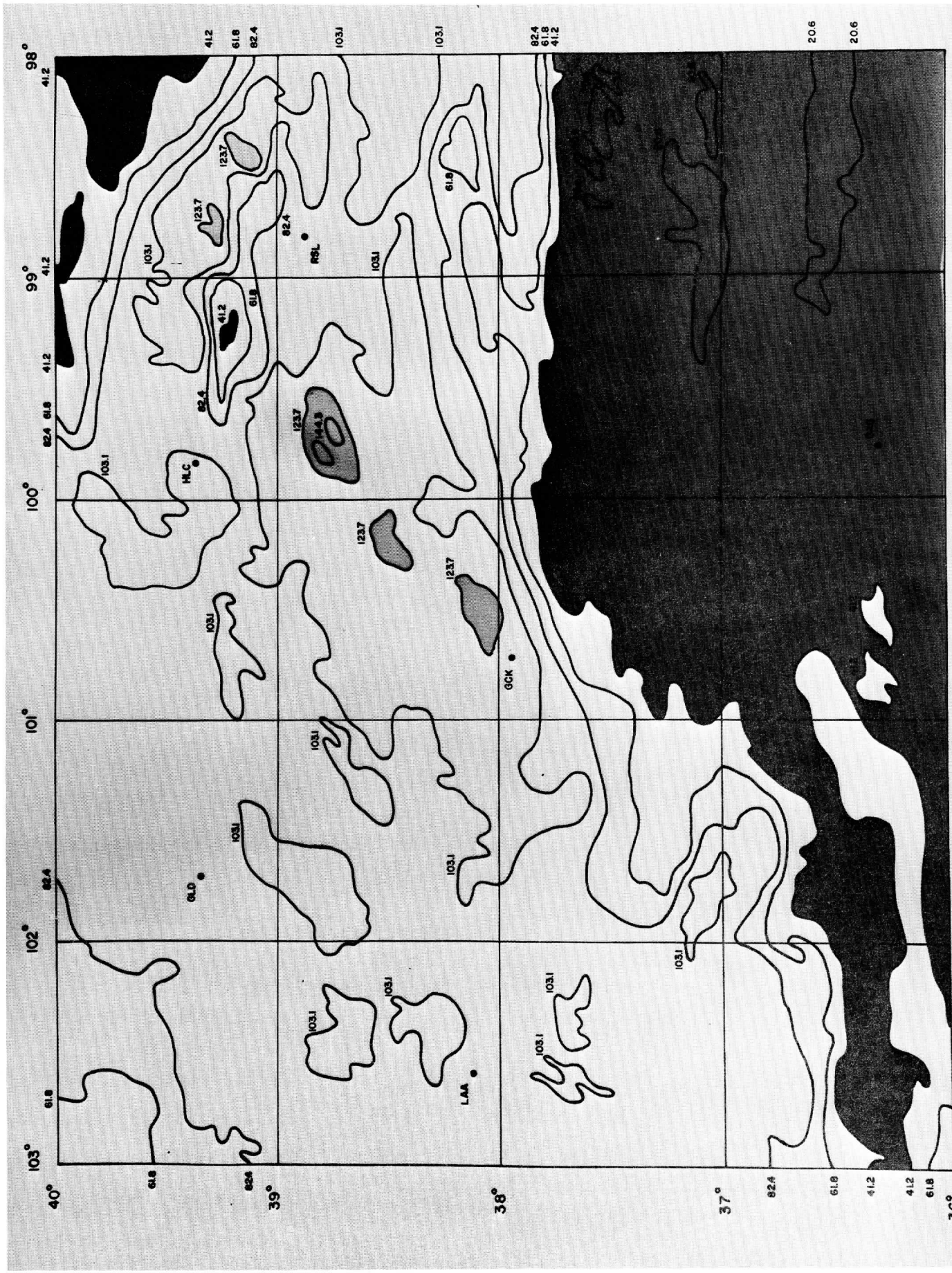

Figure 20b

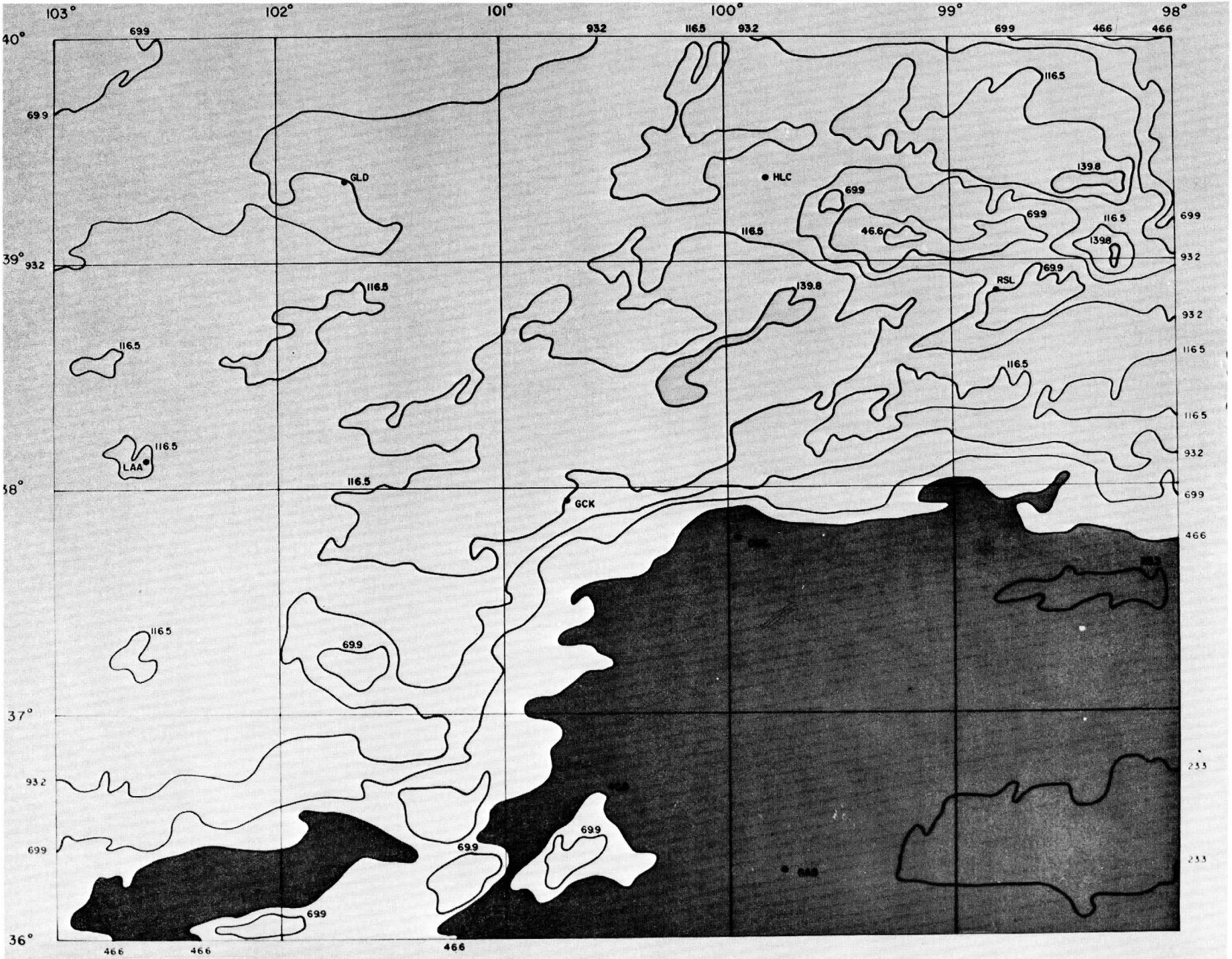

DDC APR 4 69 1556 Z

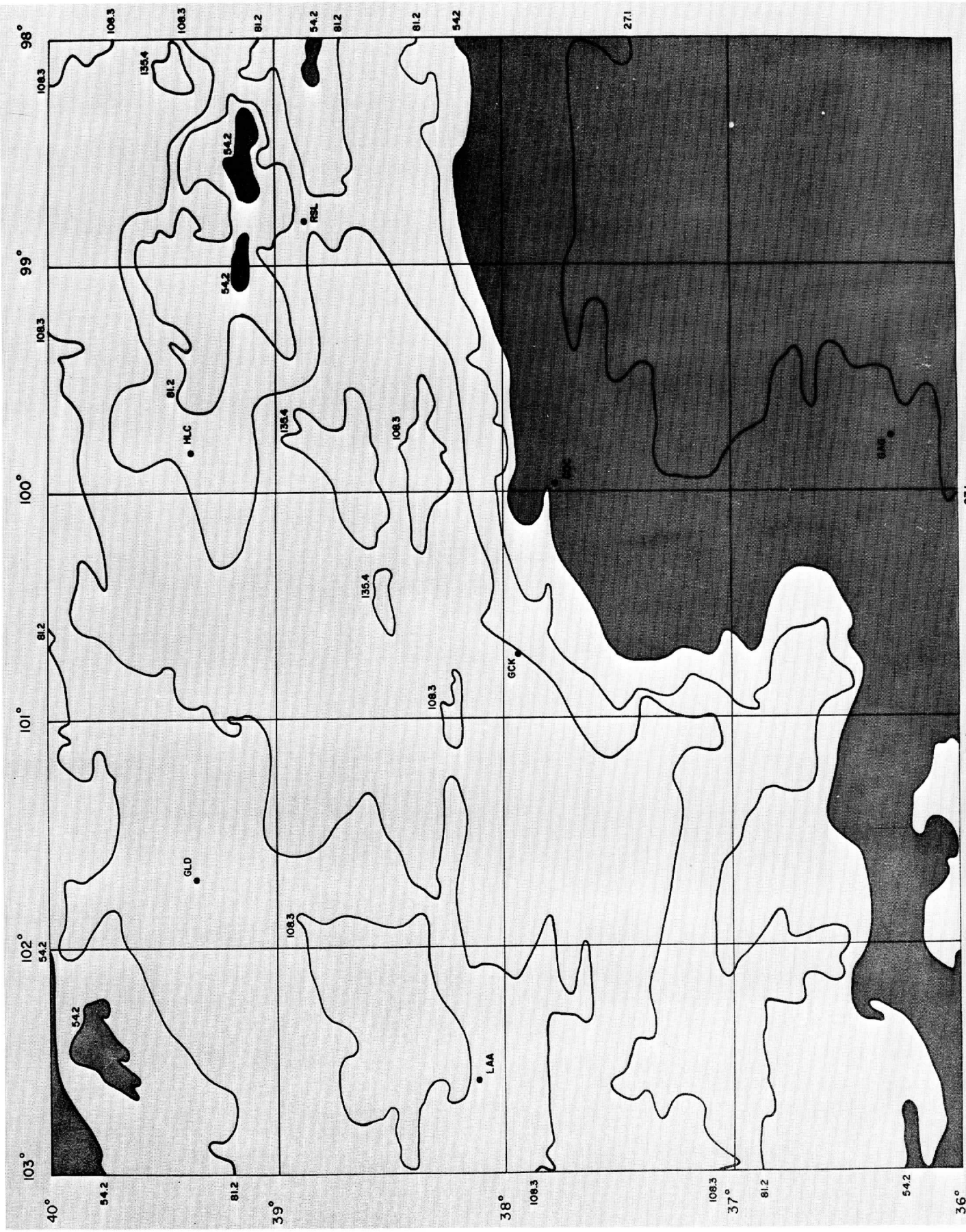
103°
102°
101°
100°
99°
98°
40°
39°
38°
37°
36°
GLD
HLC
RSL
LAA
GCK
DDC APR. 4, 69 1648 Z

Figure 20d

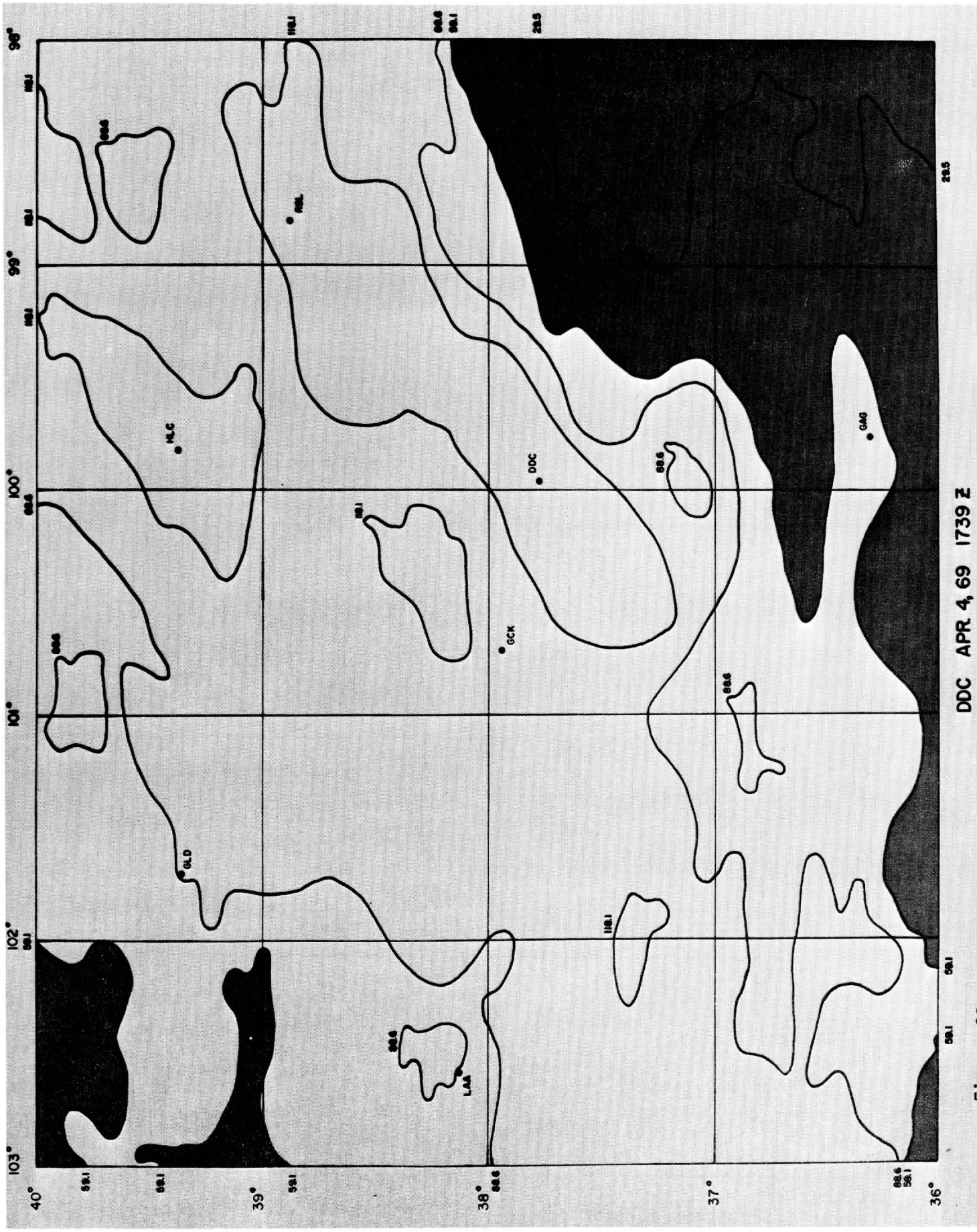
DDC APR 4, 69 1739 Z
GLD
HLC
GCK
DDC
GAG
LAA
103°
102°
101°
100°
99°
98°
40°
39°
38°
37°
36°

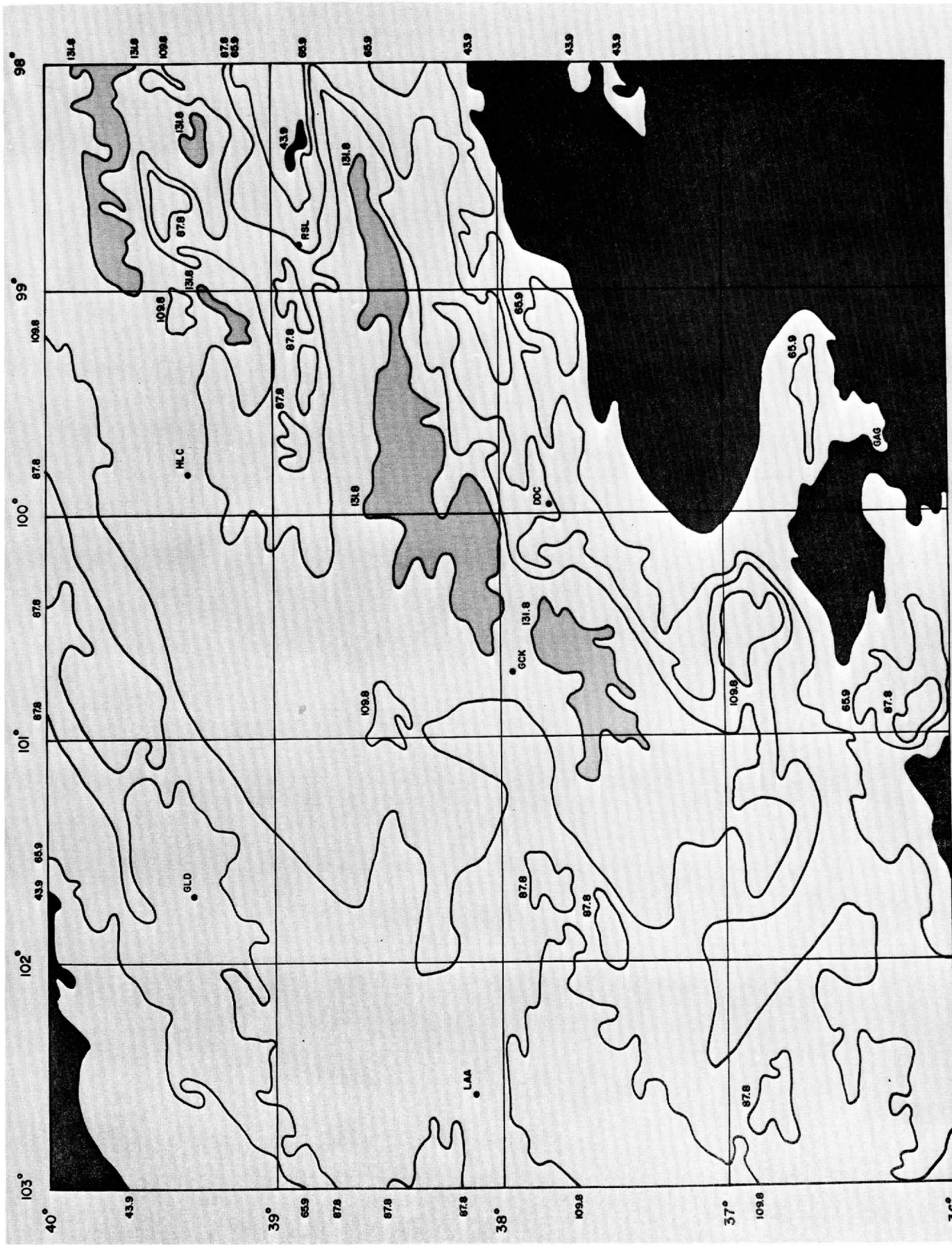

Figure 20f

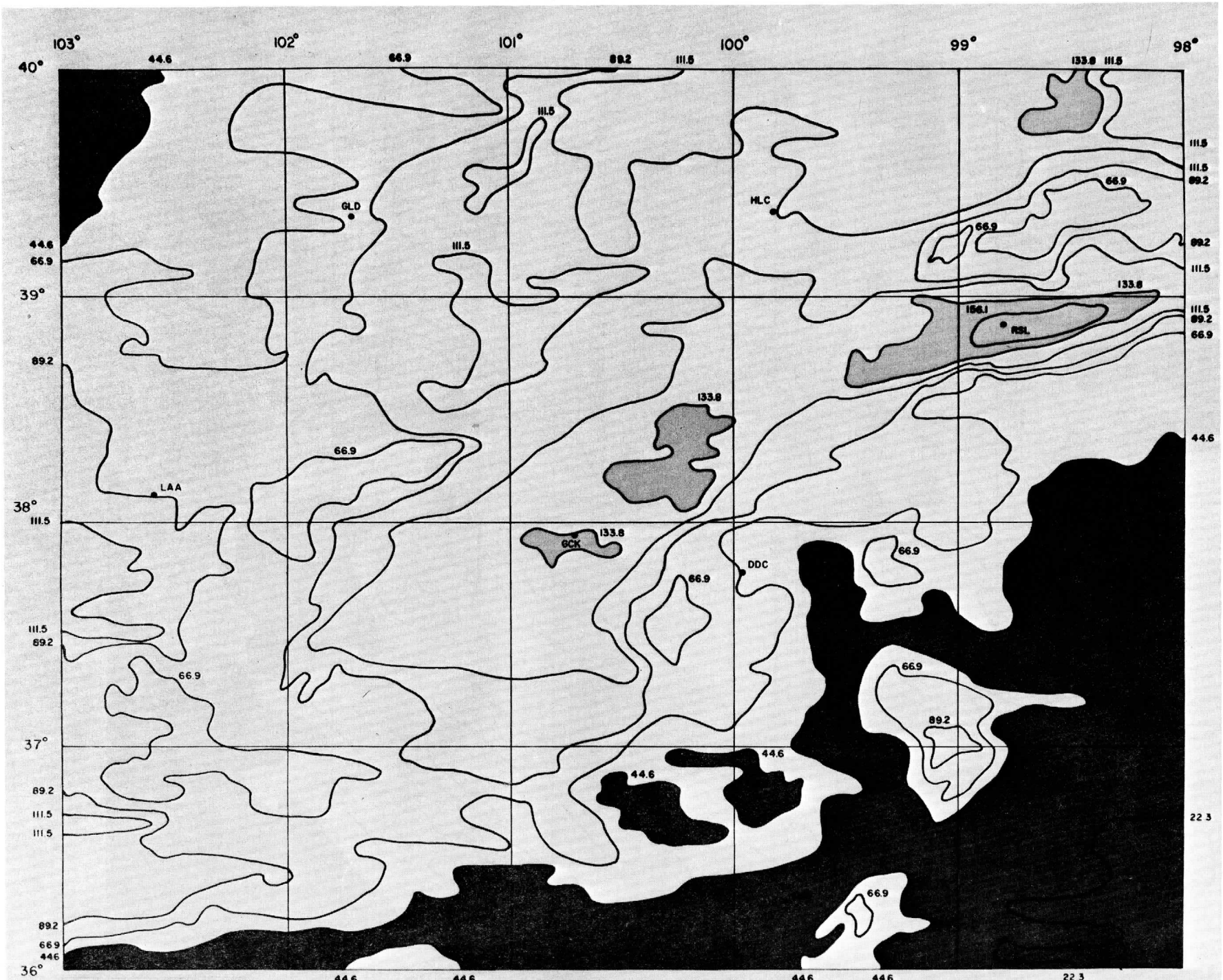

Figure 20a

DDC APR. 4, 69 1855 Z

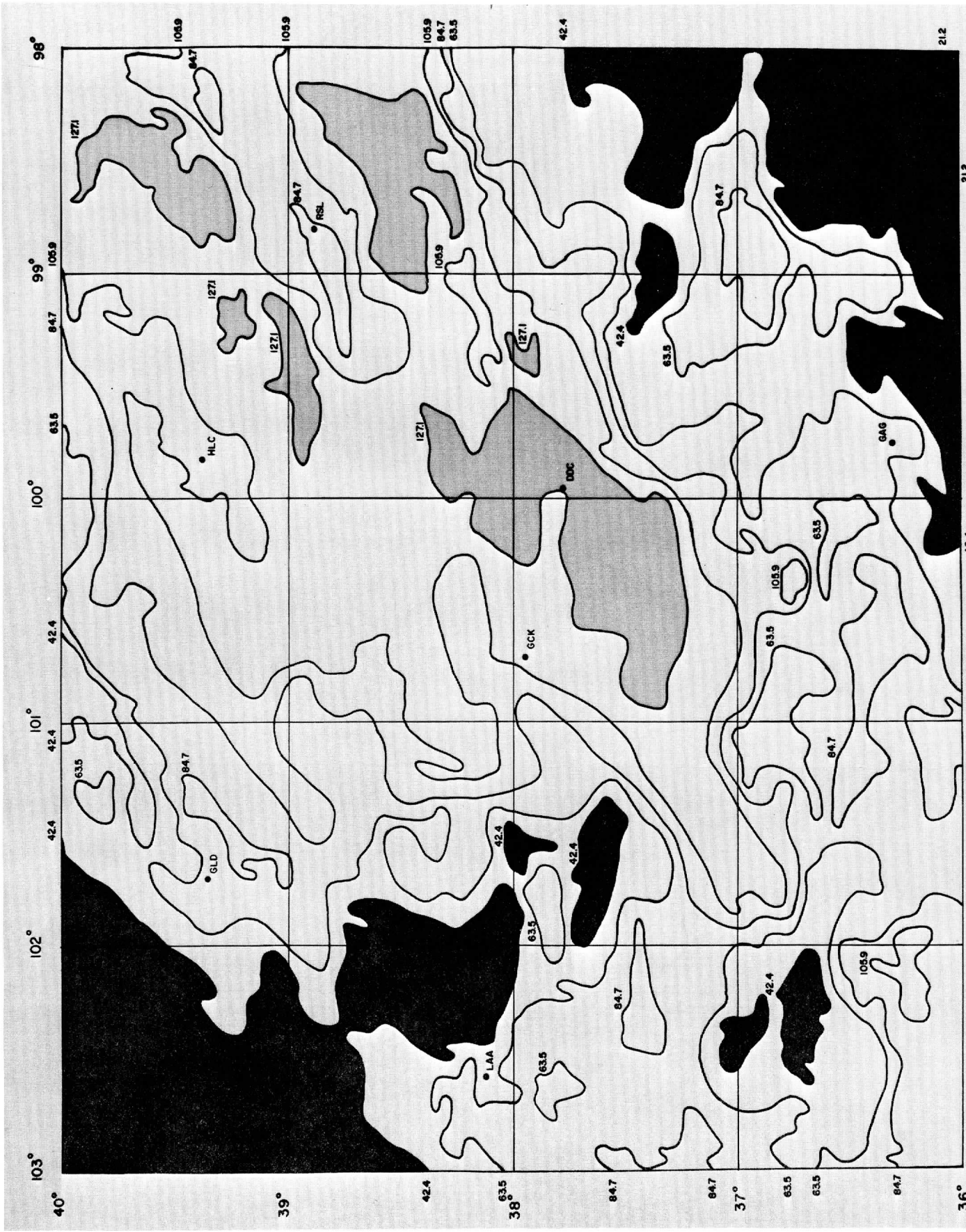

Figure 20h

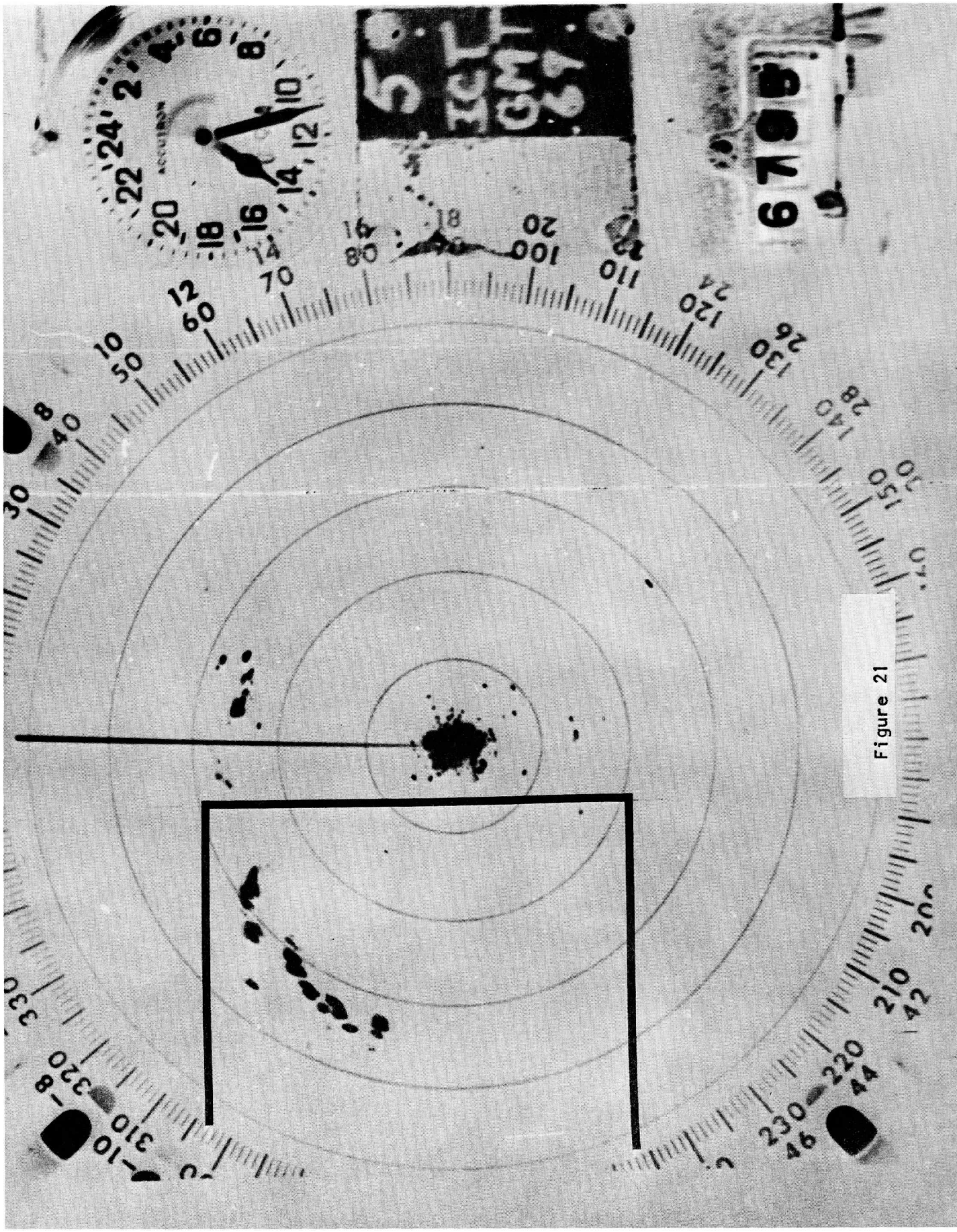

Figure 21

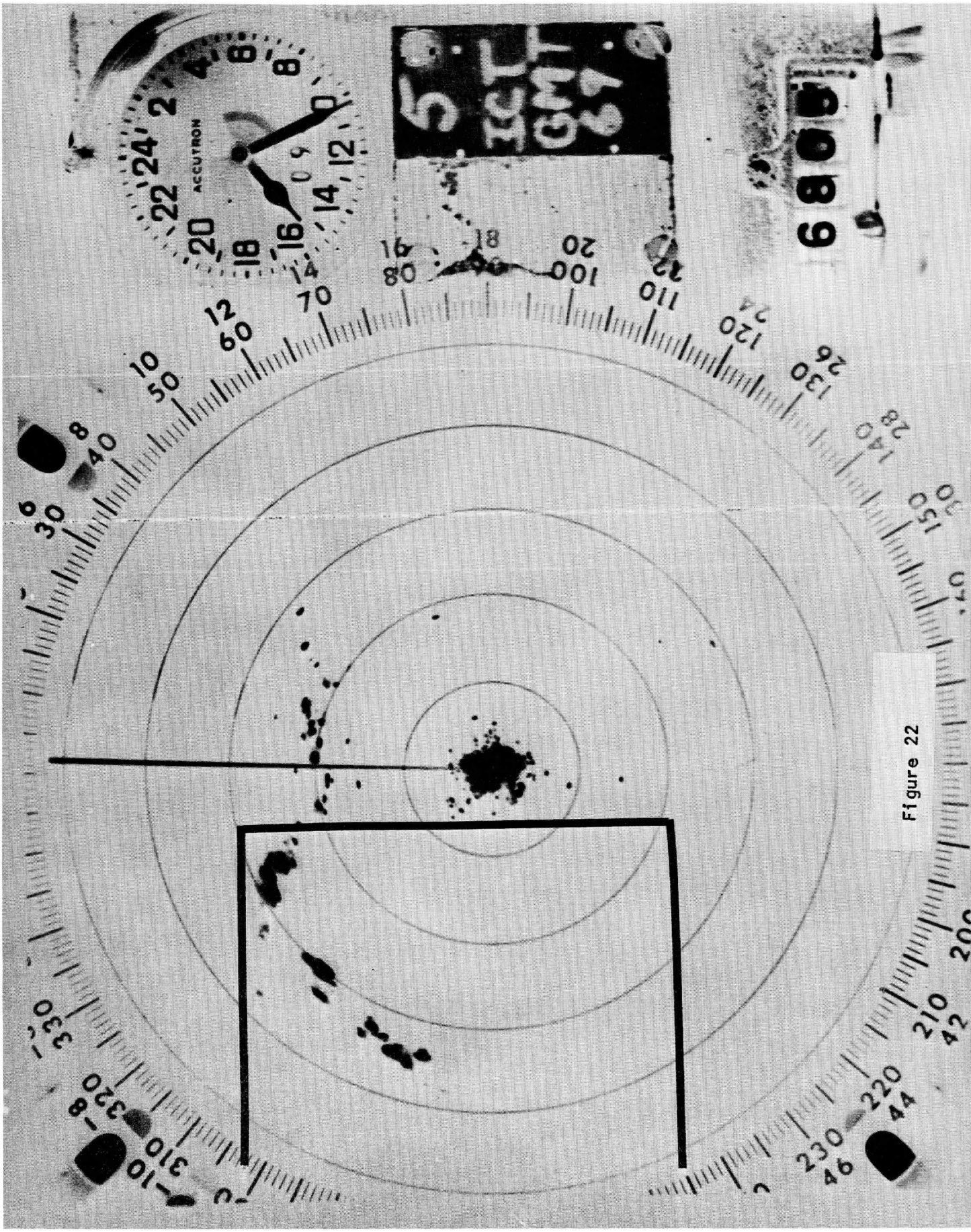

Figure 22

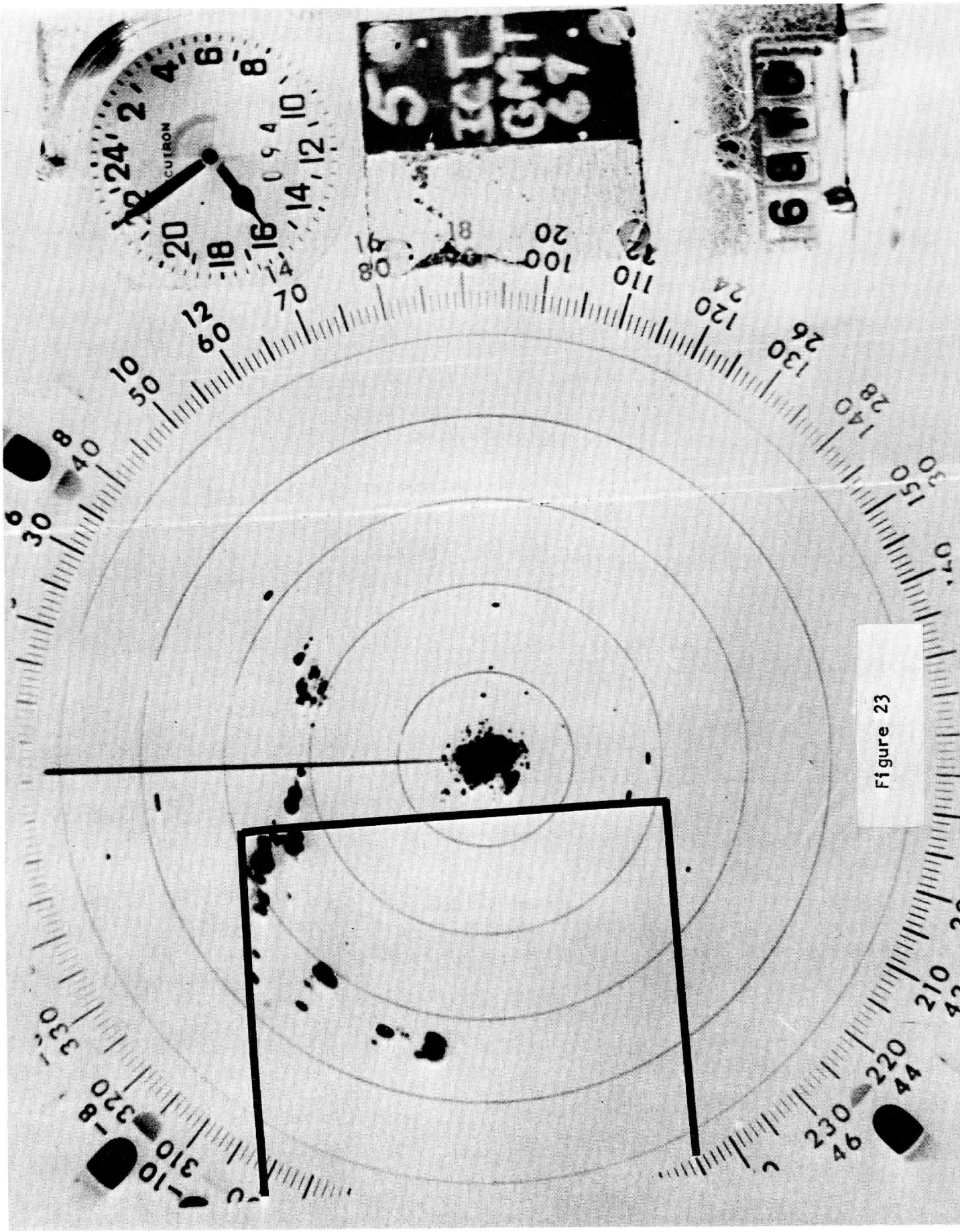

Figure 23

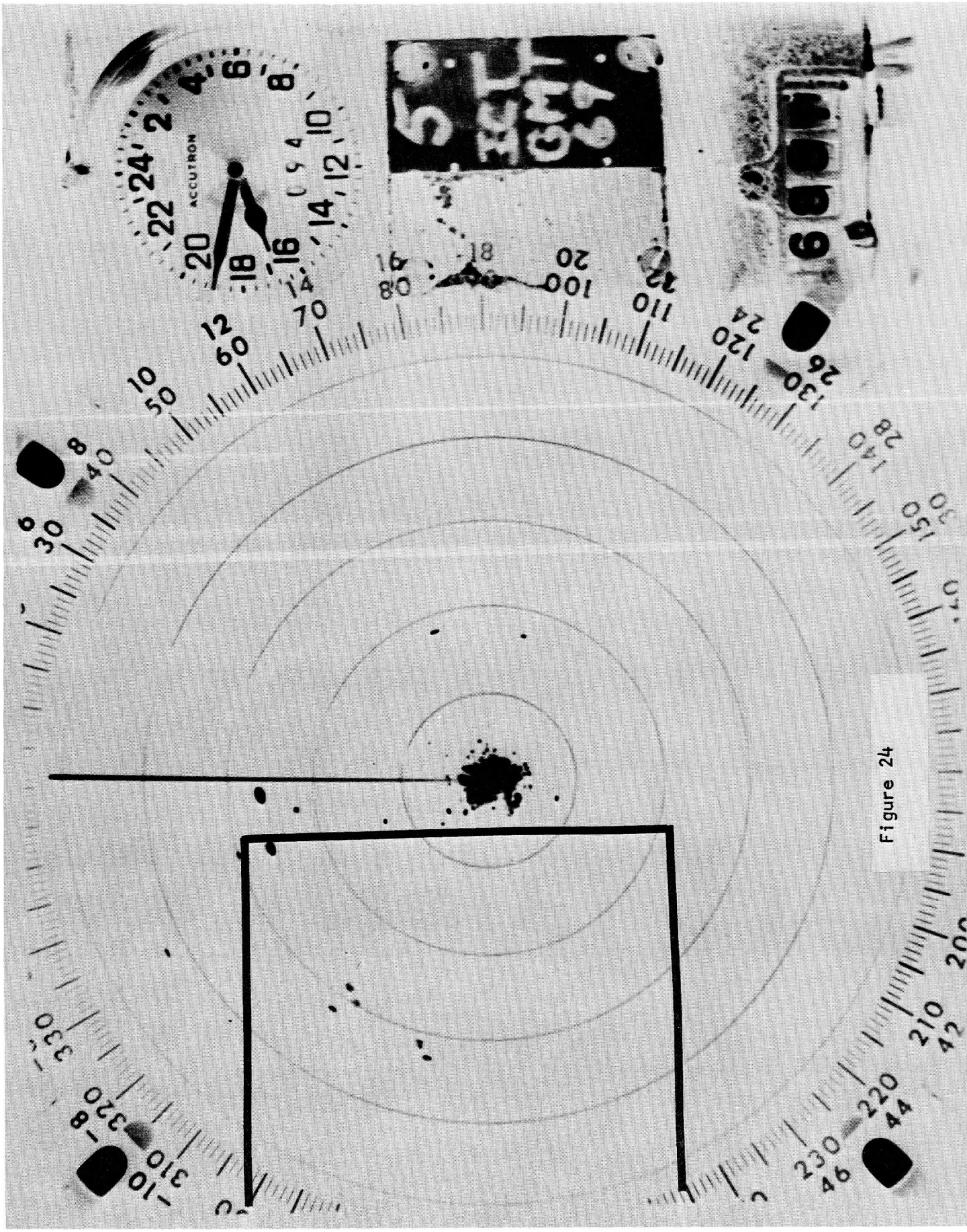

Figure 24

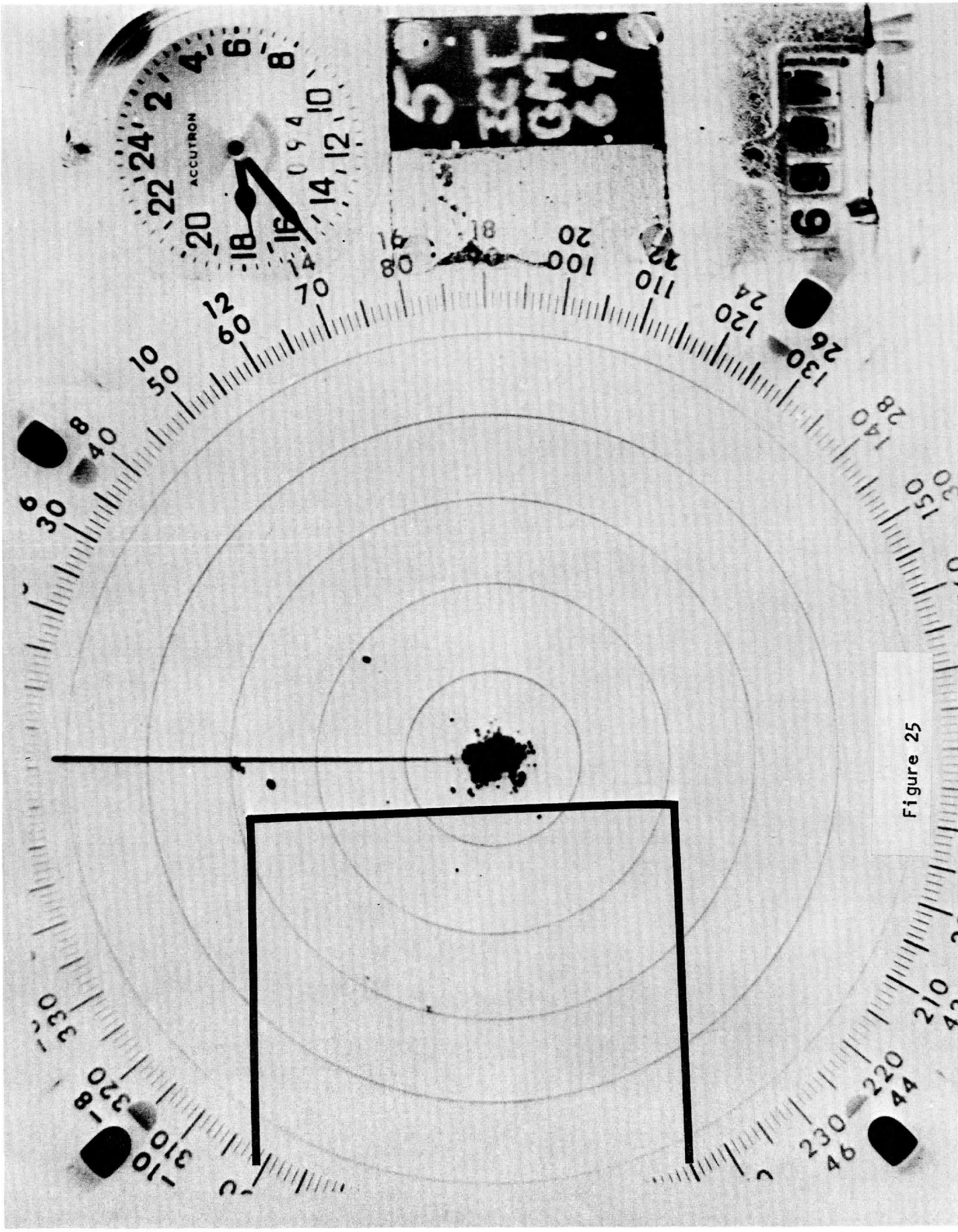

Figure 25

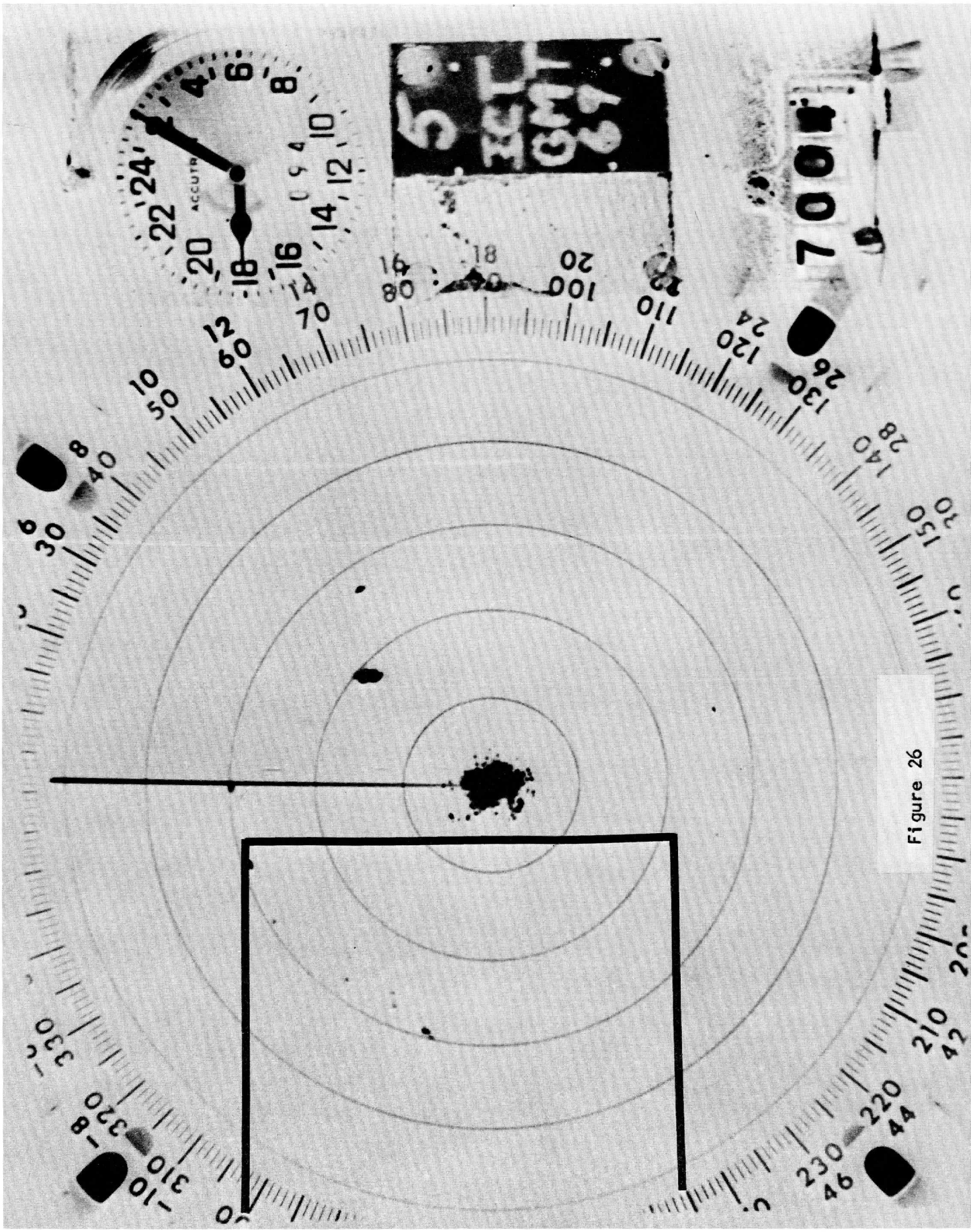

Figure 26

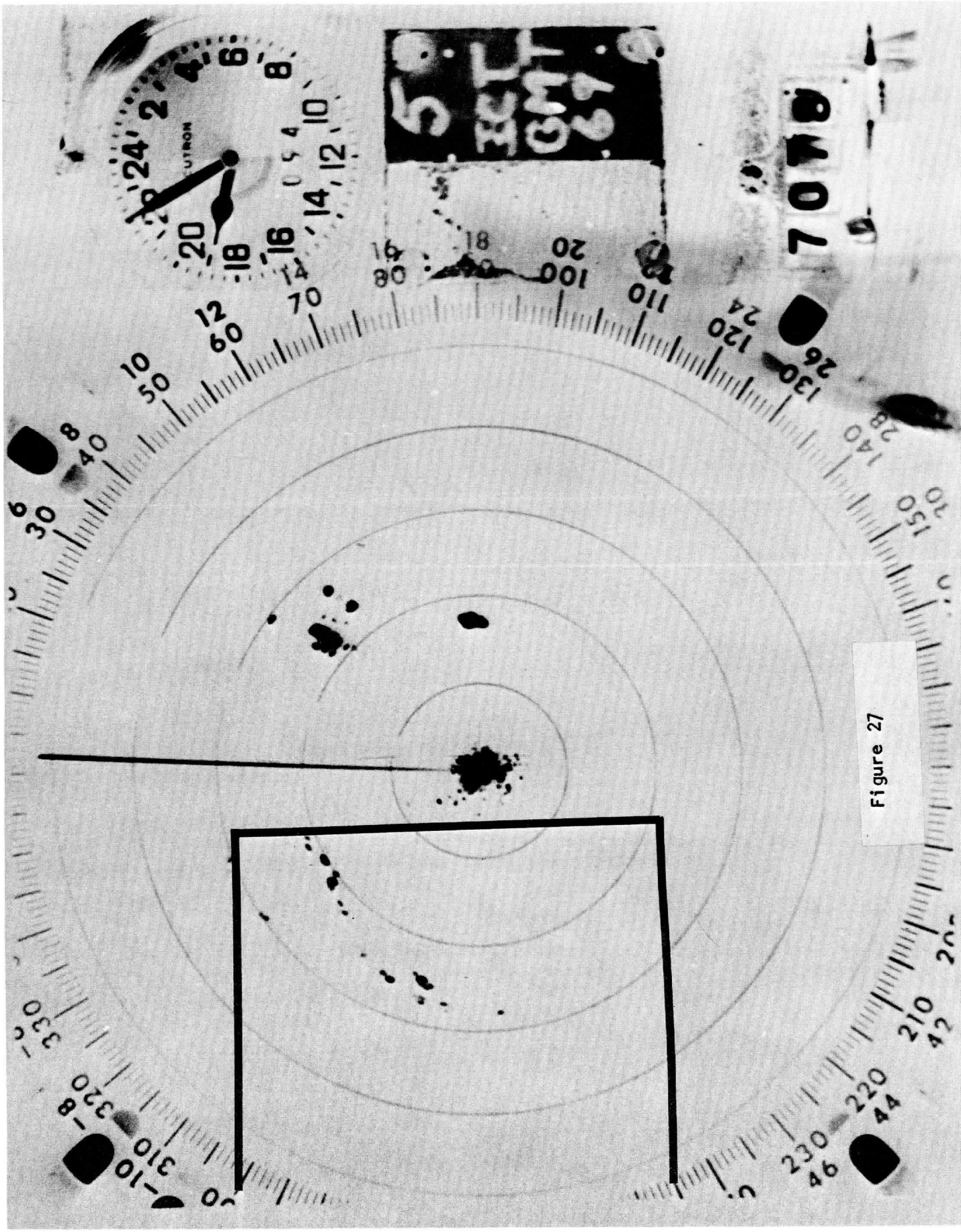

Figure 27

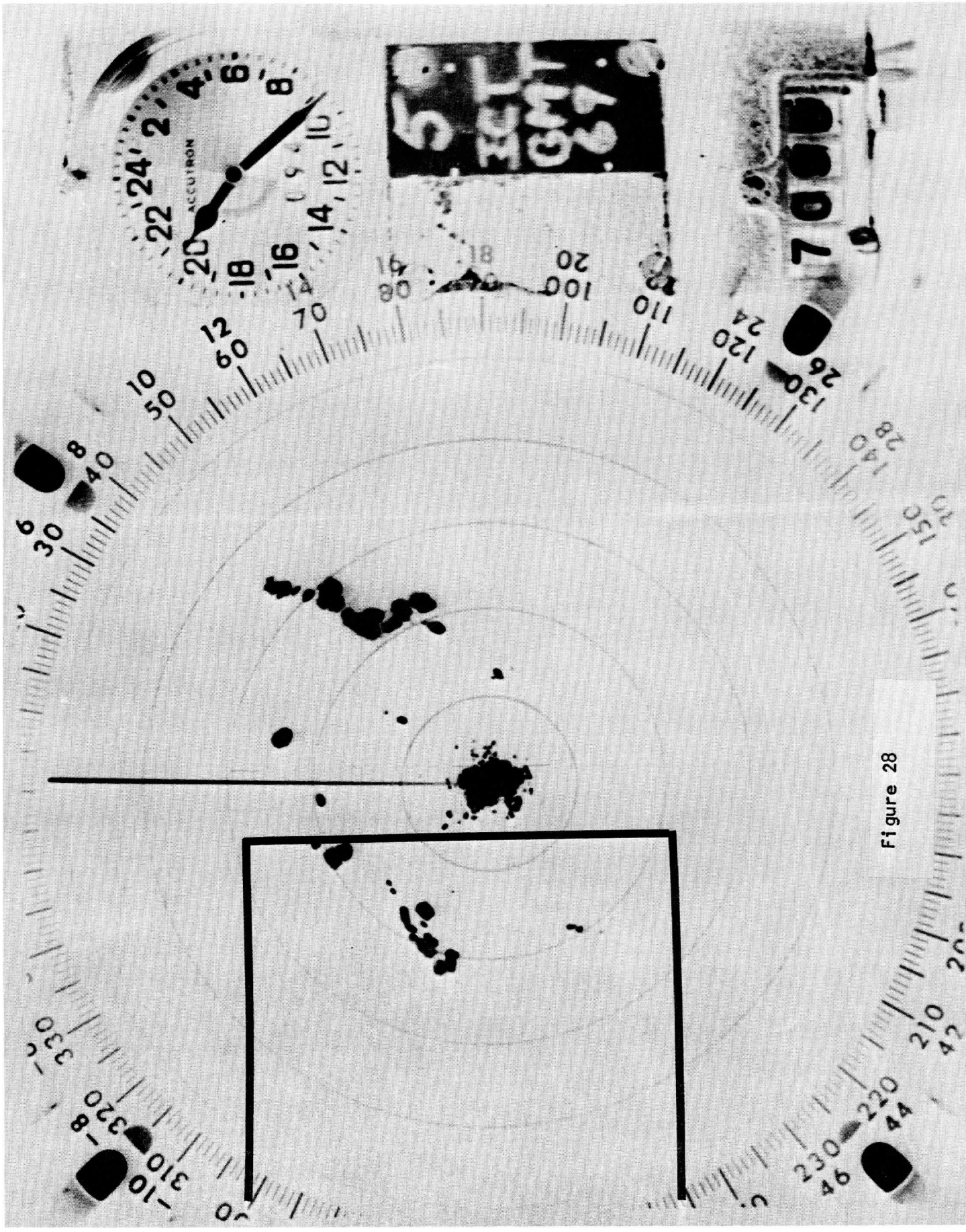

Figure 28

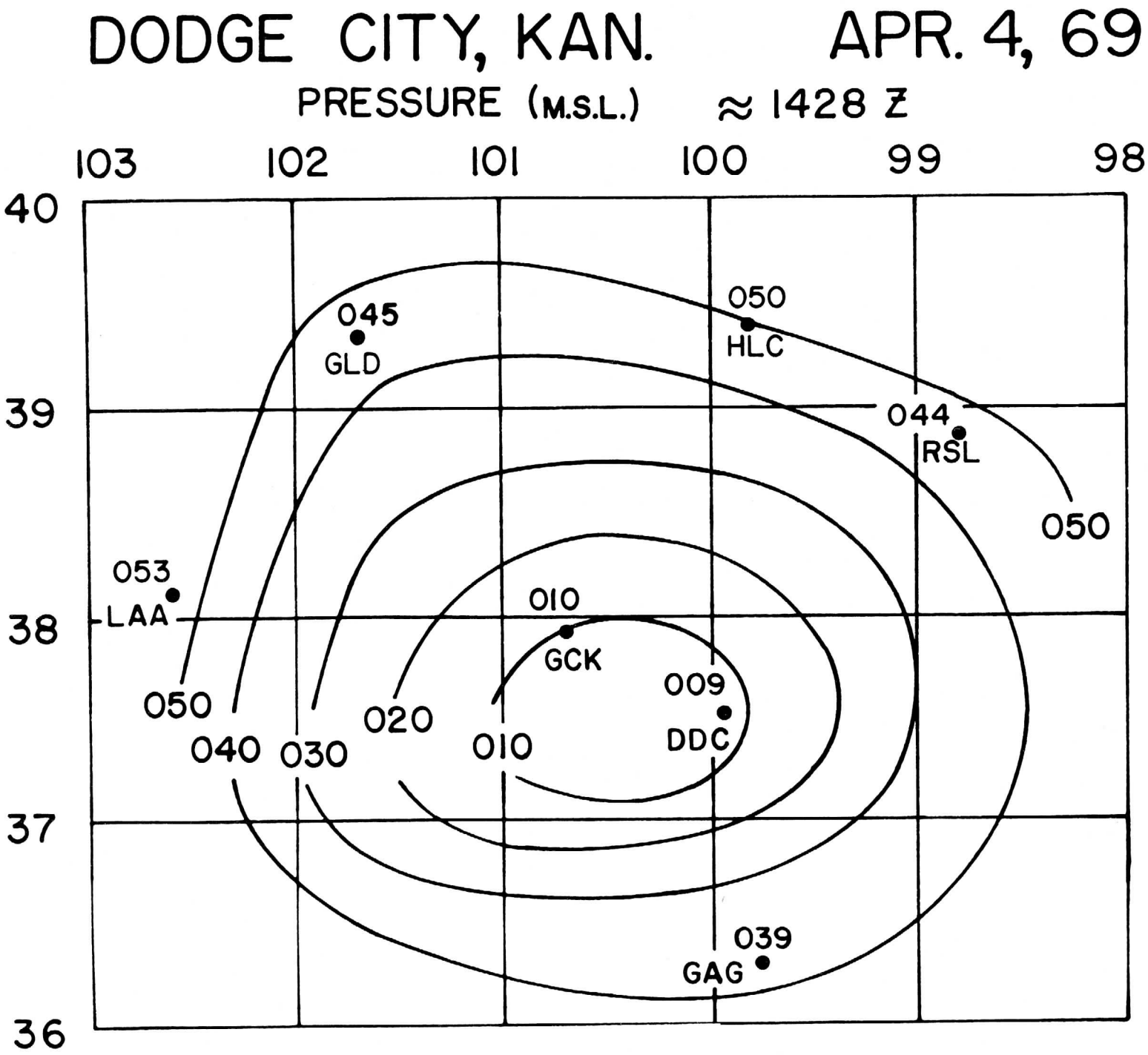
DODGE CITY, KAN. APR. 4, 69
PRESSURE (M.S.L.) ≈ 1428 Z
103
102
101
100
99
98
40
39
38
37
36
045
GLD
050
HLC
044
RSL
050
053
LAA
010
GCK
009
DDC
050
040
030
020
010
039
GAG

Figure 29

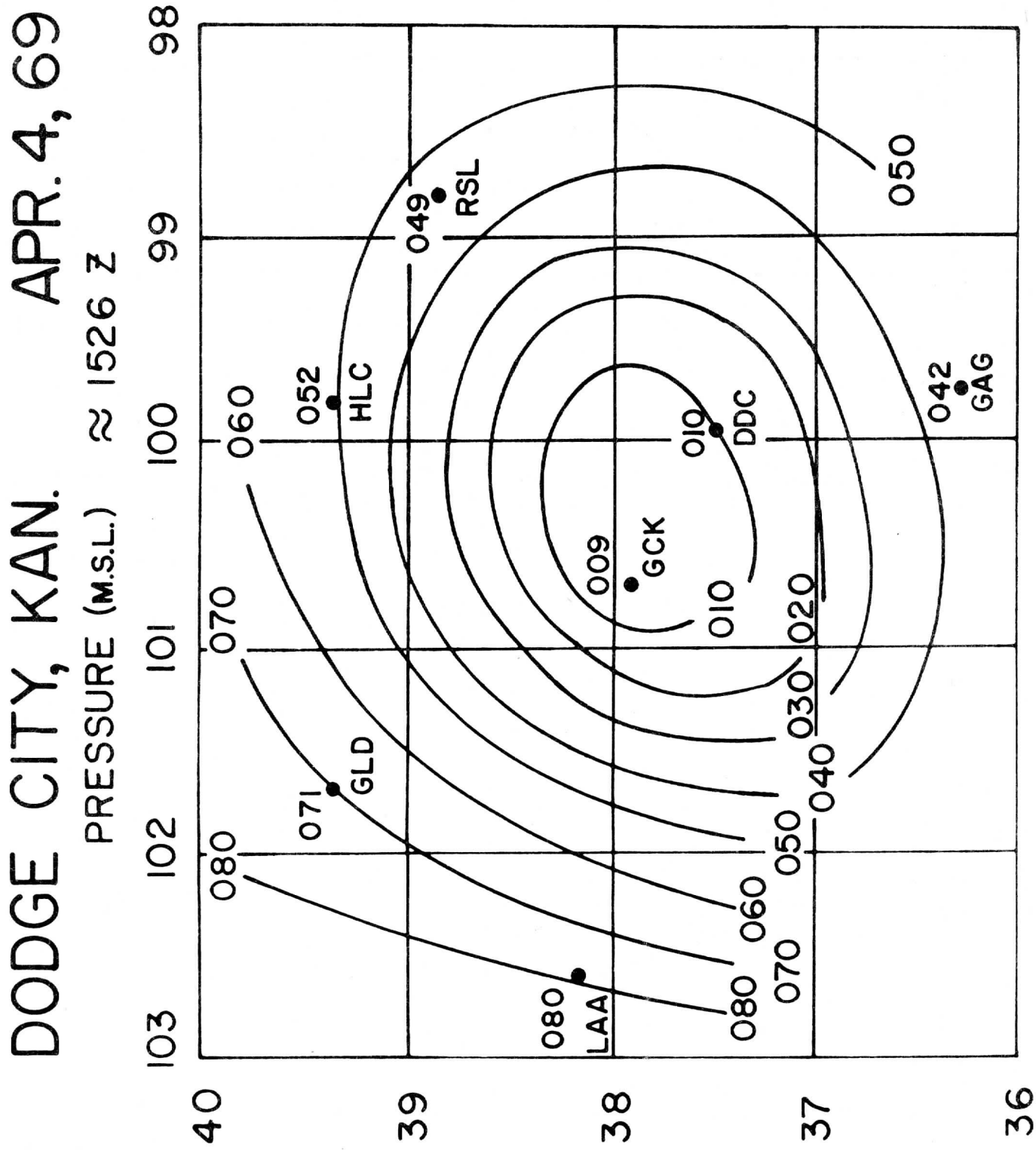
DODGE CITY, KAN. APR. 4, 69
PRESSURE (M.S.L.) ≈ 1526 Z
103
102
101
100
99
98
40
39
38
37
36
080
071
GLD
080
LAA
060
052
HLC
049
RSL
050
070
060
050
040
030
020
010
009
GCK
010
DDC
042
GAG

Figure 30

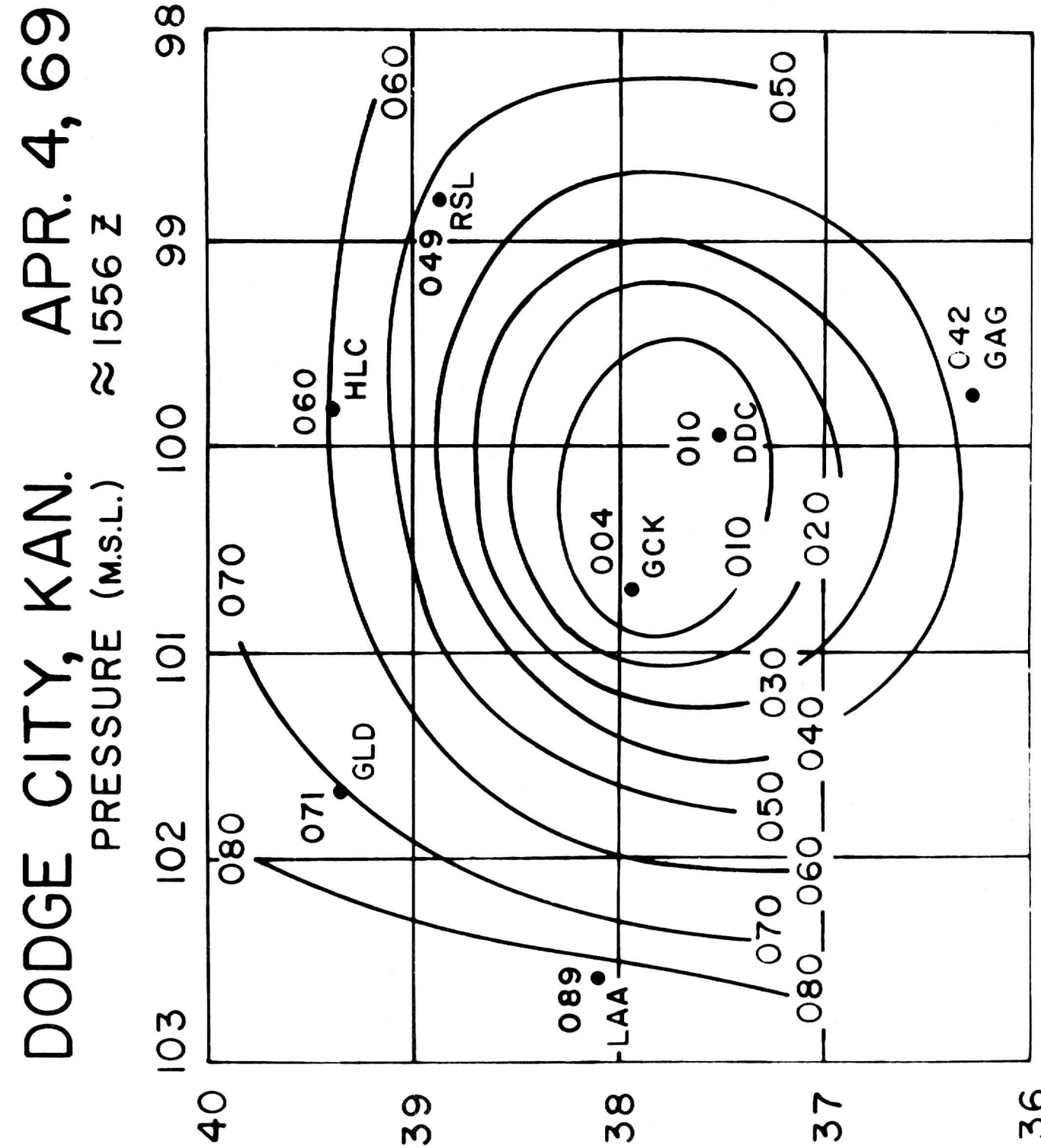
DODGE CITY, KAN. APR. 4, 69
PRESSURE (M.S.L.) ≈1556 Z
103
102
101
100
99
98
40
39
38
37
36
080
071
GLD
070
060
HLC
060
049
RSL
050
042
GAG
089
LAA
080
070
060
050
040
030
020
010
004
GCK
010
DDC

Figure 31

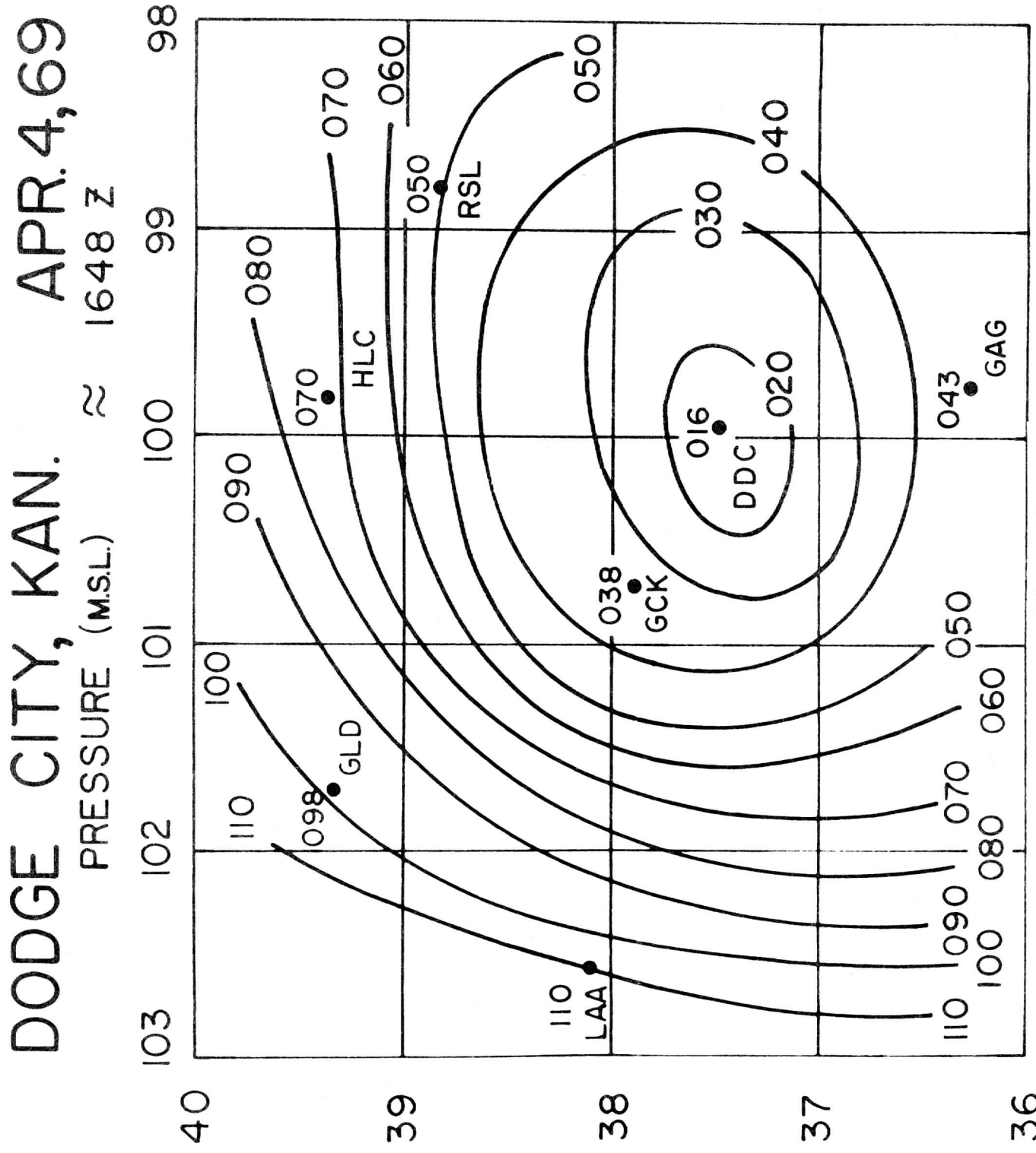
DODGE CITY, KAN. APR. 4, 69
PRESSURE (M.S.L.) ≈ 1648 Z
103
102
101
100
99
98
40
39
38
37
36
110
100
090
080
070
060
050
040
030
020
016
038
043
098
GLD
LAA
GCK
DDC
HLC
RSL
GAG

Figure 32

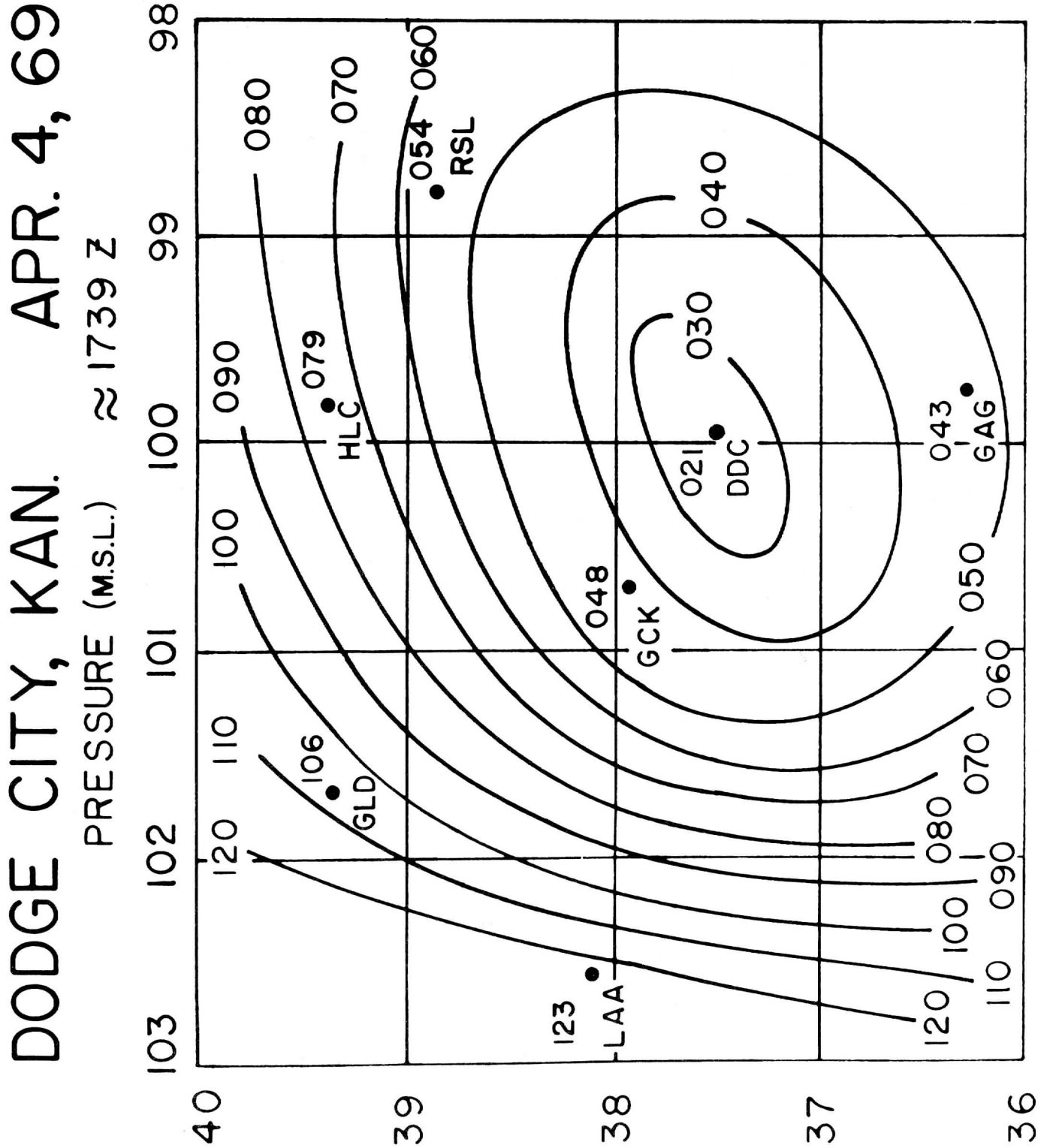
DODGE CITY, KAN. APR. 4, 69
PRESSURE (M.S.L.) ≈1739 Z
103
102
101
100
99
98
40
39
38
37
36
080
070
060
054
RSL
090
079
HLC
100
110
106
GLD
120
123
LAA
040
030
021
DDC
048
GCK
043
GAG
050
060
070
080
090
100
110
120

Figure 33

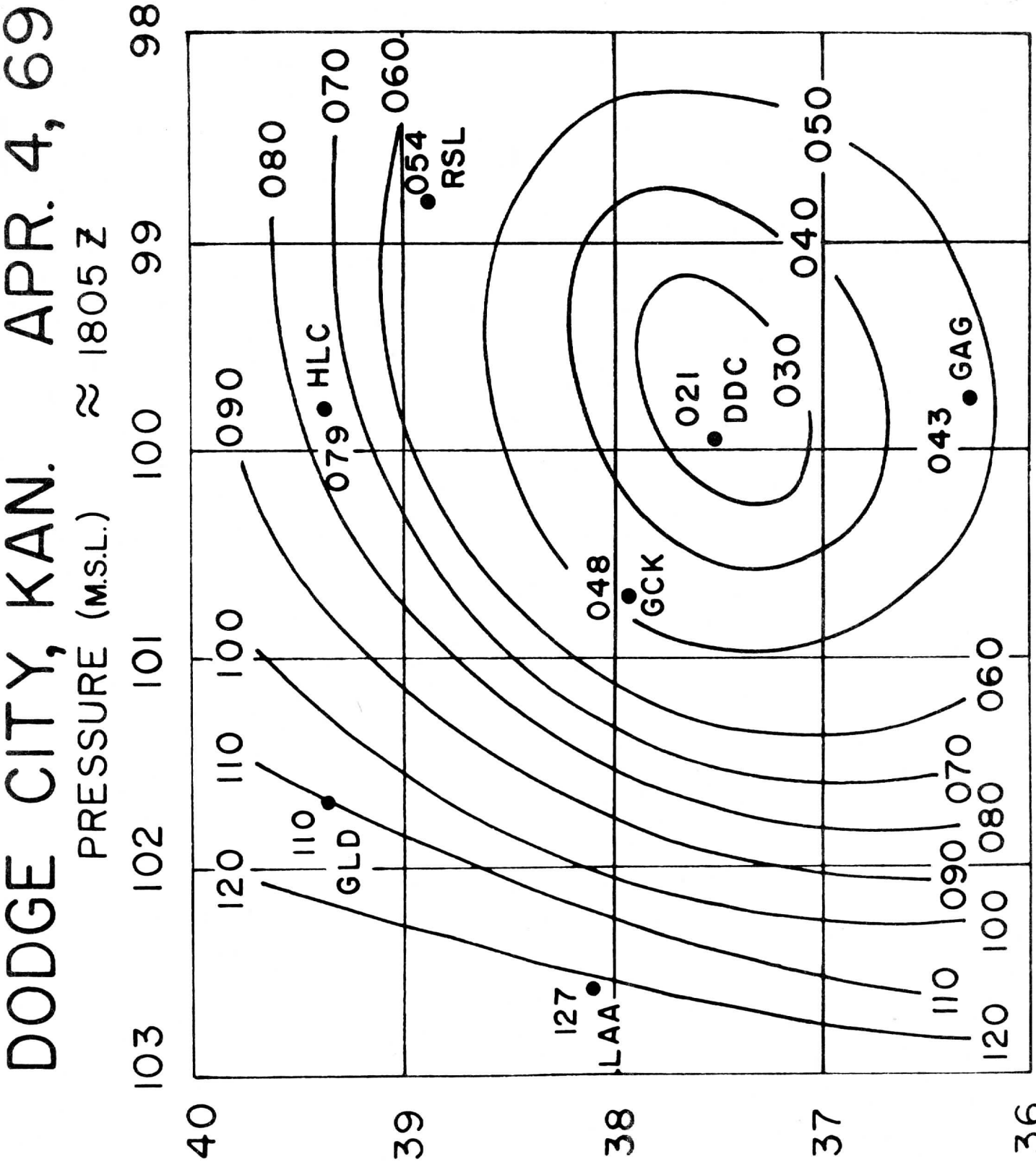
DODGE CITY, KAN. APR. 4, 69
PRESSURE (M.S.L.) ≈ 1805 Z
103
102
101
100
99
98
40
39
38
37
36
080
070
060
090
100
110
120
110
GLD
127
LAA
HLC
079
054
RSL
048
GCK
021
DDC
030
040
050
043
GAG
060
070
080
090
100
110
120

Figure 34

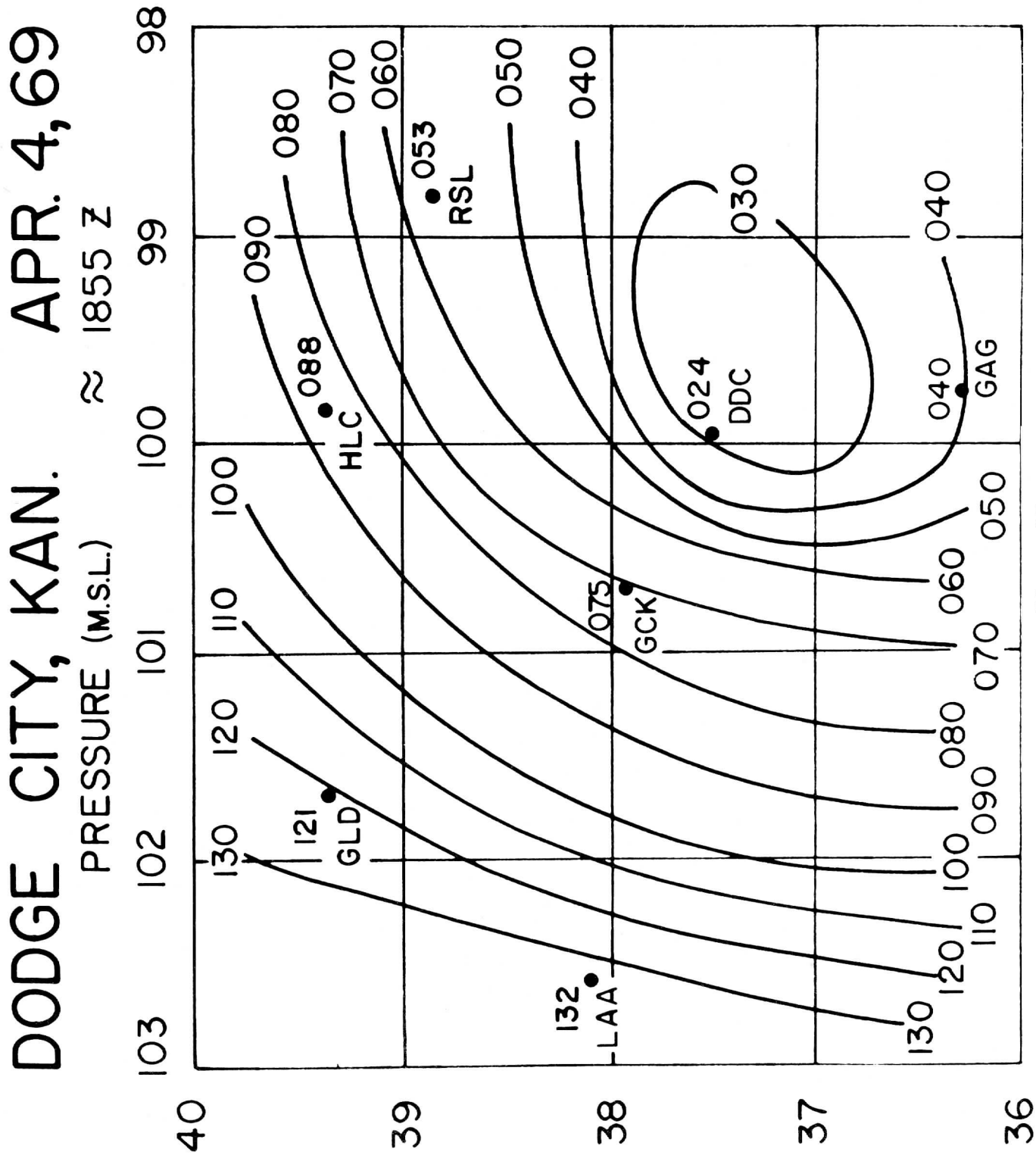
DODGE CITY, KAN. APR. 4, 69
PRESSURE (M.S.L.) ≈ 1855 Z
103
102
101
100
99
98
40
39
38
37
36
090
080
070
060
050
040
030
040
053
RSL
088
HLC
024
DDC
040
GAG
075
GCK
121
GLD
132
LAA
130
120
110
100
090
080
070
060
050
040
130
120
110
100

Figure 35

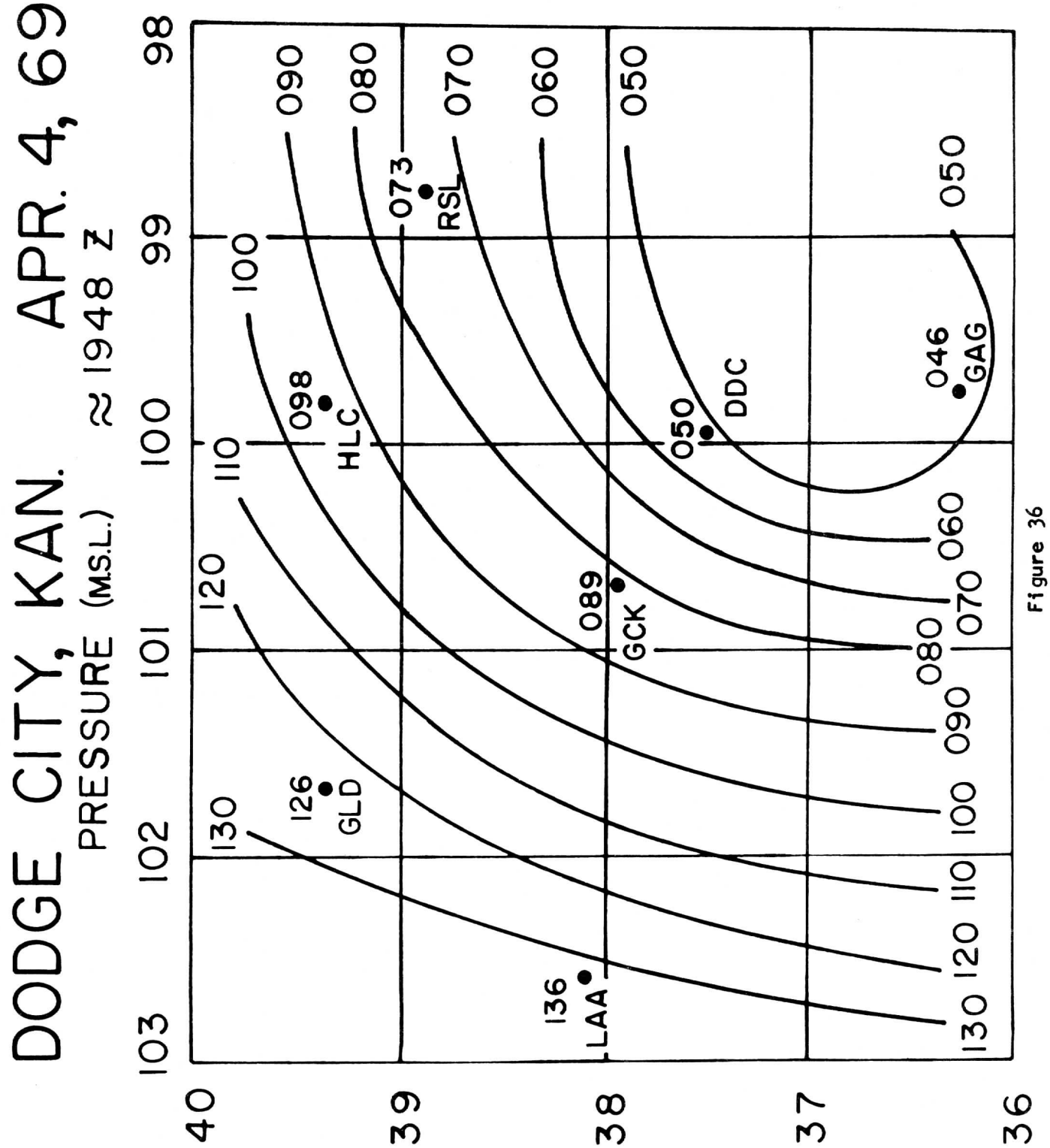
DODGE CITY, KAN. APR. 4, 69
PRESSURE (M.S.L.) ≈ 1948 Z
103
102
101
100
99
98
40
39
38
37
36
090
080
073
RSL
070
060
050
100
110
120
130
098
HLC
126
GLD
136
LAA
089
GCK
050
DDC
046
GAG

Figure 36

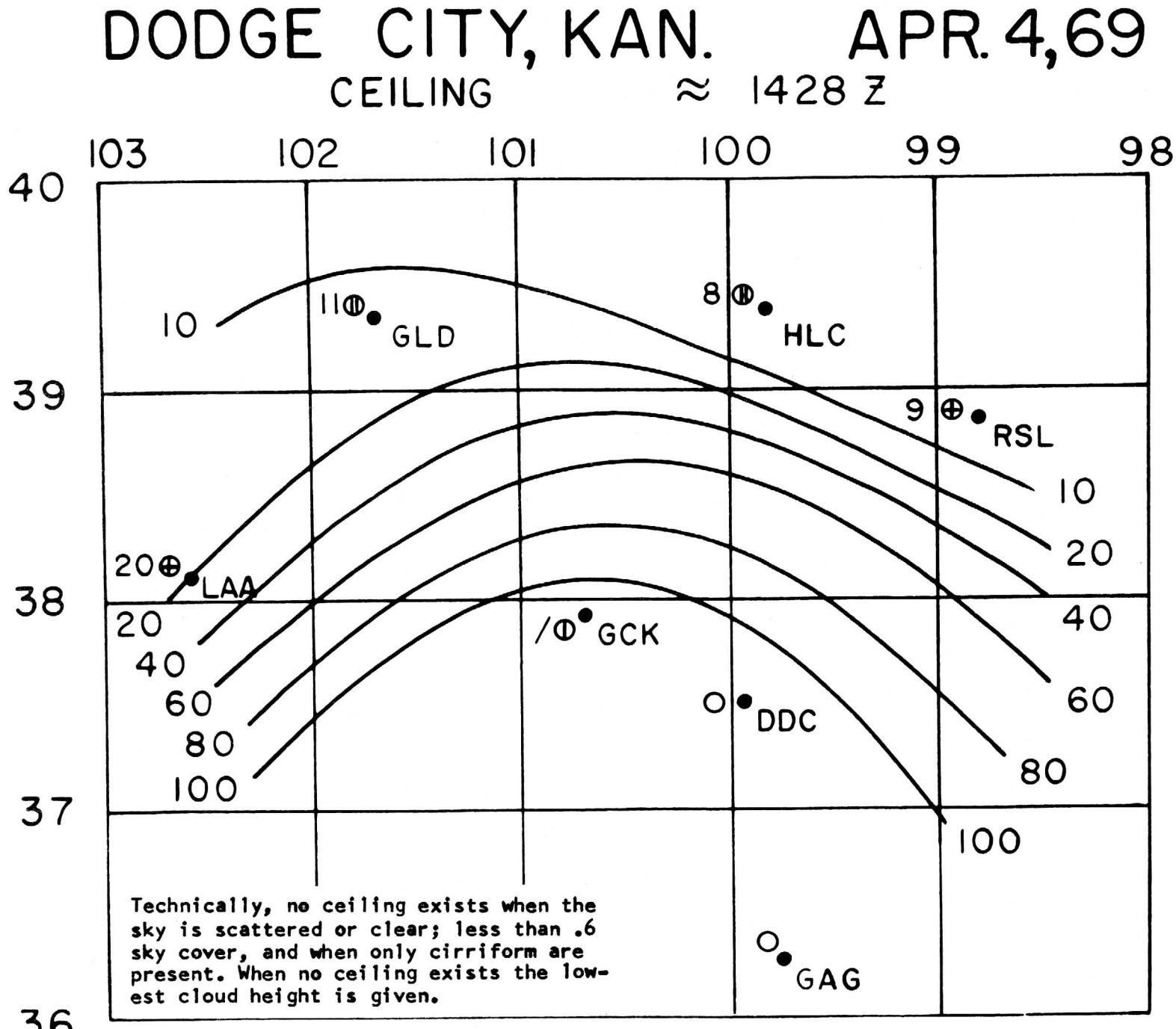
DODGE CITY, KAN. APR. 4,69
CEILING ≈ 1428 Z
103
102
101
100
99
98
40
39
38
37
36
10
11 GLD
8 HLC
9 RSL
10
20
40
60
80
100
20 LAA
20
40
60
80
100
/ GCK
O DDC
O GAG
Technically, no ceiling exists when the sky is scattered or clear; less than .6 sky cover, and when only cirriform are present. When no ceiling exists the lowest cloud height is given.

Figure 37

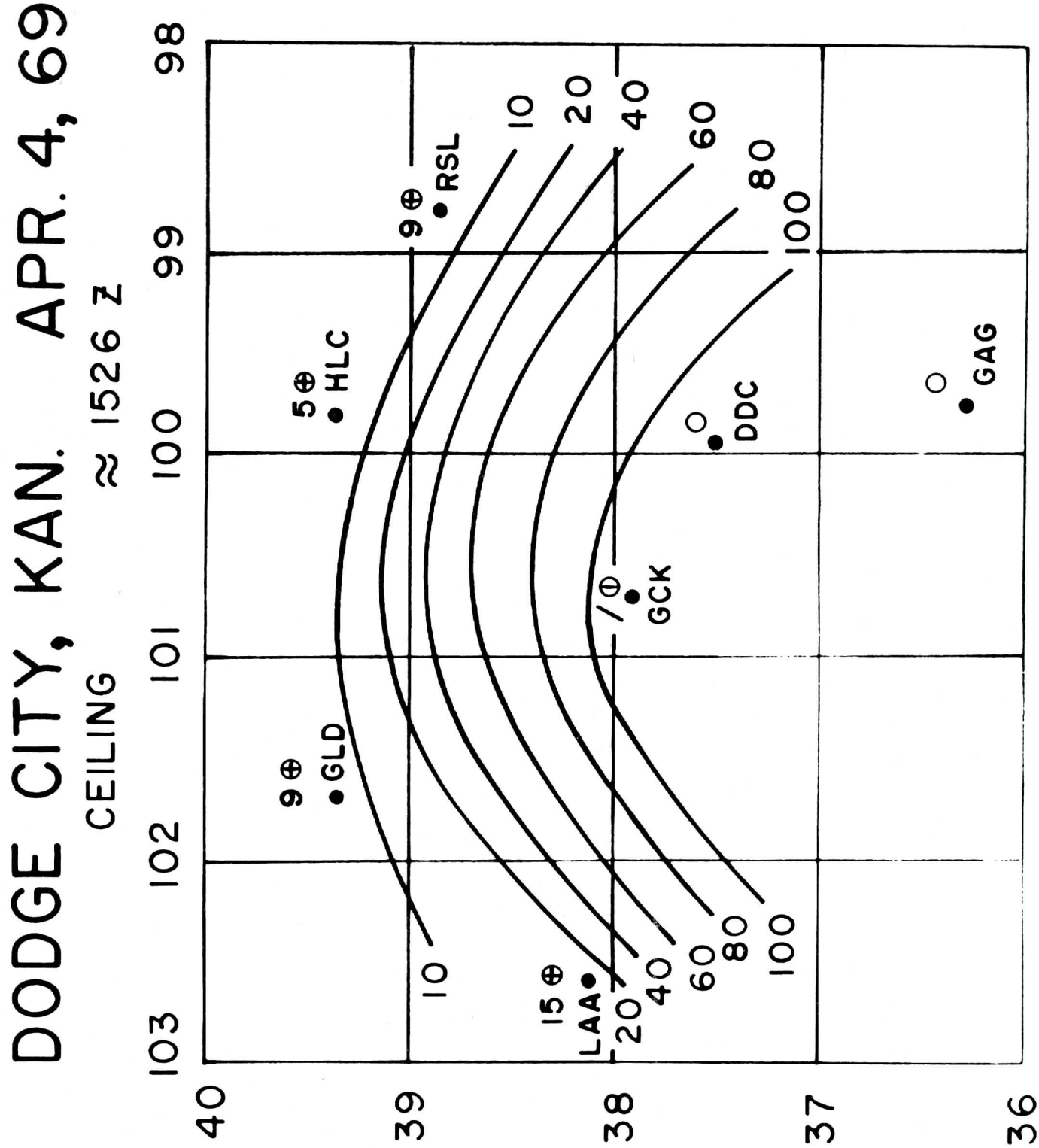
DODGE CITY, KAN. APR. 4, 69
CEILING ≈ 1526 Z
103
102
101
100
99
98
40
39
38
37
36
9⊕ GLD
5⊕ HLC
9⊕ RSL
15⊕ LAA
1⊕ GCK
DDC
GAG
10
20
40
60
80
100

Figure 38

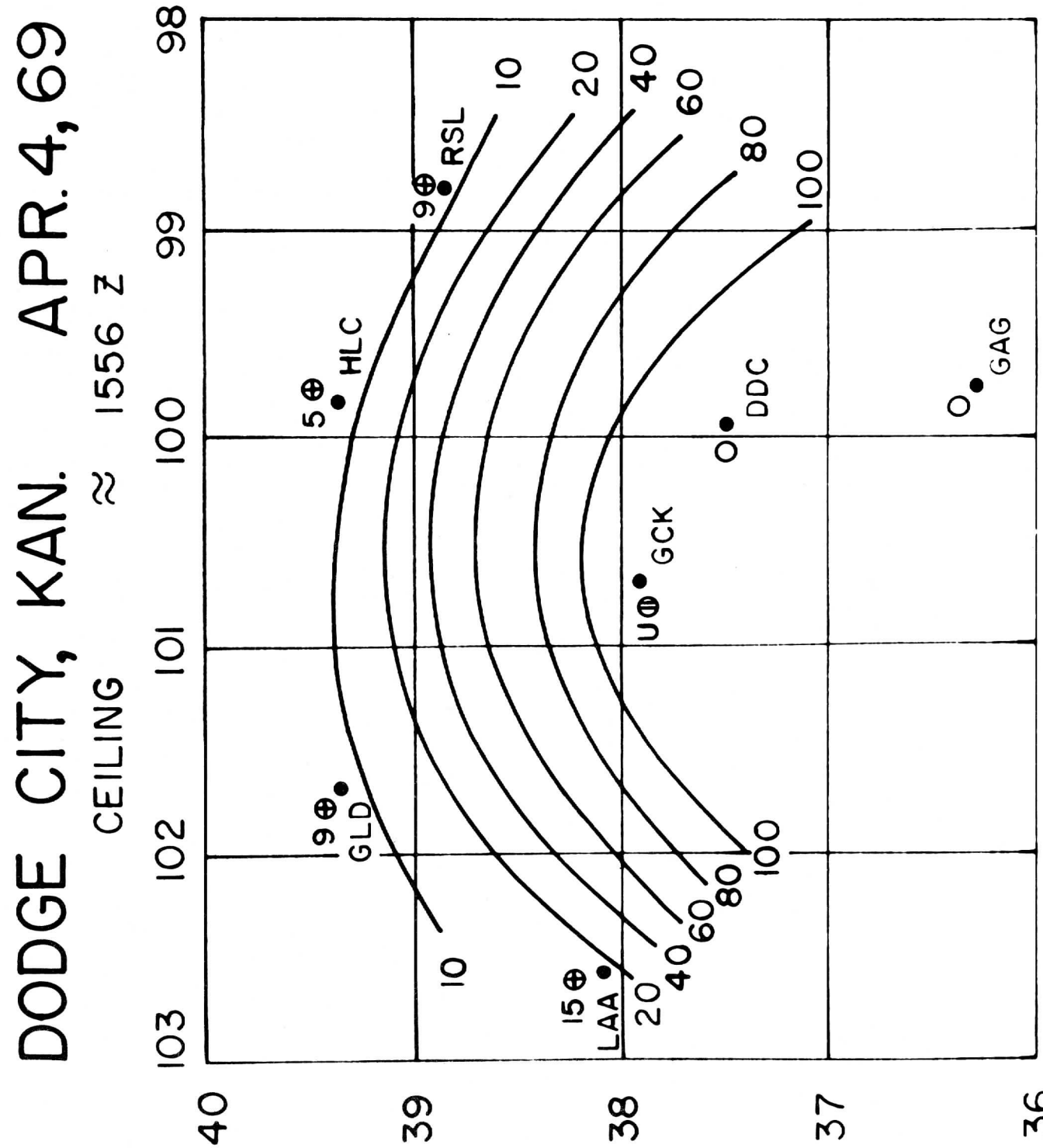
DODGE CITY, KAN. APR. 4, 69
CEILING ≈ 1556 Z
103
102
101
100
99
98
40
39
38
37
36
9⊕ GLD
5⊕ HLC
9⊕ RSL
15⊕ LAA
U⊕ GCK
O DDC
O GAG
10
20
40
60
80
100

Figure 39

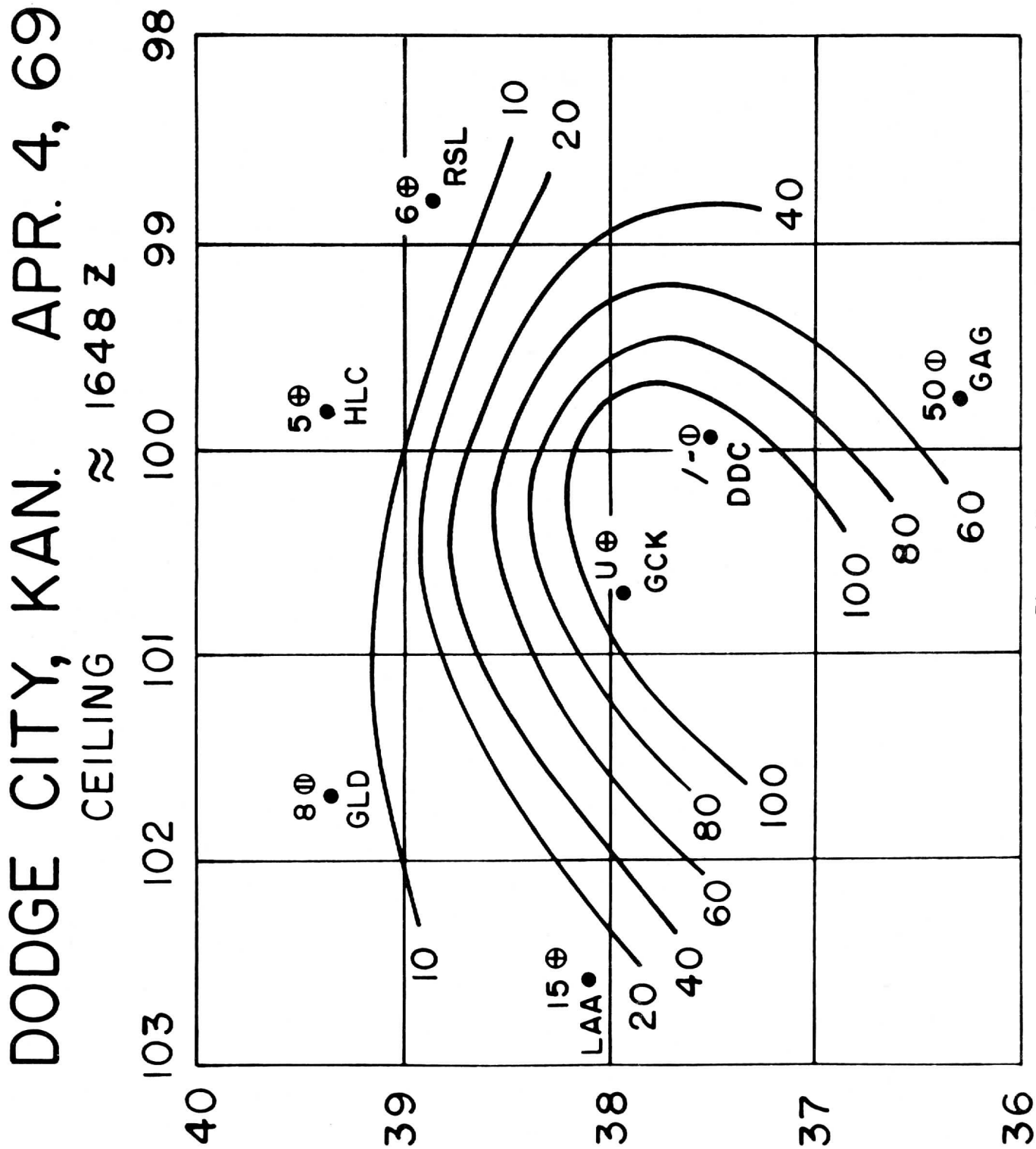
DODGE CITY, KAN. APR. 4, 69
CEILING ≈ 1648 Z
103
102
101
100
99
98
40
39
38
37
36
8Φ GLD
5Φ HLC
6Φ RSL
15Φ LAA
UΦ GCK
1-Φ DDC
50Φ GAG
10
20
40
60
80
100

Figure 40

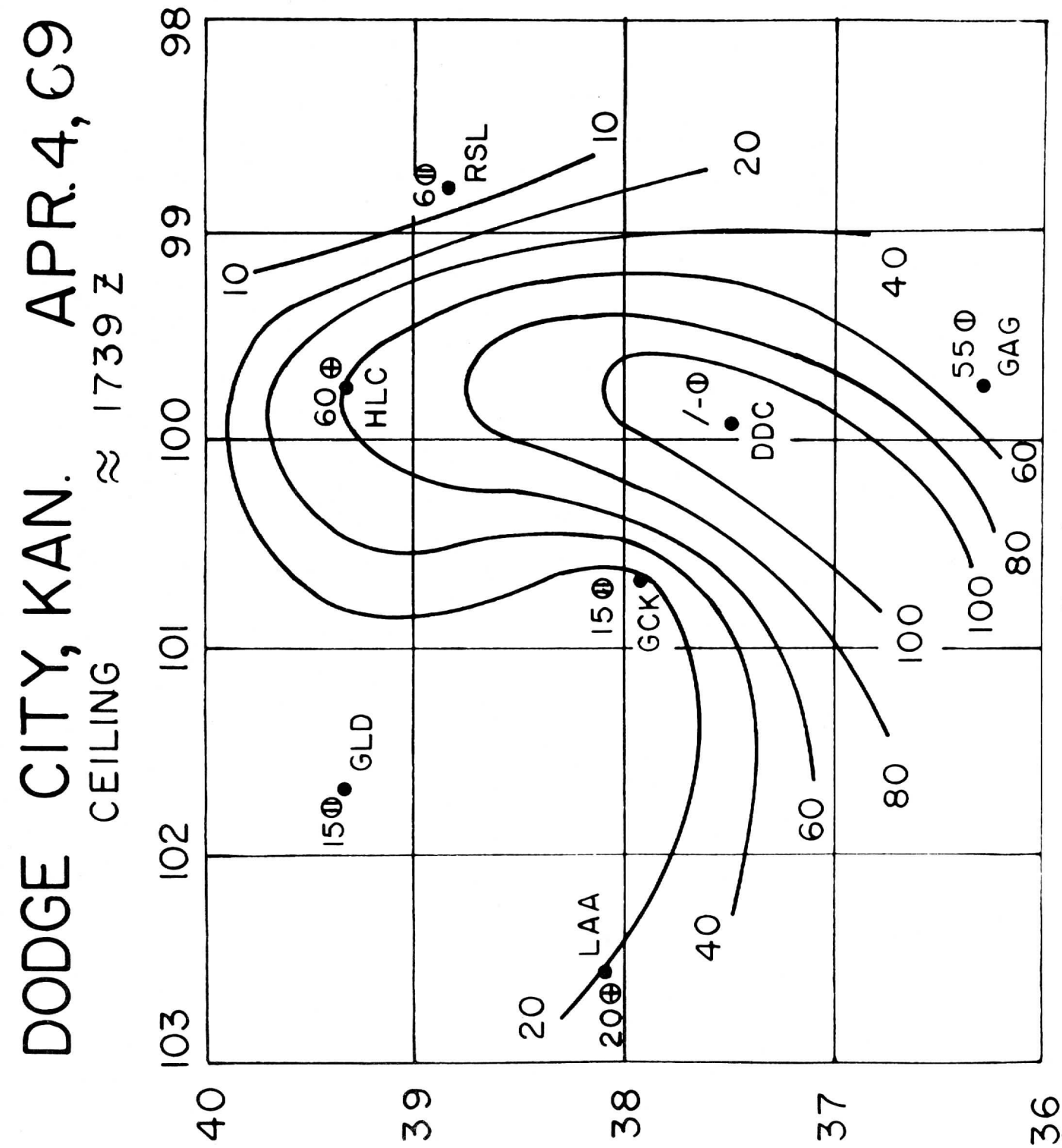
DODGE CITY, KAN. APR. 4, 69
CEILING
≈ 1739 Z
98
99
100
101
102
103
40
39
38
37
36
RSL
HLC
DDC
GAG
GCK
GLD
LAA
10
20
40
60
80
100

Figure 41

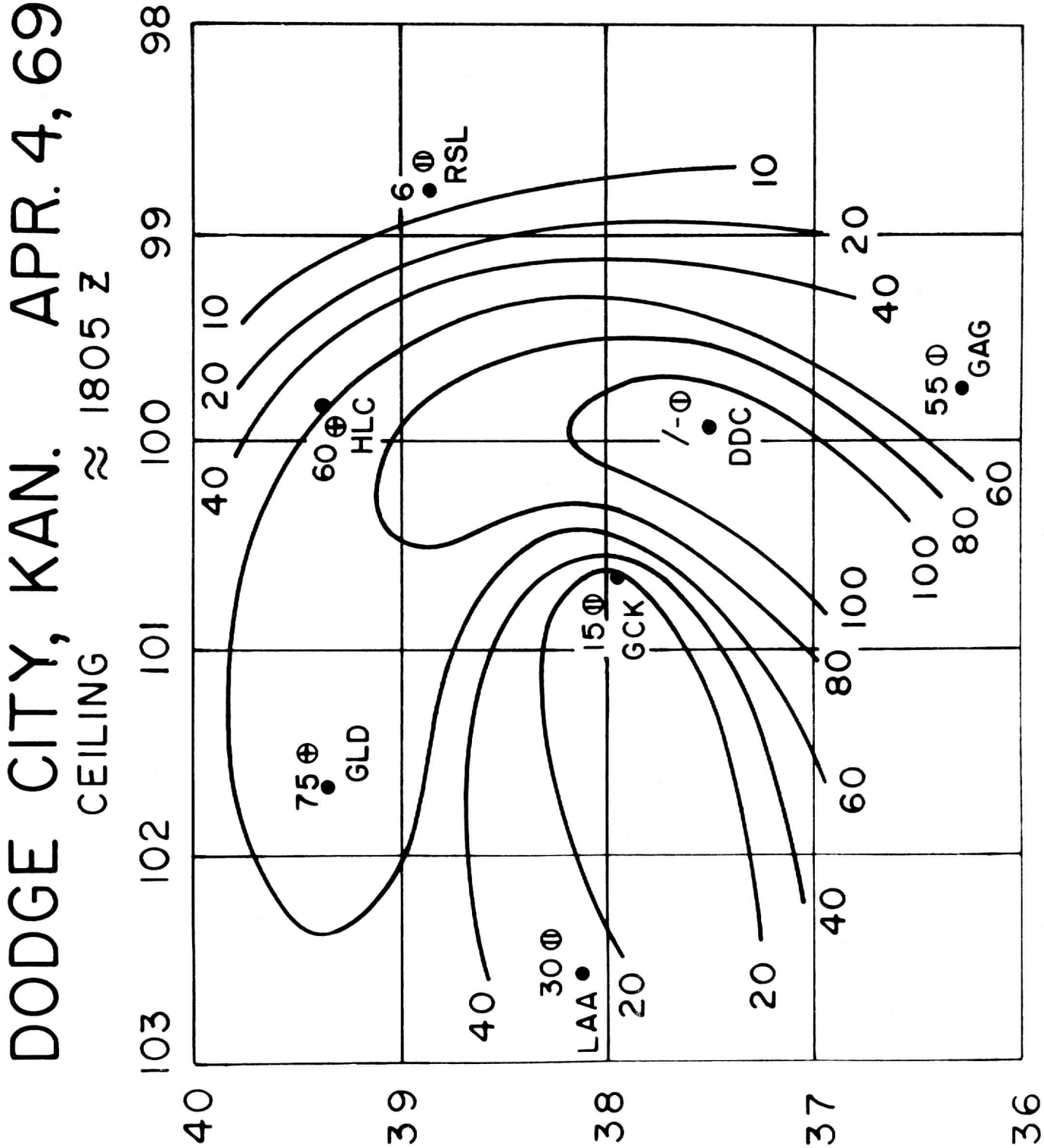
DODGE CITY, KAN. APR. 4, 69
CEILING ≈ 1805 Z
98
99
100
101
102
103
40
39
38
37
36
6 RSL
10
20
40
60 HLC
75 GLD
15 GCK
/- DDC
55 GAG
100
80
60
30 LAA

Figure 42

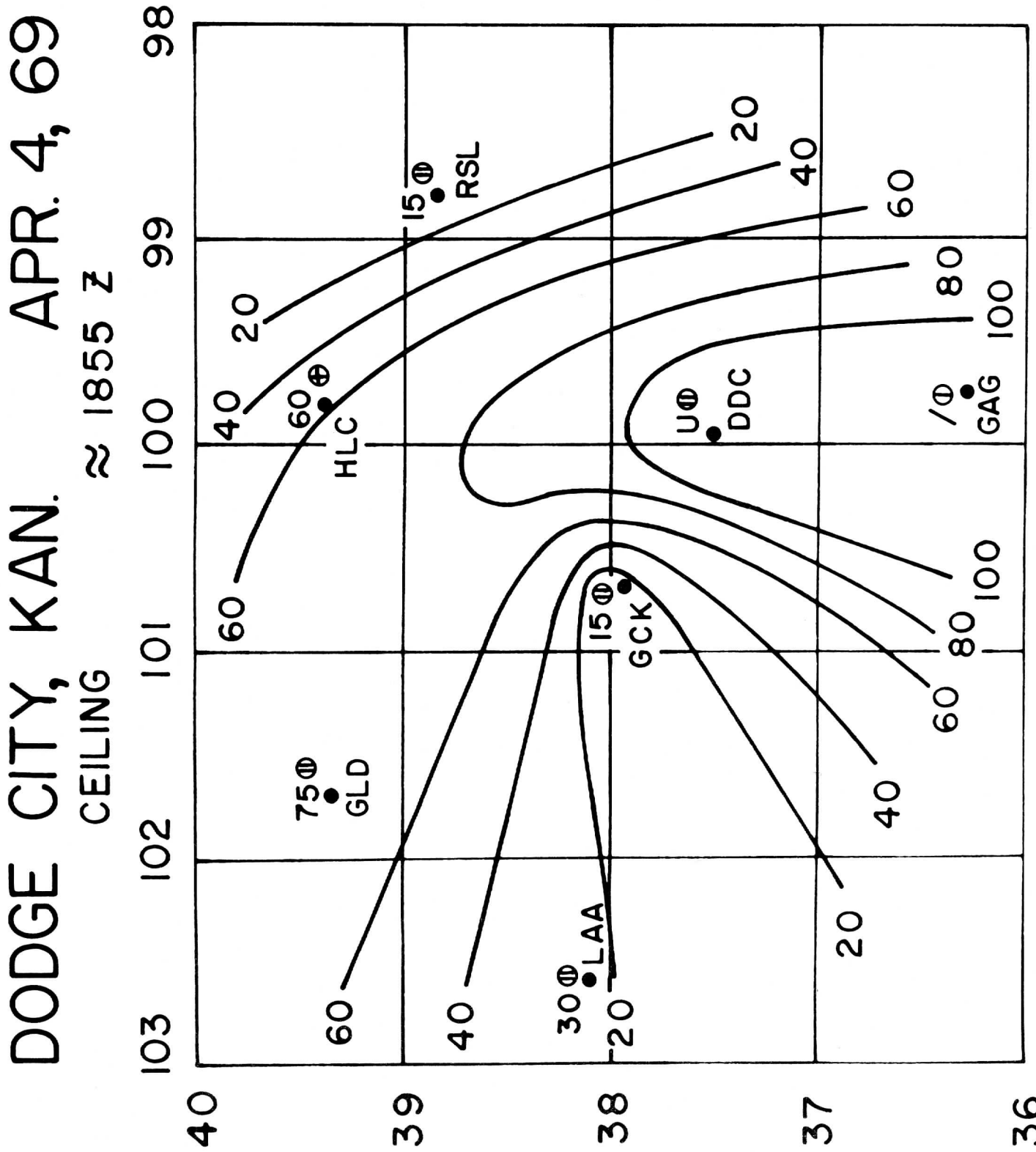
DODGE CITY, KAN. APR. 4, 69
CEILING ≈ 1855 Z
98
99
100
101
102
103
40
39
38
37
36
RSL
HLC
DDC
GAG
GCK
GLD
LAA
20
40
60
80
100

Figure 43

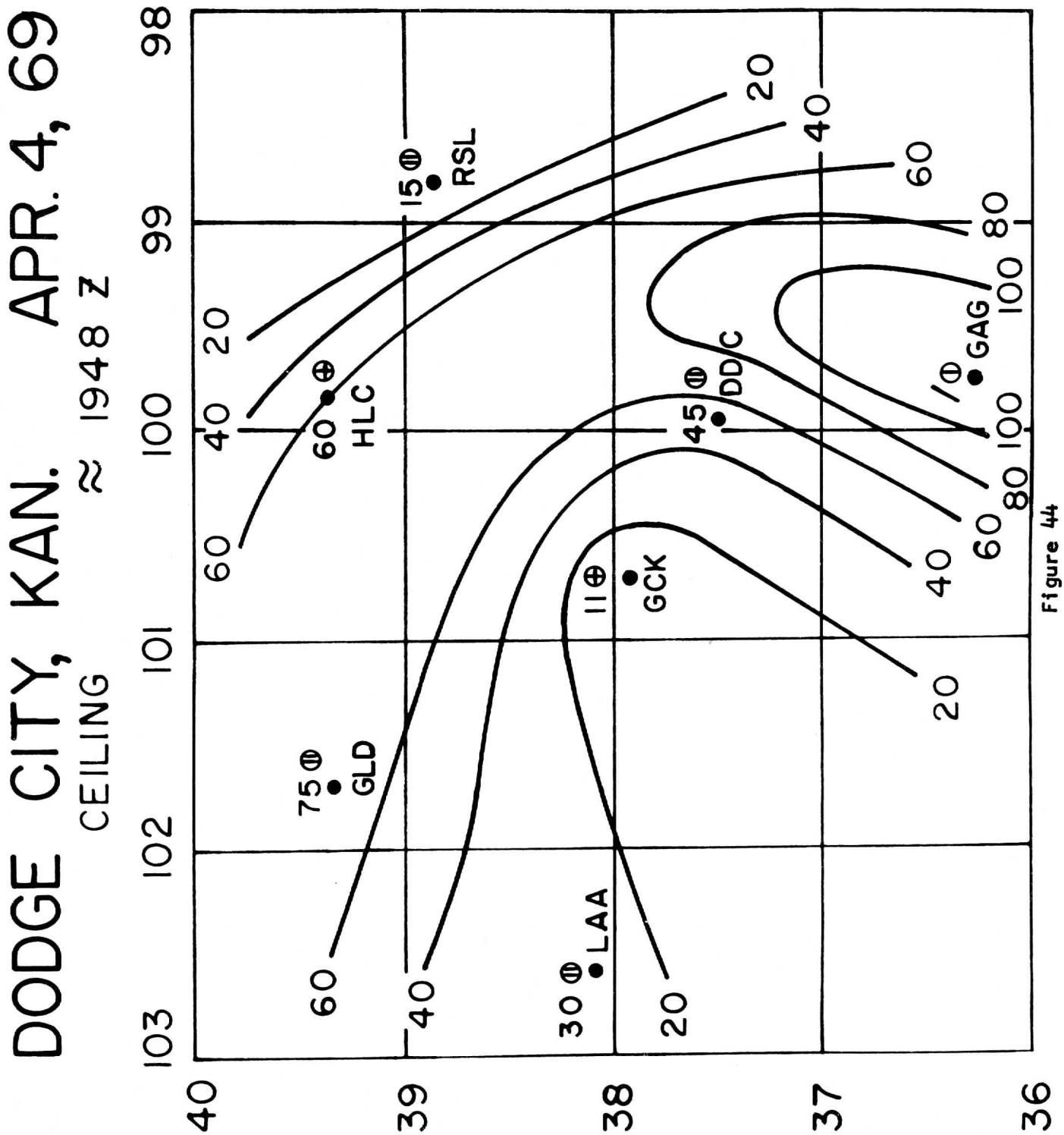
DODGE CITY, KAN. APR. 4, 69
CEILING ≈ 1948 Z
103
102
101
100
99
98
40
39
38
37
36
75Φ GLD
60Φ HLC
15Φ RSL
45Φ DDC
1Φ GAG
11Φ GCK
30Φ LAA
20
40
60
80
100

Figure 44

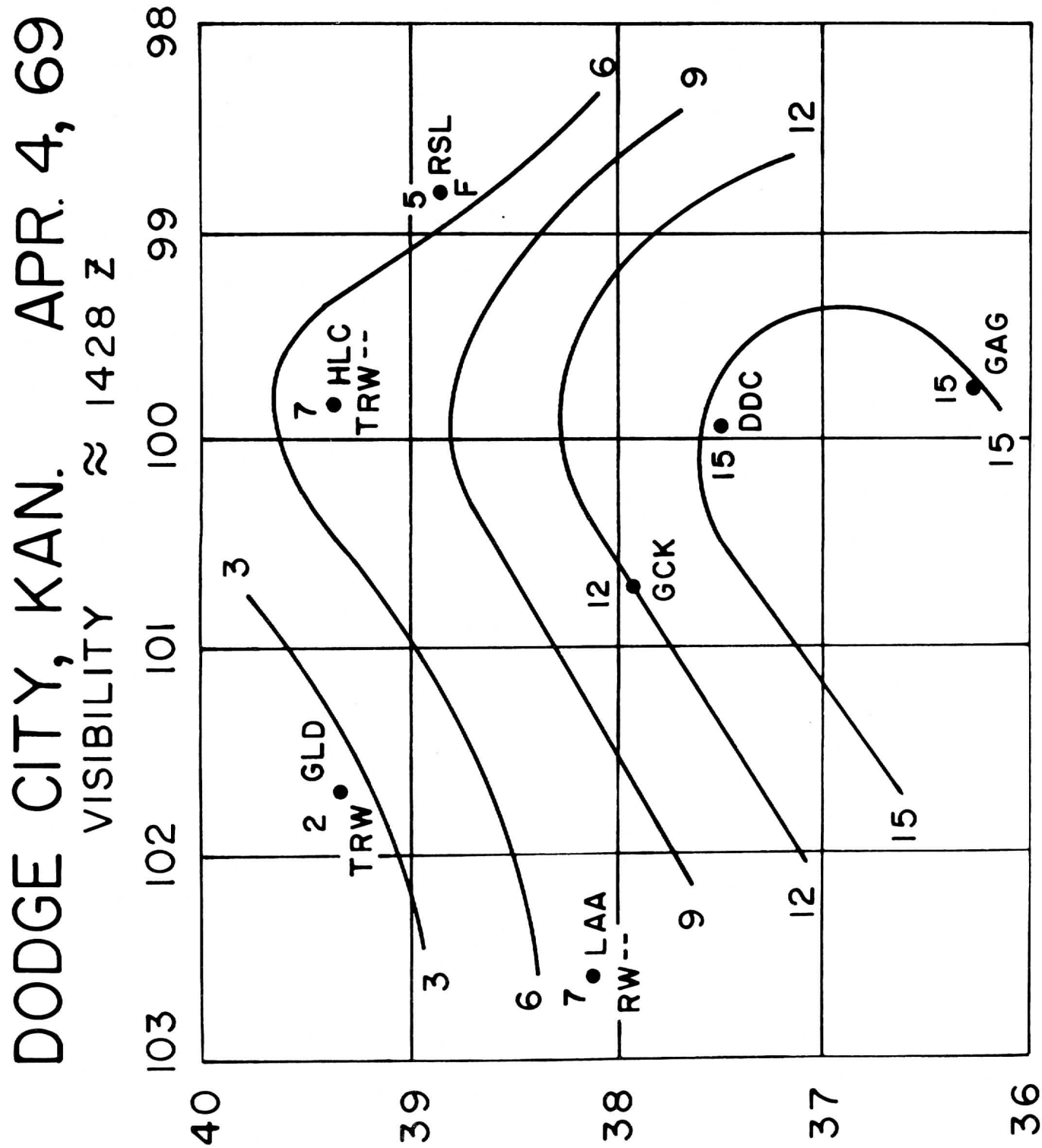
DODGE CITY, KAN. APR. 4, 69
VISIBILITY ≈ 1428 Z
103
102
101
100
99
98
40
39
38
37
36
2 GLD
TRW
7 HLC
TRW--
5 RSL
F
7 LAA
RW--
12 GCK
15 DDC
15 GAG
3
6
9
12
15

Figure 45

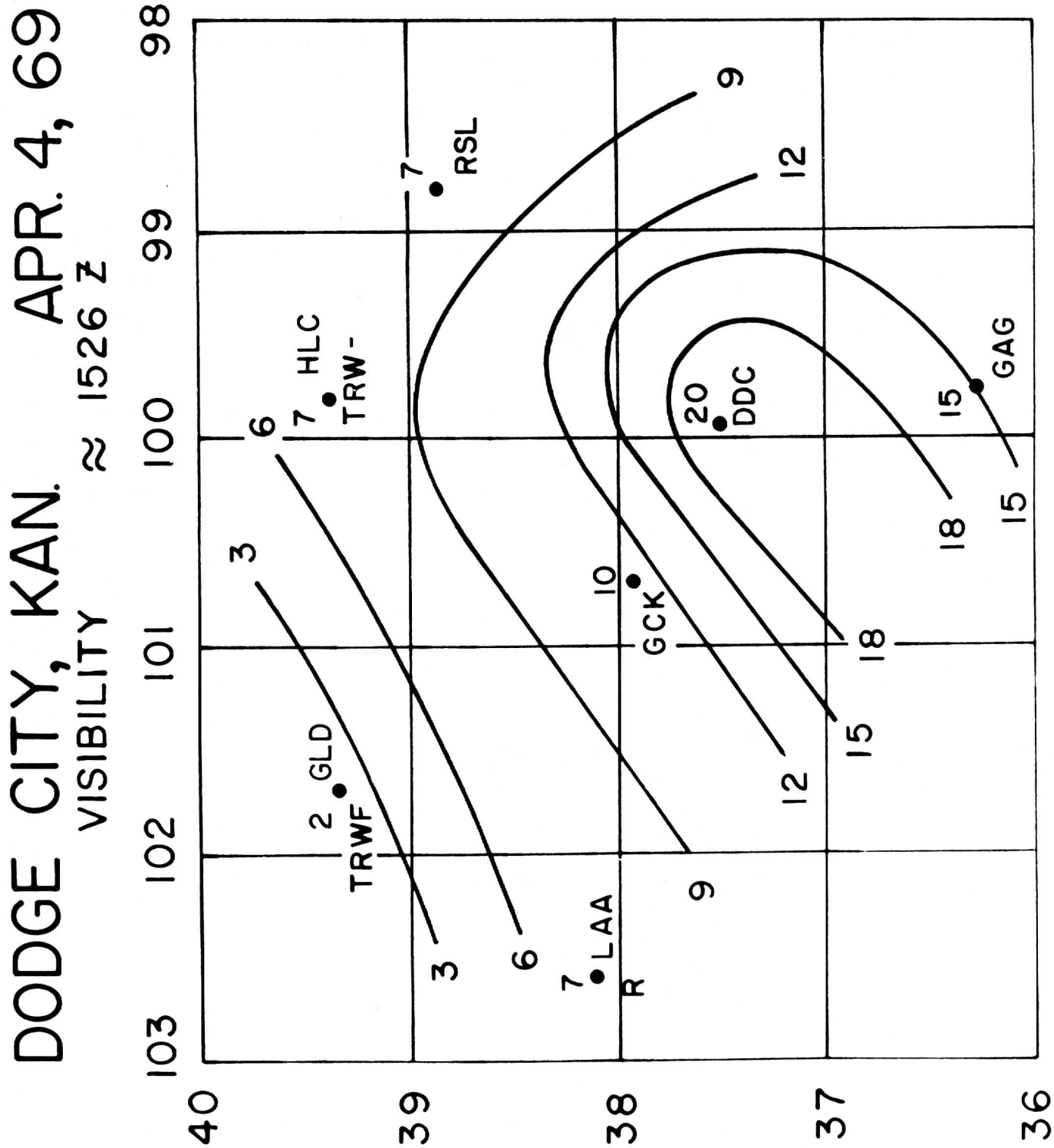
DODGE CITY, KAN. APR. 4, 69
VISIBILITY
≈ 1526 Z
103
102
101
100
99
98
40
39
38
37
36
2 GLD
TRWF
7 LAA
R
10 GCK
7 HLC
TRW-
7 RSL
20 DDC
15 GAG
3
6
9
12
15
18

Figure 46

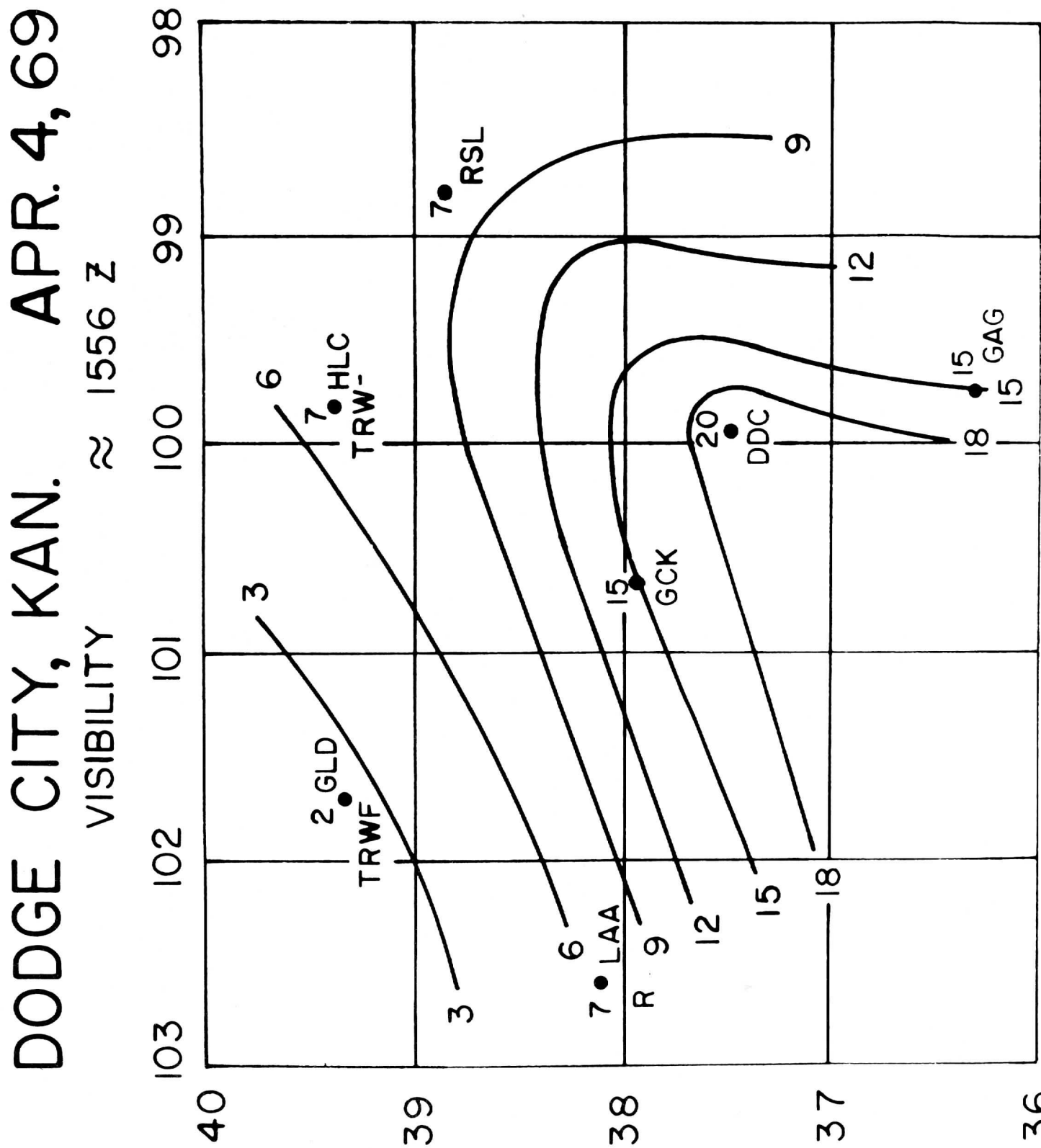
DODGE CITY, KAN. APR. 4, 69
VISIBILITY ≈ 1556 Z
98
99
100
101
102
103
40
39
38
37
36
3
6
9
12
15
18
2 GLD
TRWF
7 HLC
TRW-
7 RSL
7 LAA
R
15 GCK
20 DDC
15 GAG
18

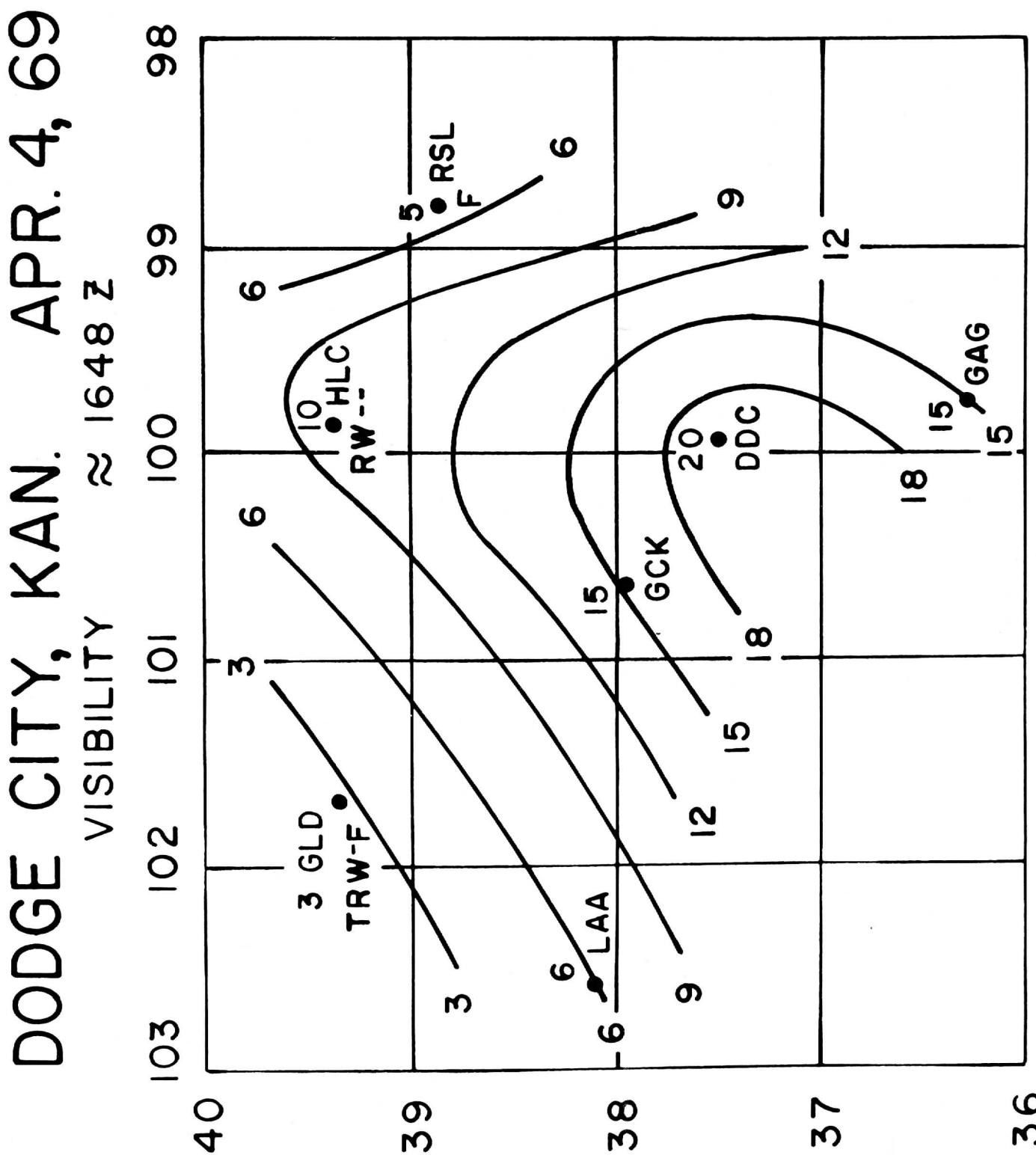
DODGE CITY, KAN. APR. 4, 69
VISIBILITY ≈ 1648 Z
103
102
101
100
99
98
40
39
38
37
36
3 GLD
TRW-F
LAA
HLC
RW--
RSL
F
GCK
DDC
GAG
3
6
9
12
15
18
20

Figure 48

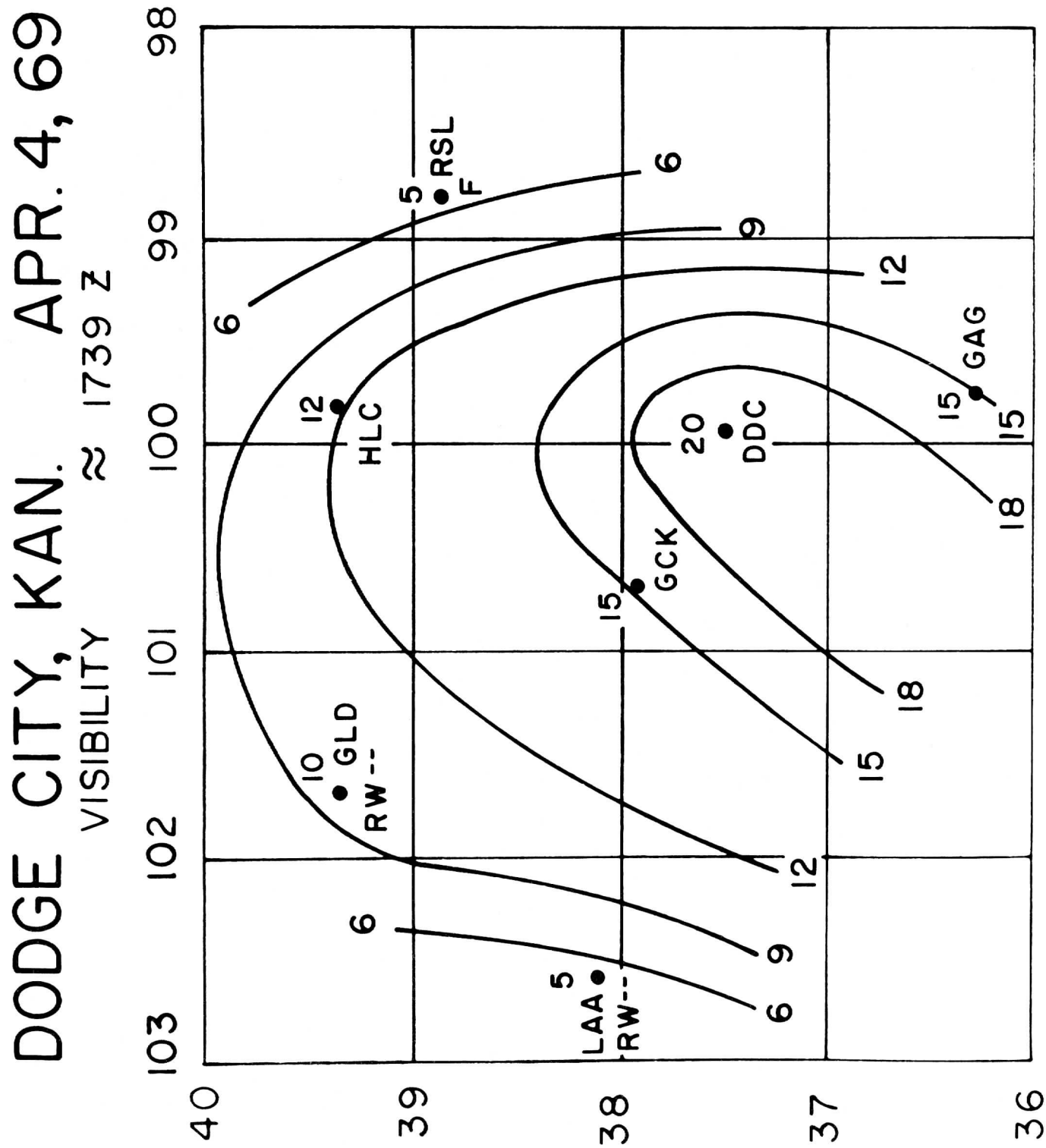
DODGE CITY, KAN. APR. 4, 69
VISIBILITY ≈ 1739 Z
103
102
101
100
99
98
40
39
38
37
36
10 GLD RW--
5 LAA RW--
12 HLC
5 RSL F
15 GCK
20 DDC
15 GAG
6
9
12
15
18

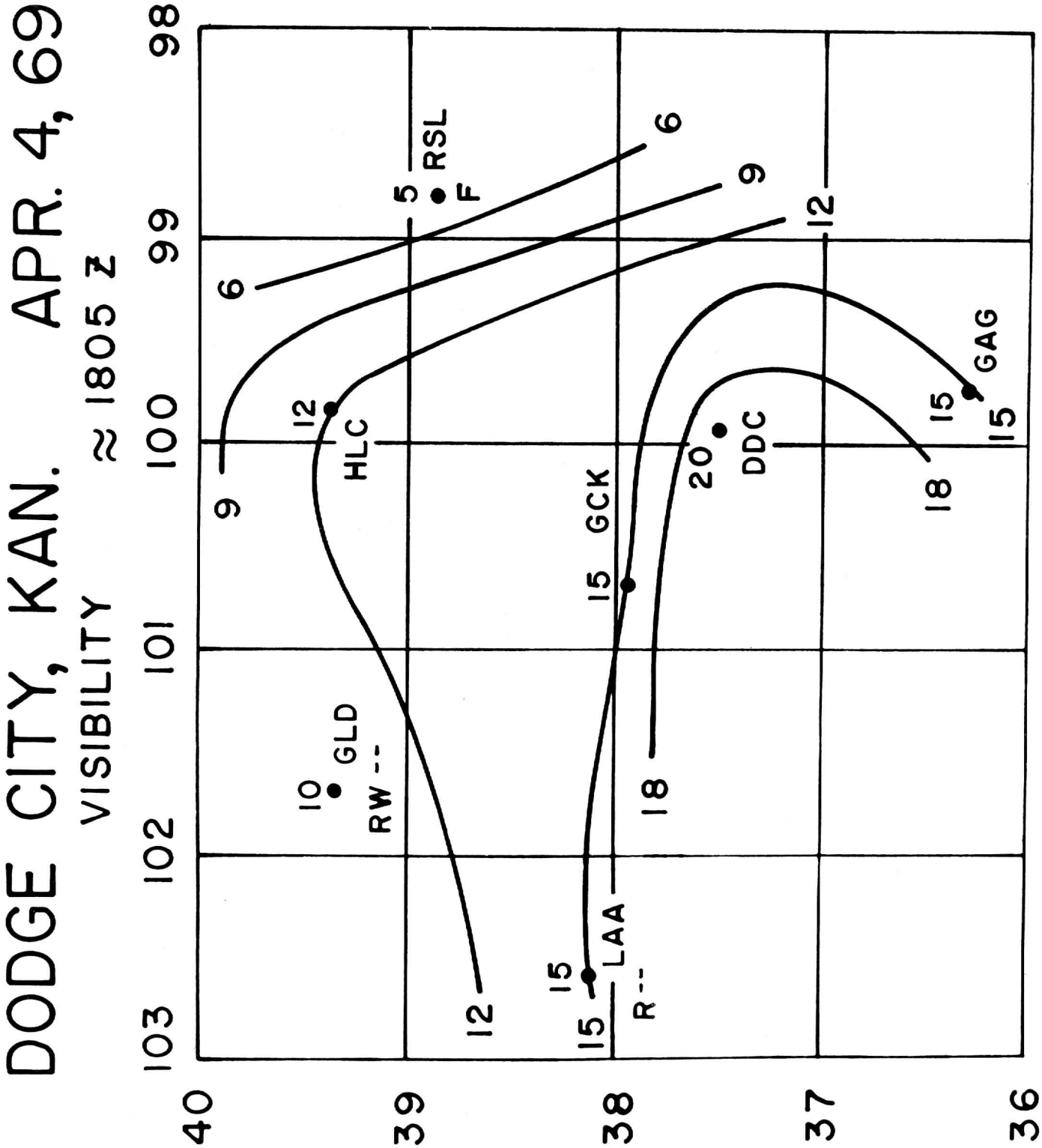
DODGE CITY, KAN. APR. 4, 69
VISIBILITY ≈ 1805 Z
98
99
100
101
102
103
40
39
38
37
36
5 RSL
F
6
6
9
12
12 HLC
9
10 GLD
RW --
15 GCK
20 DDC
18
15 GAG
15
18
12
15
15 LAA
R --

Figure 50

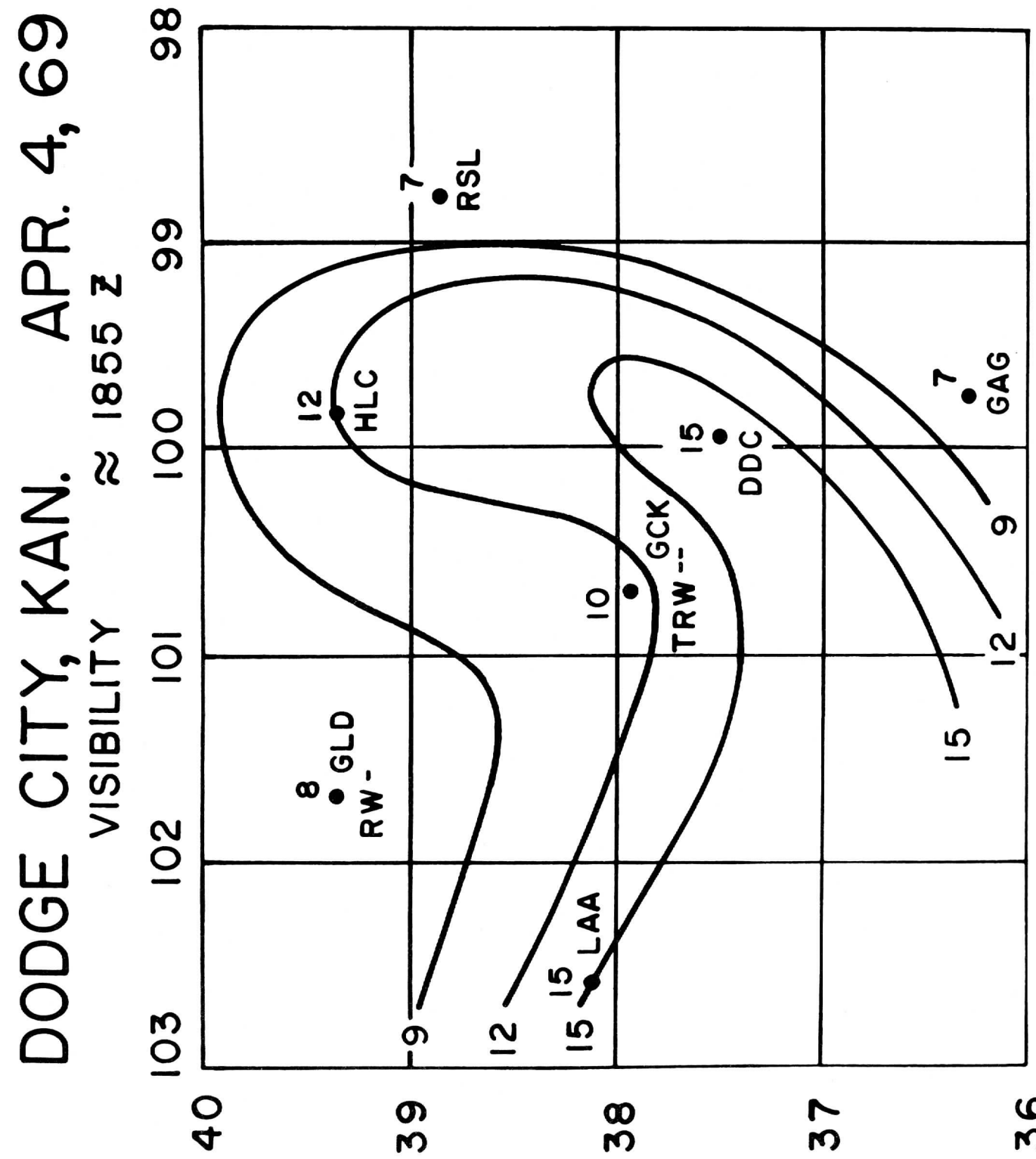
DODGE CITY, KAN. APR. 4, 69
VISIBILITY ≈ 1855 Z
98
99
100
101
102
103
40
39
38
37
36
7
RSL
12
HLC
8
GLD
RW-
10
GCK
TRW--
15
DDC
7
GAG
9
12
15
15
LAA
9
12
15

Figure 51

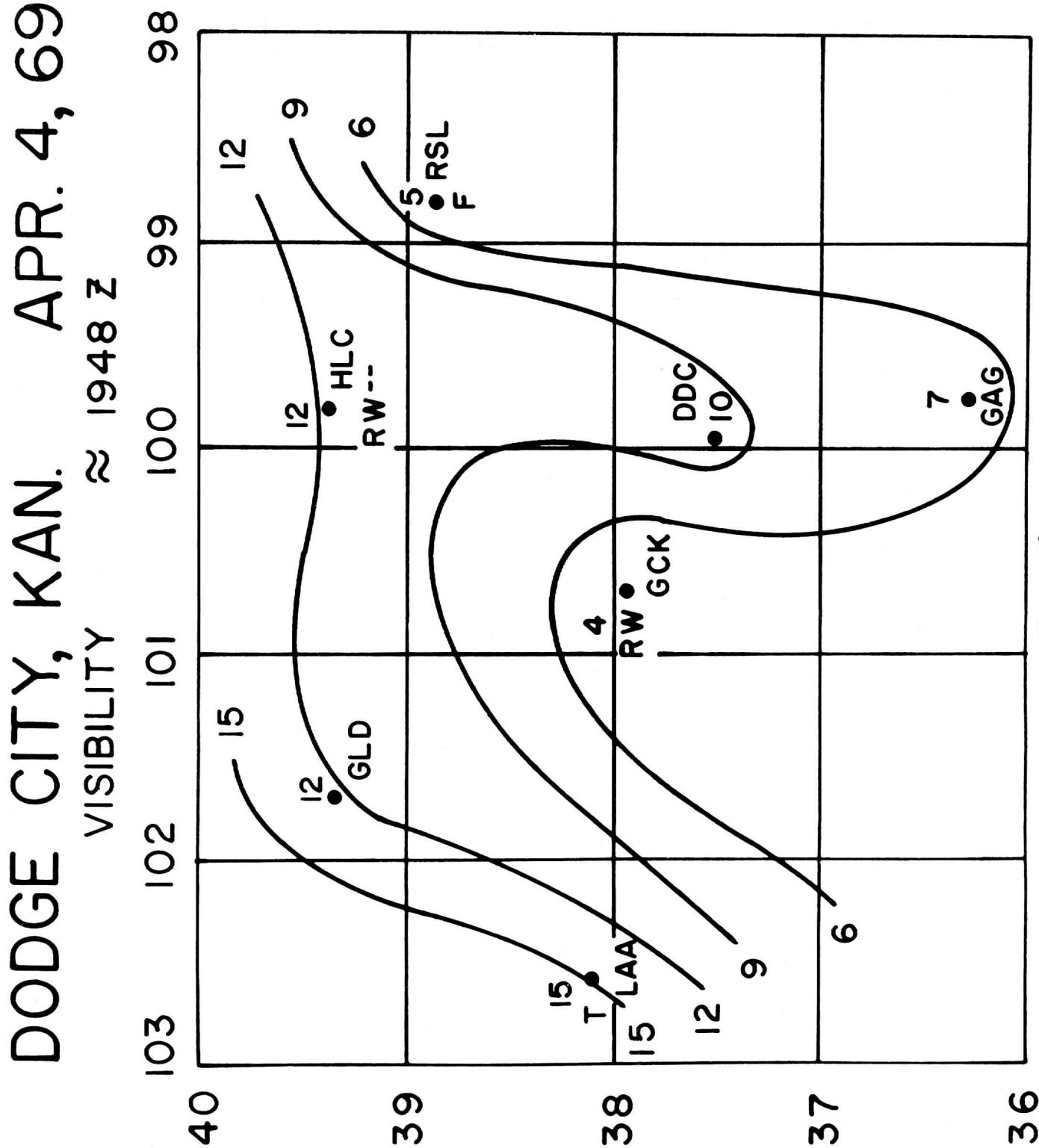
DODGE CITY, KAN. APR. 4, 69
VISIBILITY ≈ 1948 Z
103
102
101
100
99
98
40
39
38
37
36
15
12
9
6
5
12
9
6
12
15
15
12
4
7
RSL
F
HLC
RW--
GLD
DDC
10
RW
GCK
T
LAA
GAG

Figure 52

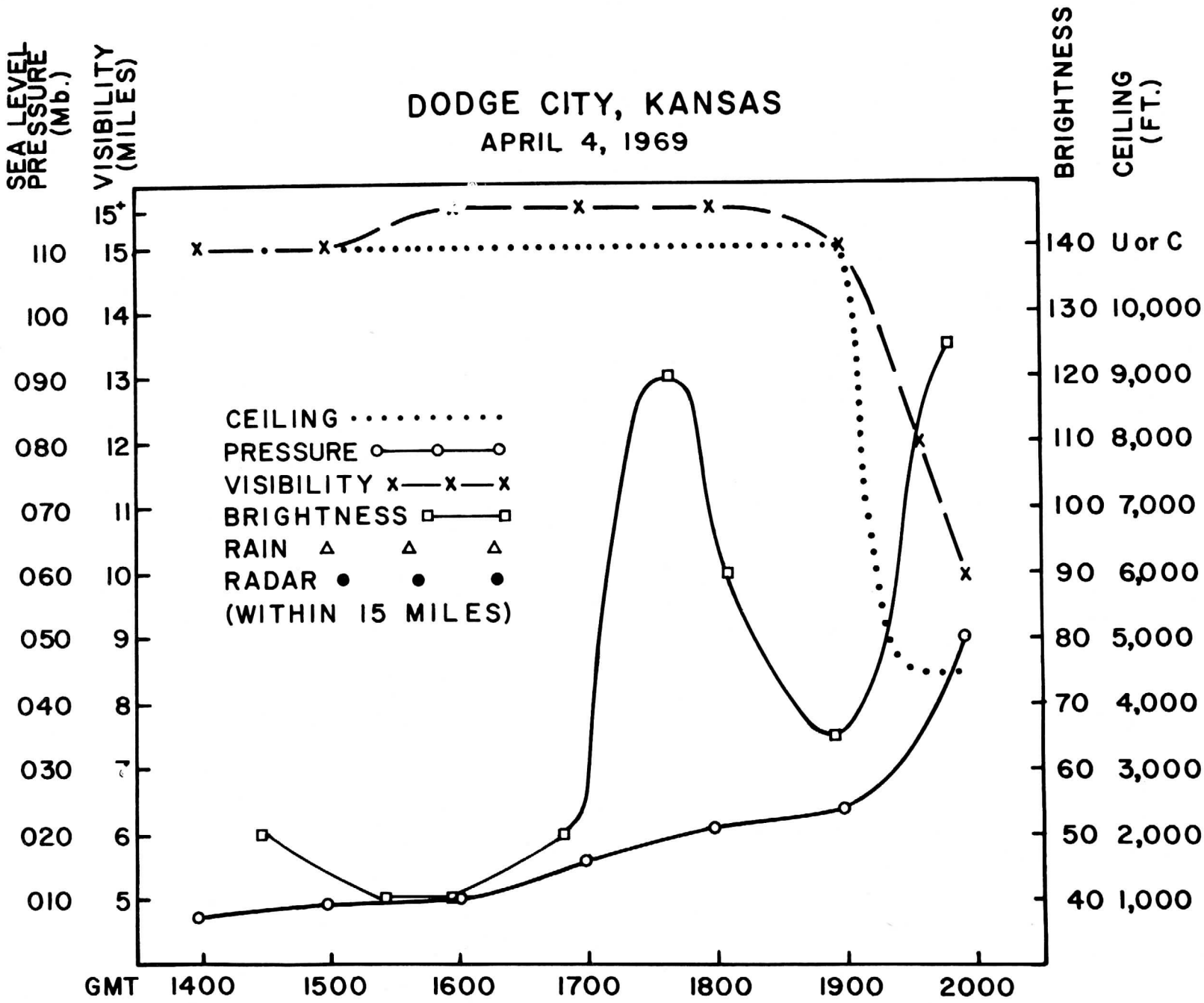
DODGE CITY, KANSAS
APRIL 4, 1969
SEA LEVEL PRESSURE (Mb.)
VISIBILITY (MILES)
BRIGHTNESS
CEILING (FT.)
CEILING
PRESSURE
VISIBILITY
BRIGHTNESS
RAIN
RADAR
(WITHIN 15 MILES)
110
100
090
080
070
060
050
040
030
020
010
15+
15
14
13
12
11
10
9
8
7
6
5
140 U or C
130 10,000
120 9,000
110 8,000
100 7,000
90 6,000
80 5,000
70 4,000
60 3,000
50 2,000
40 1,000
GMT 1400 1500 1600 1700 1800 1900 2000

Figure 53

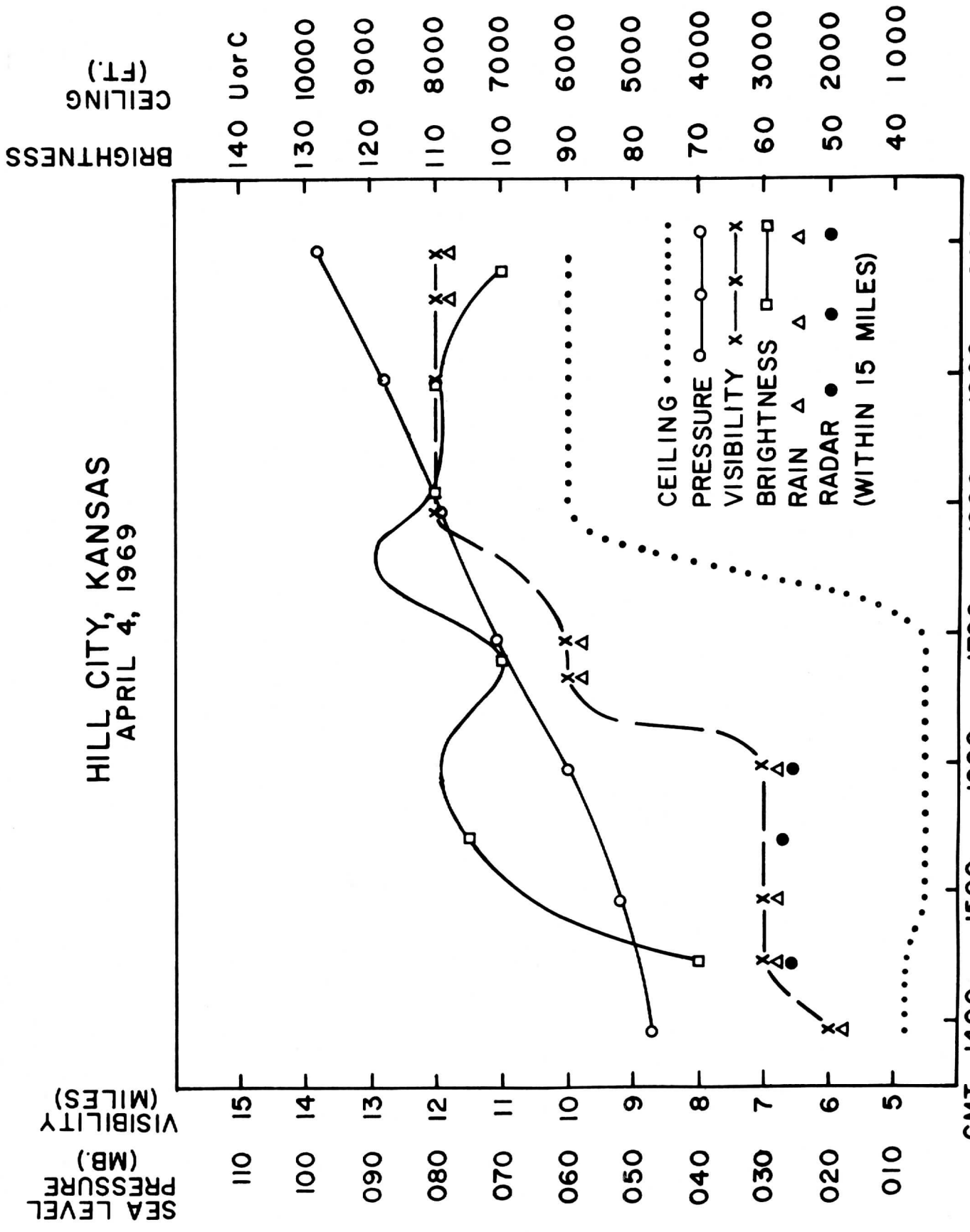
HILL CITY, KANSAS
APRIL 4, 1969
SEA LEVEL PRESSURE (MB.)
VISIBILITY (MILES)
BRIGHTNESS
CEILING (FT.)
U or C
GMT
CEILING
PRESSURE
VISIBILITY
BRIGHTNESS
RAIN
RADAR
(WITHIN 15 MILES)

Figure 54

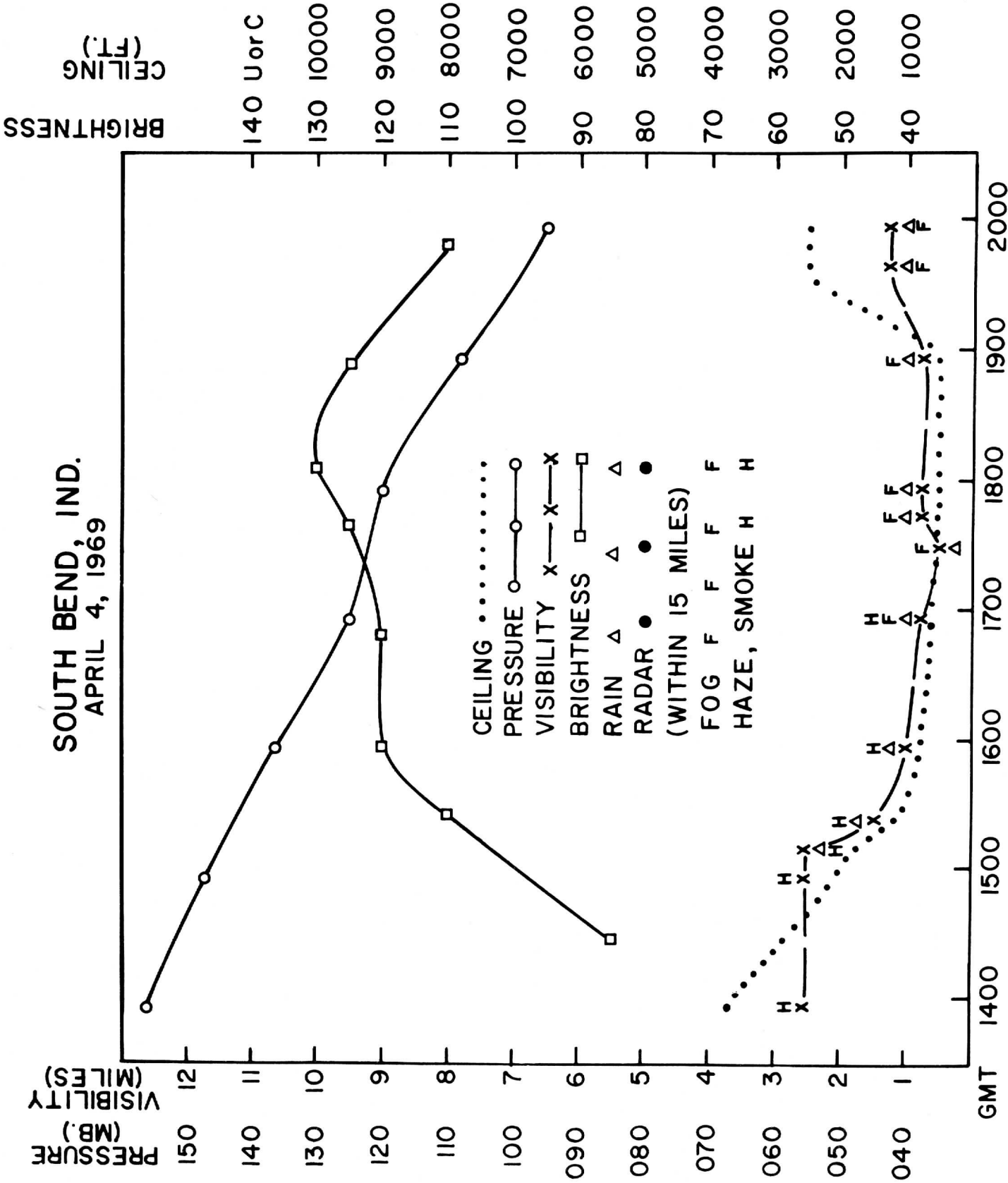
SOUTH BEND, IND.
APRIL 4, 1969
PRESSURE (MB.)
VISIBILITY (MILES)
BRIGHTNESS
CEILING (FT.)
GMT
CEILING
PRESSURE
VISIBILITY
BRIGHTNESS
RAIN
RADAR
(WITHIN 15 MILES)
FOG
HAZE, SMOKE

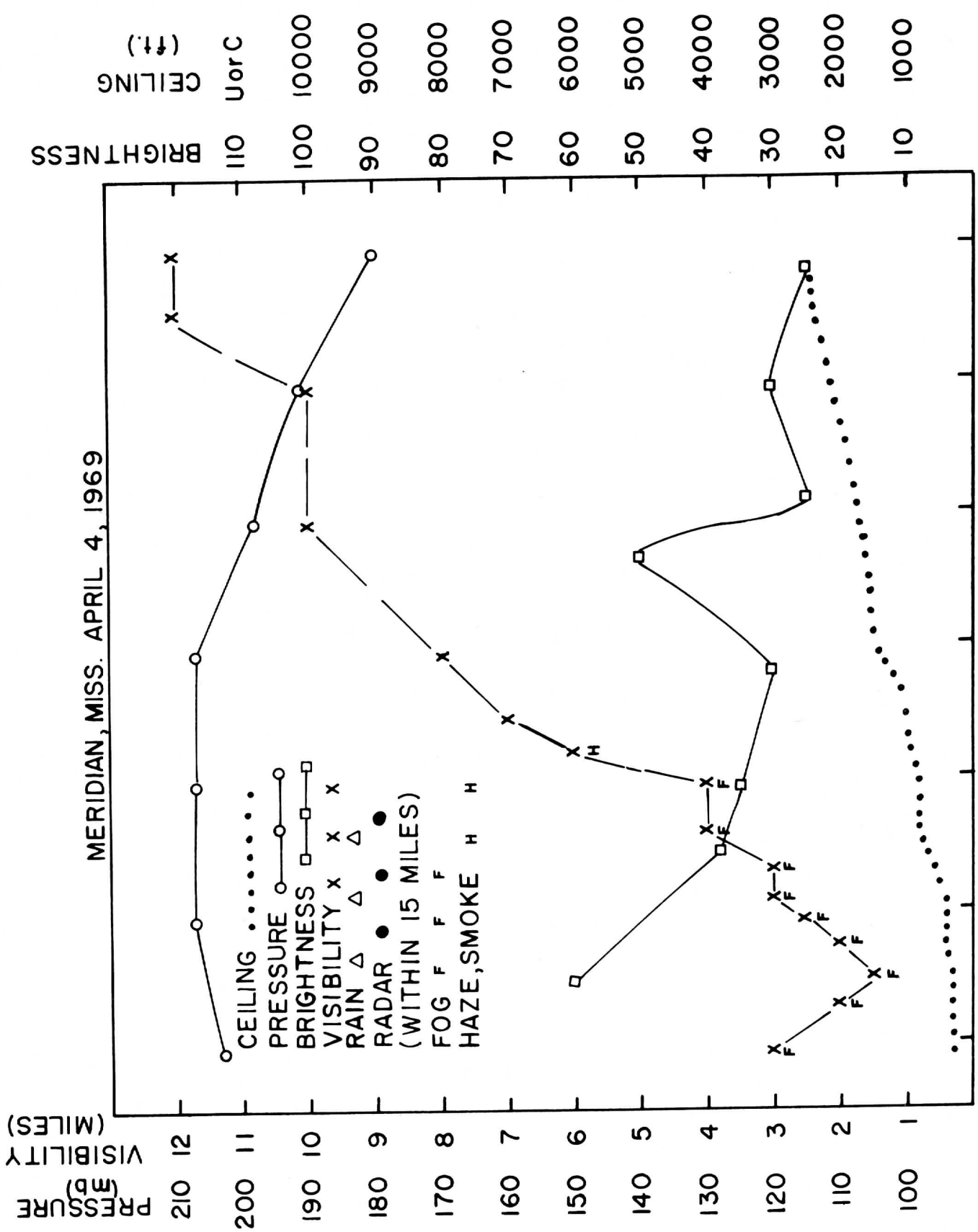
MERIDIAN, MISS. APRIL 4, 1969
PRESSURE (mb)
VISIBILITY (MILES)
BRIGHTNESS
CEILING (ft.) U or C
GMT
CEILING
PRESSURE
BRIGHTNESS
VISIBILITY x x x
RAIN △ △
RADAR ● ●
(WITHIN 15 MILES)
FOG F F F
HAZE, SMOKE H H

Figure 56

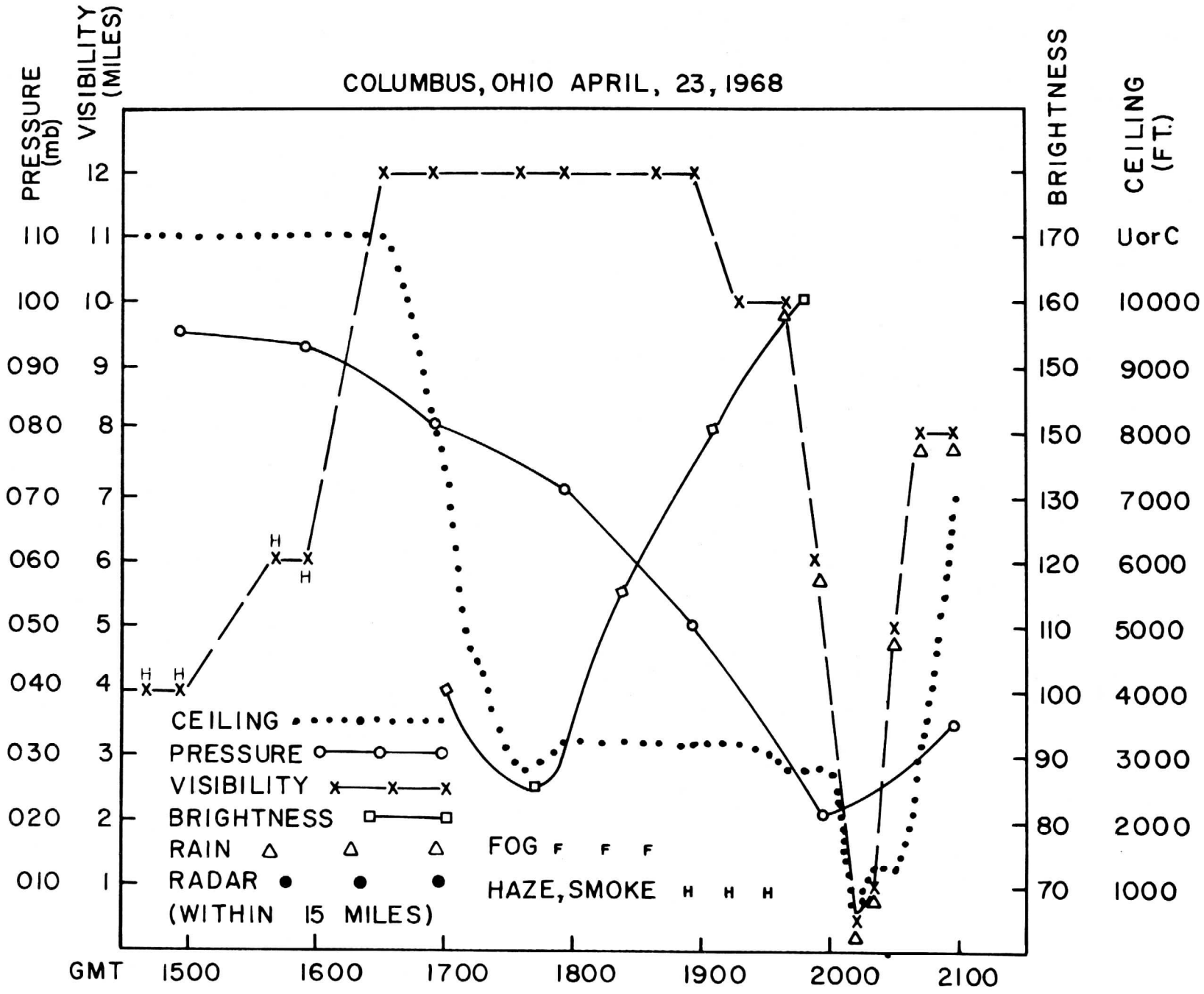
COLUMBUS, OHIO APRIL, 23, 1968
PRESSURE (mb)
VISIBILITY (MILES)
BRIGHTNESS
CEILING (FT.)
110
100
090
080
070
060
050
040
030
020
010
12
11
10
9
8
7
6
5
4
3
2
1
170
160
150
150
130
120
110
100
90
80
70
UorC
10000
9000
8000
7000
6000
5000
4000
3000
2000
1000
CEILING
PRESSURE
VISIBILITY
BRIGHTNESS
RAIN
RADAR
(WITHIN 15 MILES)
FOG F F F
HAZE, SMOKE H H H
GMT
1500
1600
1700
1800
1900
2000
2100

Figure 57

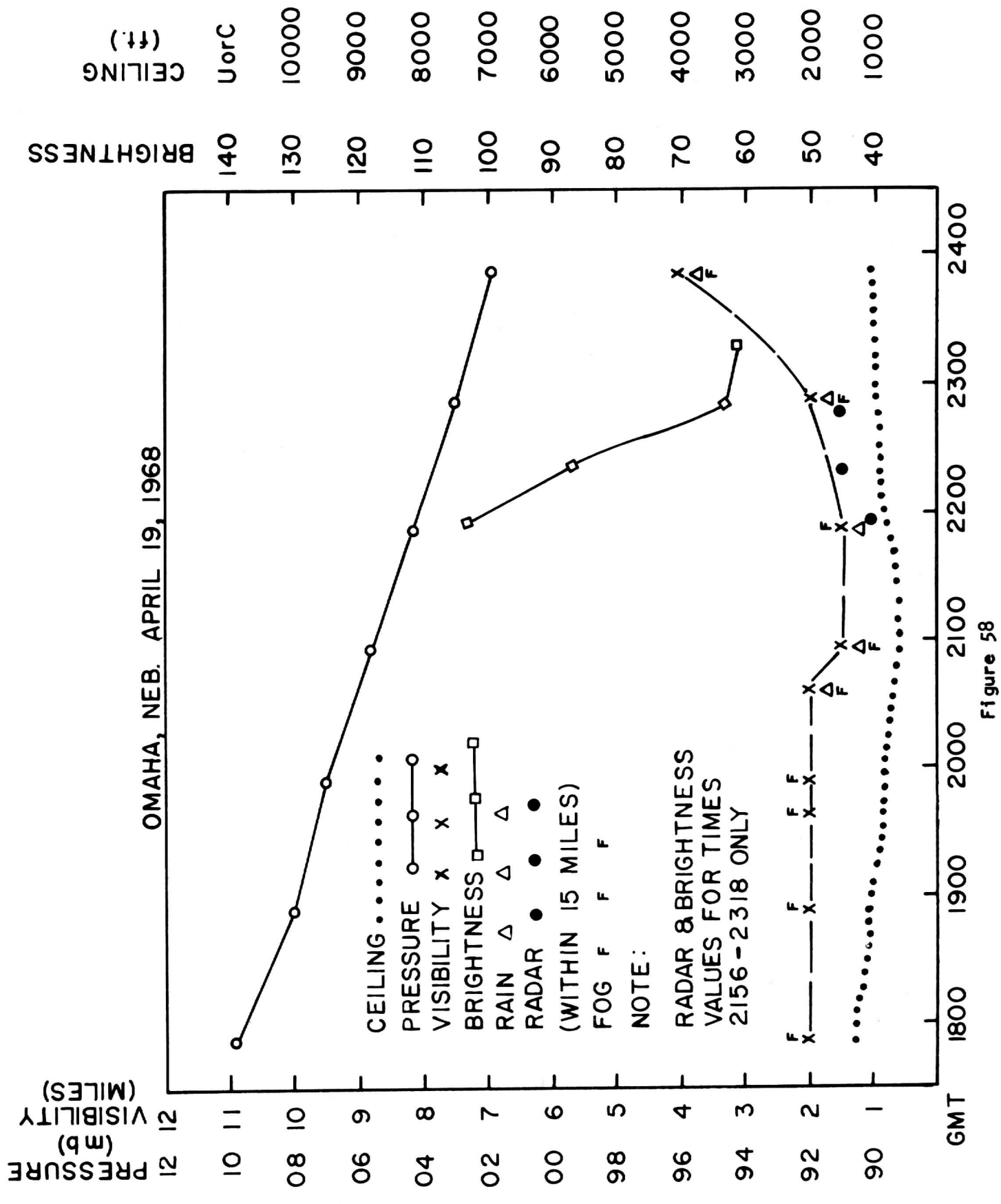
OMAHA, NEB. APRIL 19, 1968
PRESSURE (mb)
VISIBILITY (MILES)
CEILING (ft.)
BRIGHTNESS
UorC
GMT
1800
1900
2000
2100
2200
2300
2400
CEILING
PRESSURE
VISIBILITY
BRIGHTNESS
RAIN
RADAR
(WITHIN 15 MILES)
FOG
NOTE:
RADAR & BRIGHTNESS VALUES FOR TIMES 2156-2318 ONLY

Figure 58

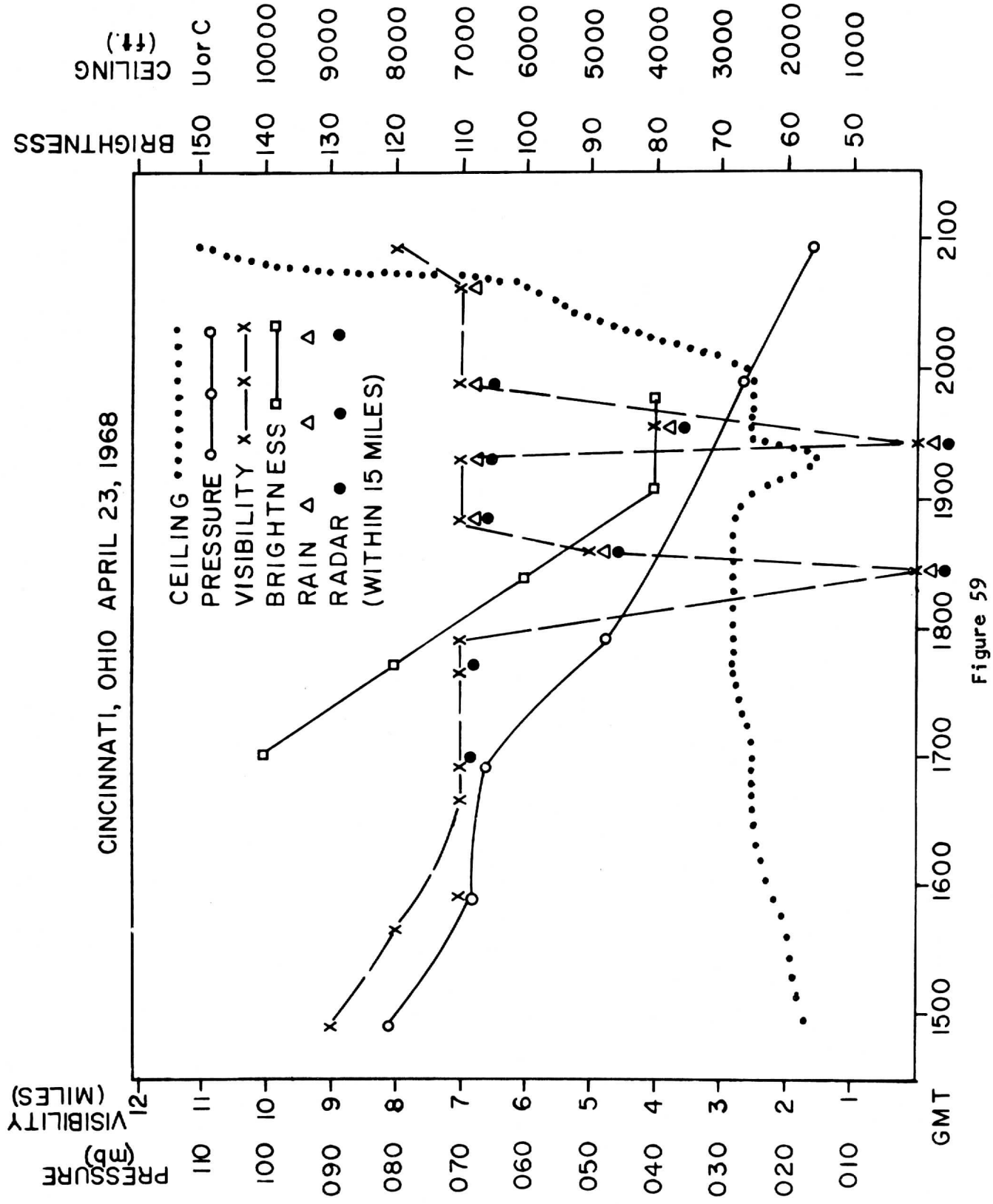
CINCINNATI, OHIO APRIL 23, 1968
CEILING
PRESSURE
VISIBILITY
BRIGHTNESS
RAIN
RADAR
(WITHIN 15 MILES)
PRESSURE (mb)
VISIBILITY (MILES)
BRIGHTNESS
CEILING (ft.) U or C
GMT
1500
1600
1700
1800
1900
2000
2100

Figure 59

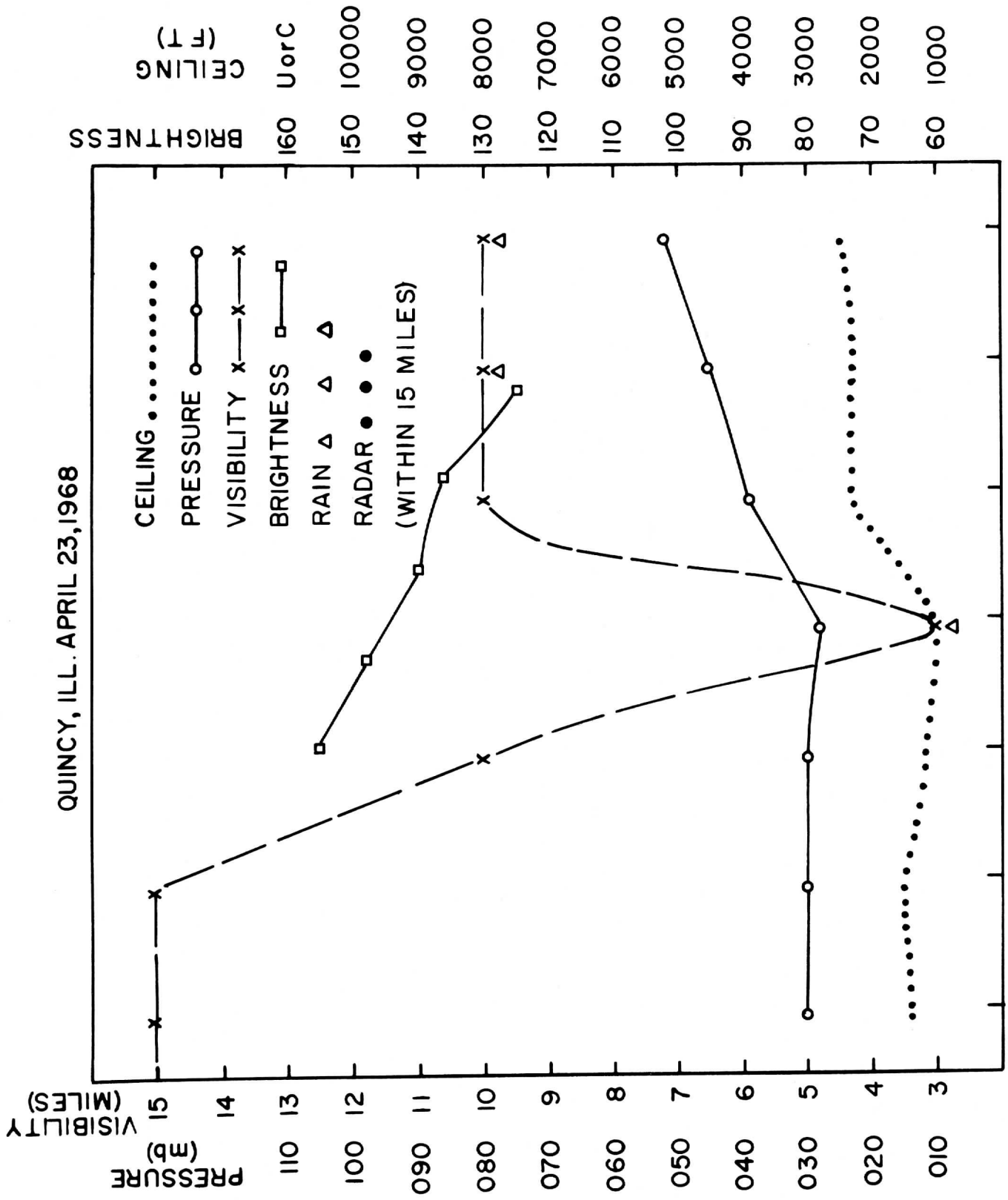
QUINCY, ILL. APRIL 23, 1968
CEILING
PRESSURE
VISIBILITY
BRIGHTNESS
RAIN
RADAR
(WITHIN 15 MILES)
VISIBILITY (MILES)
PRESSURE (mb)
BRIGHTNESS
CEILING (FT)
UorC
GMT
1500
1600
1700
1800
1900
2000
2100

Figure 60

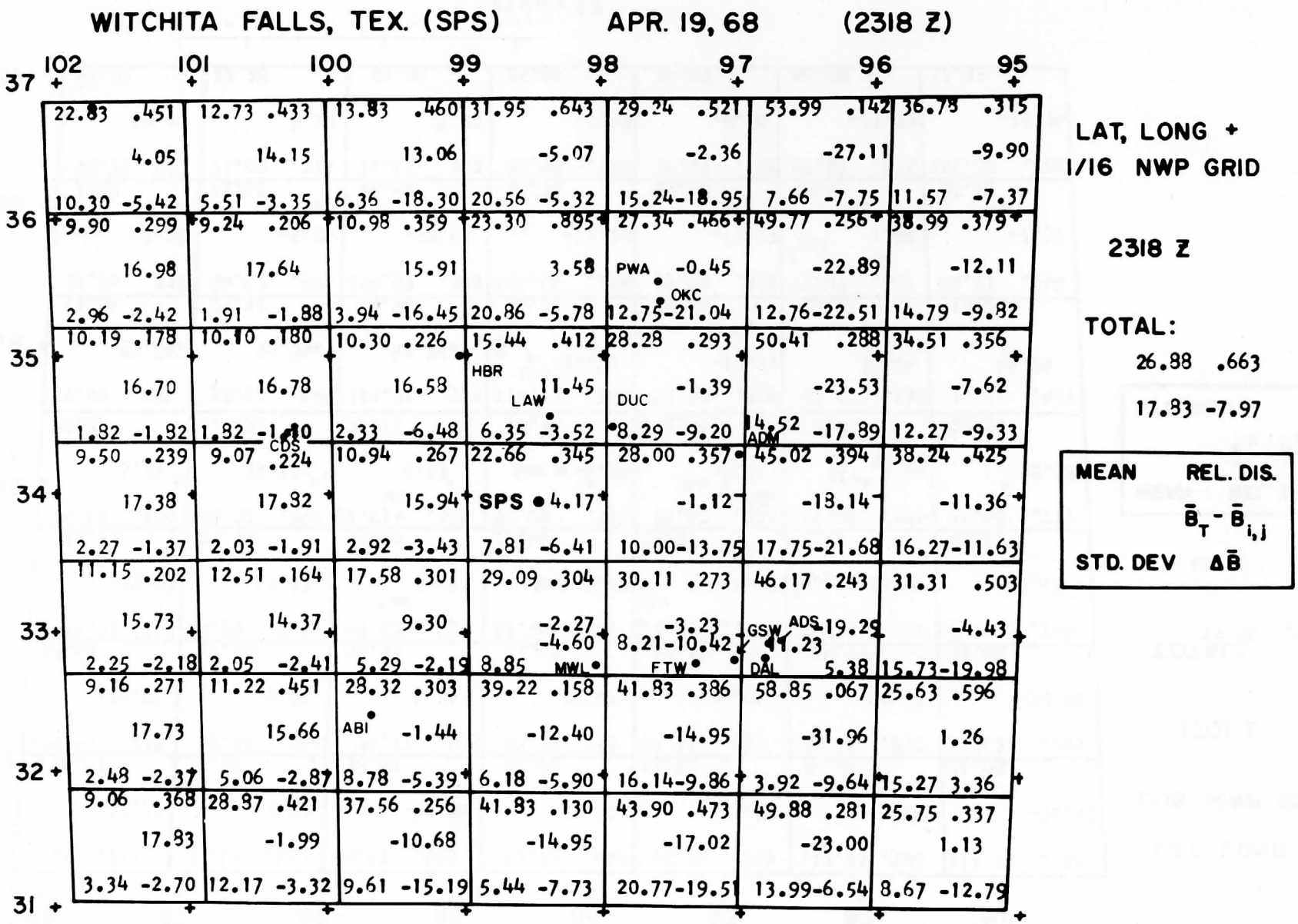

LAT, LONG +
1/16 NWP GRID

2318 Z

TOTAL:
26.88 .663
17.83 -7.97

MEAN	REL. DIS.
	$\bar{B}_T - \bar{B}_{i,j}$
STD. DEV	$\Delta\bar{B}$

Figure 61

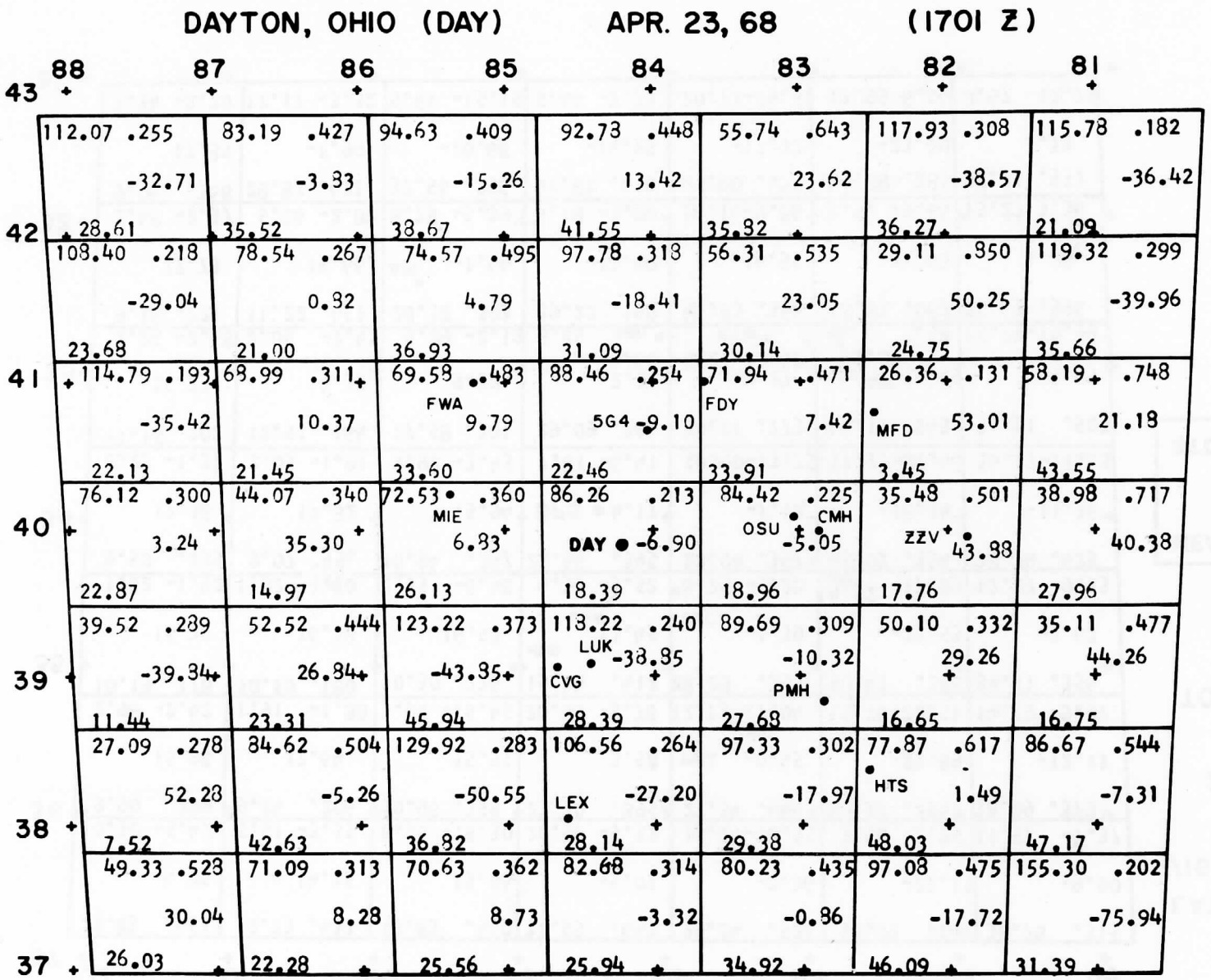
DAYTON, OHIO (DAY) APR. 23, 68 (1701 Z)
88 87 86 85 84 83 82 81
43
42
41
40
39
38
37
112.07 .255
-32.71
28.61
83.19 .427
-3.33
35.52
94.63 .409
-15.26
38.67
92.73 .448
13.42
41.55
55.74 .643
23.62
35.82
117.93 .308
-38.57
36.27
115.78 .182
-36.42
21.09
108.40 .218
-29.04
23.68
78.54 .267
0.82
21.00
74.57 .495
4.79
36.93
97.78 .318
-18.41
31.09
56.31 .535
23.05
30.14
29.11 .850
50.25
24.75
119.32 .299
-39.96
35.66
114.79 .193
-35.42
22.13
68.99 .311
10.37
21.45
69.58 .483
FWA
9.79
33.60
88.46 .254
5G4 -9.10
22.46
71.94 .471
FDY
7.42
33.91
26.36 .131
MFD 53.01
3.45
58.19 .748
21.18
43.55
76.12 .300
3.24
22.87
44.07 .340
35.30
14.97
72.53 .360
MIE
6.83
26.13
86.26 .213
DAY -6.90
18.39
84.42 .225
OSU CMH
-5.05
18.96
35.48 .501
ZZV 43.88
17.76
38.98 .717
40.38
27.96
39.52 .289
-39.34
11.44
52.52 .444
26.84
23.31
123.22 .373
-43.85
45.94
118.22 .240
LUK -38.85
CVG
28.39
89.69 .309
-10.32
PMH
27.68
50.10 .332
29.26
16.65
35.11 .477
44.26
16.75
27.09 .278
52.28
7.52
84.62 .504
-5.26
42.63
129.92 .283
-50.55
36.82
106.56 .264
LEX -27.20
28.14
97.33 .302
-17.97
29.38
77.87 .617
HTS 1.49
48.03
86.67 .544
-7.31
47.17
49.33 .523
30.04
26.03
71.09 .313
8.28
22.28
70.63 .362
8.73
25.56
82.68 .314
-3.32
25.94
80.23 .435
-0.86
34.92
97.08 .475
-17.72
46.09
155.30 .202
-75.94
31.39
LAT, LONG +
1/16 NWP GRID
1701 Z
TOTAL:
79.36 .533
42.30
MEAN REL. DIS.
$\bar{B}_T - \bar{B}_{i,j}$
STD. DEV.

Figure 62

DAYTON, OHIO (DAY) APR. 23, 68 (1946 Z)

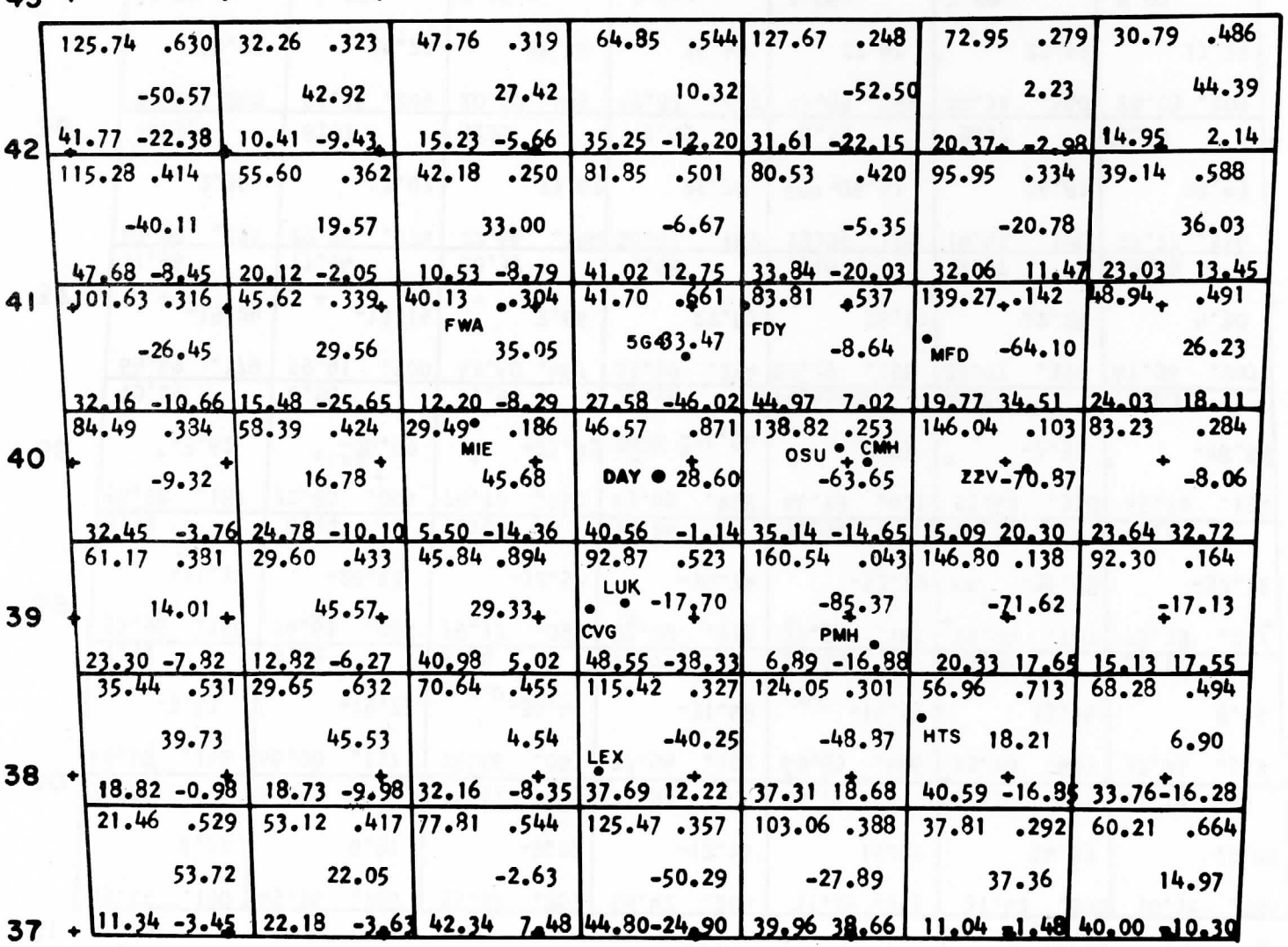

LAT, LONG +
1/16 NWP GRID

1946 Z

TOTAL:

75.18 .630

47.37 -2.83

MEAN	REL. DIS.
	$\bar{B}_T - \bar{B}_{I,J}$
STD. DEV.	$\Delta \bar{B}$

Figure 63

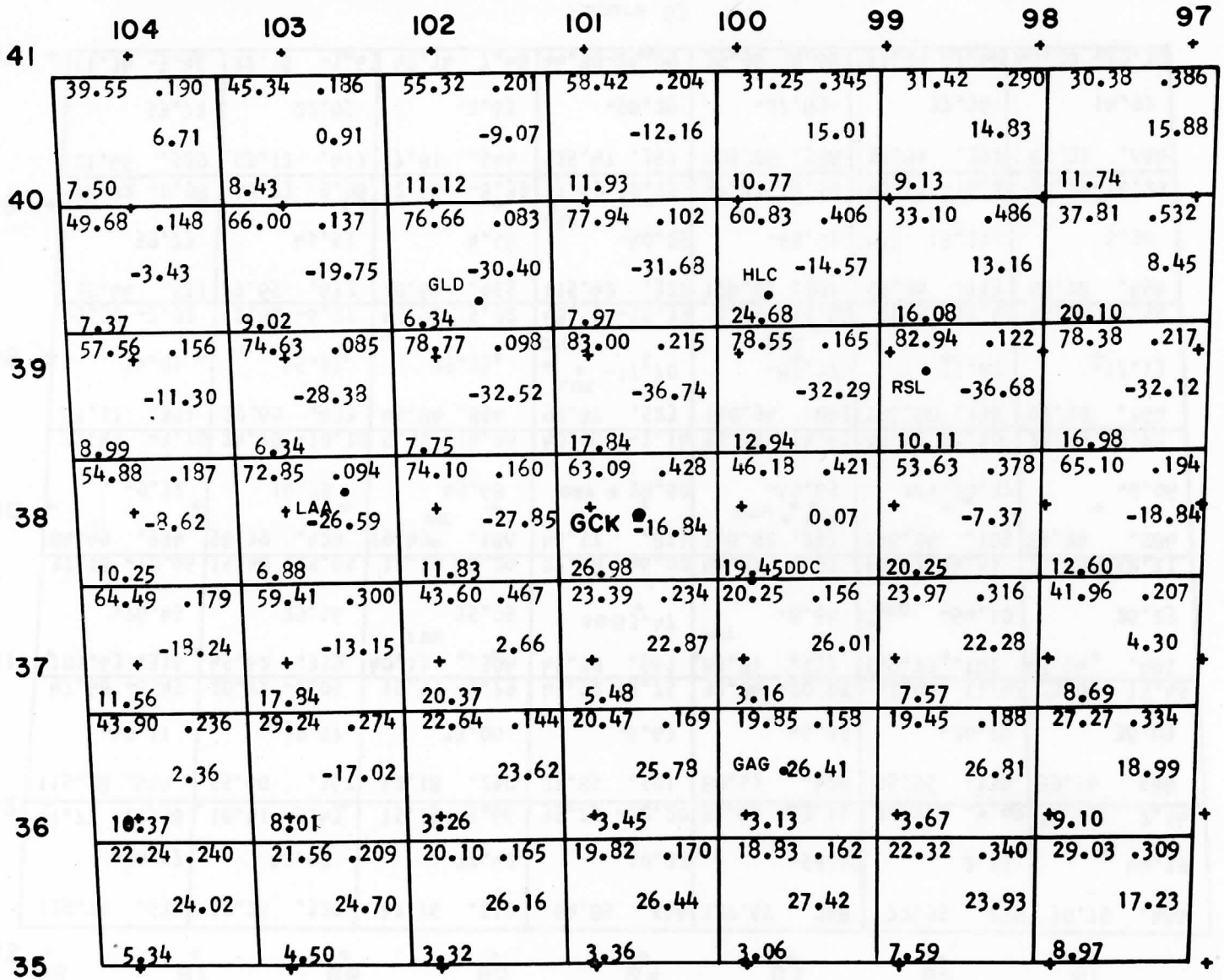

LAT, LONG +

1/16 NWP GRID

1428 Z

TOTAL:
46.26 .525

24.31

MEAN REL. DIS.

$\bar{B}_T - \bar{B}_{i,j}$

STD. DEV.

Figure 64

GARDEN CITY, KAN. (GCK) APR. 4, 69 (1526 Z)

	104	103	102	101	100	99	98	97
41	50.63 .380	61.46 .191	70.15 .118	73.60 .152	41.61 .360	40.42 .235	43.34 .399	
	10.65	-0.18	-8.87	-12.32	19.67	20.86	17.95	
40	19.22 11.08	11.72 16.12	8.25 14.83	11.18 15.18	14.99 10.36	9.49 9.00	17.31 12.96	
	74.50 .126	67.83 .220	87.31 .073	94.75 .093	88.90 .236	66.76 .461	33.15 .303	
	-13.22	-6.55	GLD 26.03	-33.47	HLC -27.61	-5.48	28.13	
	9.42 24.82	14.93 1.33	6.39 10.65	8.79 16.81	21.02 28.07	30.77 33.66	10.03 -4.66	
39	74.68 .107	94.68 .086	97.38 .084	103.75 .092	107.61 .150	99.90 .128	90.40 .382	
	-13.39	-33.40	-36.10	-42.47	-46.32	RSL -38.62	-29.11	
	7.98 17.12	8.17 20.05	8.15 18.61	9.56 20.75	16.18 29.06	12.84 16.96	34.57 12.02	
	83.72 .117	97.99 .053	99.47 .084	92.38 .328	61.58 .461	61.70 .442	82.56 .278	
38	-22.44	LAA -36.71	-38.19	GCK -31.09	-0.29	-0.43	-21.28	
	9.83 28.84	5.17 25.14	8.31 25.37	30.32 29.29	28.41 15.40	27.31 8.07	22.92 17.46	
	85.10 .125	93.49 .064	76.90 .277	34.47 .321	26.39 DDC .131	23.94 .148	47.16 .356	
37	-23.81	32.21	-15.62	24.82	34.94	37.34	14.12	
	10.65 20.61	5.94 34.08	21.29 33.30	11.72 11.08	3.44 6.30	3.54 -0.03	16.78 5.20	
	61.20 .354	53.68 .323	39.32 .296	33.15 .299	24.31 .141	21.94 .152	38.65 .446	
	0.08	7.60	21.97	28.14	GAG 36.48	39.34	22.63	
36	21.64 17.30	17.36 24.44	11.65 16.68	9.91 12.68	3.50 4.96	3.33 2.49	17.23 11.38	
	30.27 .266	33.77 .269	26.04 .185	23.92 .151	22.72 .141	22.71 .159	41.34 .345	
	31.01	27.52	35.25	37.36	38.57	38.57	19.94	
35	8.07 8.03	9.09 12.21	4.82 5.94	3.62 4.10	3.21 3.89	3.61 0.39	14.26 12.31	

LAT, LONG +
1/16 NWP GRID

1526 Z

TOTAL:
61.28 .505

30.92 15.02

MEAN REL. DIS.
$\bar{B}_T - \bar{B}_{I,J}$
STD. DEV. $\Delta\bar{B}$

Figure 65

GARDEN CITY, KAN. (GCK) APR. 4, 69 (1556 Z)

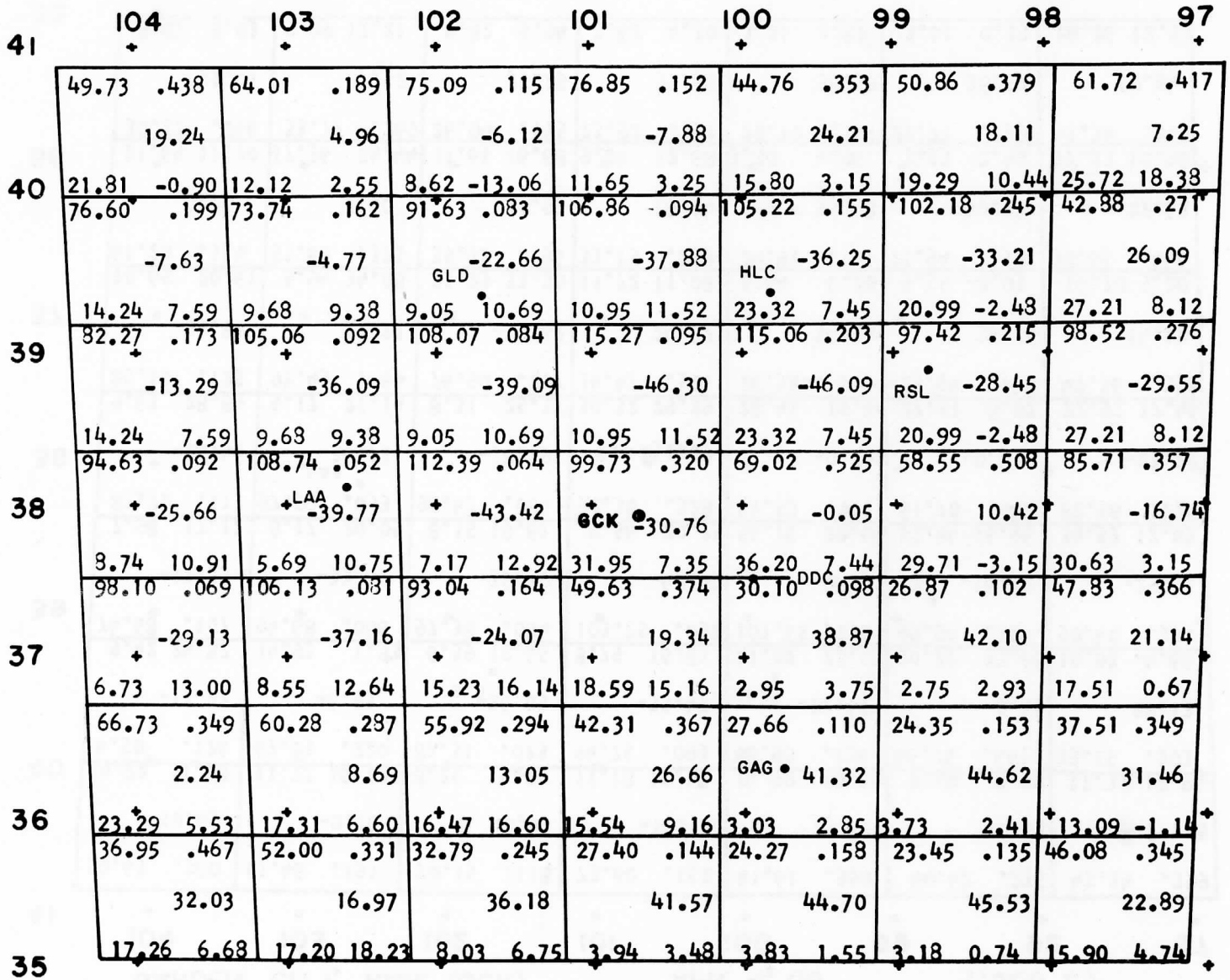

LAT, LONG +
1/16 NWP GRID

1556 Z

TOTAL:
68.97 .487

33.60 7.69

MEAN	REL. DIS.
	$\bar{B}_T - \bar{B}_{i,j}$
STD. DEV.	$\Delta \bar{B}$

Figure 66

GARDEN CITY, KAN. (GCK) APR. 4, 69 (1648 Z)

	104	103	102	101	100	99	98	97
41	33.88 .317	46.60 .235	53.12 .197	62.46 .257	52.47 .283		84.50 .117	94.47 .055
	28.76	21.04	14.53	5.18	15.17		-16.86	-26.83
40	12.33 -10.85	10.95 -17.41	10.46 -21.97	16.02 -14.39	14.86 7.71		9.91 33.64	5.20 32.75
	59.73 .228	55.14 .242	76.92 .196	97.64 .172	101.01 .146		110.88 .143	79.59 .333
	7.91	12.50	GLD -9.28	-30.00	HLC -33.37		-43.24	-11.95
	13.61 -16.87	13.36 -18.60	15.09 -14.71	16.77 -9.22	14.78 -4.21		15.86 8.70	26.51 36.71
39	79.02 .130	95.97 .117	105.77 .066	117.60 .076	108.48 .226		82.23 .276	75.64 .350
	-11.38	-28.33	-38.13	-49.96	-40.84		RSL -14.59	-8.00
	10.28 -3.25	11.26 -9.19	7.03 -2.30	8.99 2.33	24.56 -6.58		22.72 -15.19	26.44 -22.88
	93.37 .098	107.36 .054	112.63 .063	108.48 .177	82.76 .389		63.87 .414	78.65 .314
38	-25.73	LAA -39.72	-44.99	GCK -40.84	-15.12		3.77	-11.01
	9.14 -1.26	5.79 -1.38	7.05 0.24	19.23 8.75	32.17 13.74		26.42 5.32	24.68 -7.06
	99.25 .088	104.03 .111	103.28 .175	64.34 .447	28.58 .148		25.30 .154	38.48 .258
37	-31.61	-36.39	-36.64	3.30	39.06		42.34	29.16
	8.69 1.15	11.53 -2.10	18.09 10.24	28.75 14.71	4.22 -1.52		3.89 -1.57	9.94 -9.35
	69.13 .348	62.69 .232	60.50 .316	53.46 .435	29.61 .185		23.92 .145	29.08 .238
	-1.49	4.95	7.14	14.18	GAG 38.03		43.72	38.56
36	24.04 2.40	14.53 2.41	19.14 4.58	23.24 11.15	5.47 1.95		3.46 -0.43	6.93 -8.43
	39.82 .278	37.83 .188	39.75 .370	36.93 .405	24.53 .153		22.95 .146	39.43 .447
	27.82	29.81	27.89	30.71	43.11		44.69	28.21
35	11.07 2.87	7.11 -14.17	14.71 6.96	14.94 9.53	3.75 0.26		3.34 -0.50	17.63 -6.65

LAT, LONG +

1/16 NWP GRID

1648 Z

TOTAL:

67.64 .489

33.07 -1.33

MEAN REL. DIS. $\bar{B}_T - \bar{B}_{i,j}$

STD. DEV. $\Delta \bar{B}$

Figure 67

GARDEN CITY, KAN. (GCK) APR. 4, 69 (1739 Z)

	104	103	102	101	100	99	98	97
41	54.65 .755	52.48 .772	55.42 .747	69.11 .638	86.57 .331	98.54 .373	114.93 .328	
	18.26	20.42	17.48	3.79	-13.67	-25.63	-42.03	
40	41.28 15.77	40.54 5.88	41.40 2.30	44.08 6.65	28.69 34.10	36.73 14.04	37.65 20.46	
	73.94 .352	59.75 .412	73.32 .299	92.49 .177	110.25 .163	102.37 .212	97.88 .292	
	-1.04	13.15	-0.42	-19.59	-37.35	-29.47	-24.98	
	26.00 14.21	24.60 4.61	GLD 21.92 -3.60	16.41 -5.15	HLC 17.95 9.24	21.72 -8.51	28.56 18.29	
39	81.66 .285	67.86 .388	91.43 .180	107.31 .147	115.01 .187	118.77 .188	87.31 .301	
	-8.76	5.05	-18.53	-34.41	-42.11	RSL -45.87	-14.41	
	23.25 2.64	26.33 -28.11	16.45-14.34	15.79 -10.29	21.48 6.53	22.31 36.54	26.27 11.67	
	76.14 .311	95.50 .208	112.52 .225	119.79 .199	110.10 .323	68.25 .618	51.28 .839	
38	-3.24	LAA -22.60	-39.62	GCK -46.89	-37.20	4.65	21.62	
	23.71 -17.23	19.89-11.86	25.35 -0.11	23.90 11.31	35.59 27.34	42.15 4.38	43.02 -27.37	
	86.86 .215	104.08 .112	98.10 .166	94.00 .209	72.00 .373	32.78 .296	23.21 .163	
37	-13.96	-31.18	-25.20	-21.10	DDC 0.90	40.13	49.69	
	18.65-12.39	11.63 0.05	16.29 -5.18	19.61 29.66	26.84 43.42	9.72 7.48	3.78 -15.27	
	51.51 .611	76.77 .355	75.03 .444	69.98 .413	58.83 .436	40.91 .742	27.63 .672	
	21.39	-3.87	-2.13	2.92	GAG 14.07	31.99	45.28	
36	31.45 -17.62	27.29 14.08	33.29 14.53	28.90 16.52	25.68 29.22	30.37 16.99	18.55 -1.45	
	28.54 .298	36.93 .290	32.35 .194	41.29 .580	37.79 .507	27.90 .668	25.03 .772	
	44.36	35.97	40.56	31.61	35.12	45.00	47.87	
35	8.52 -11.28	10.72 -0.90	6.26 -7.40	23.93 4.36	19.15 13.26	18.64 4.95	19.33-14.40	

LAT, LONG +
1/16 NWP GRID

1739 Z

TOTAL:
72.90 .534

38.90 5.26

MEAN	REL. DIS.
	$\bar{B}_T - \bar{B}_{i,j}$
STD. DEV.	$\Delta \bar{B}$

Figure 68

GARDEN CITY, KAN. (GCK) APR. 4, 69 (1805 Z)

	104	103	102	101	100	99	98	97
41	30.06 .108	29.85 .140	36.09 .290	62.86 .314	80.13 .253	99.58 .123	103.82 .069	
	40.21	40.43	34.18	7.41	-9.86	-29.30	-33.55	
40	3.25 -24.59	4.19 -22.63	10.48 -19.33	19.76 -6.25	20.24 -6.44	12.29 1.04	7.16 -11.11	
	38.24 .226	49.46 .315	74.54 .222	98.94 .170	112.71 .116	120.93 .123	118.29 .161	
	32.04	20.82	GLD -4.27	-28.67	HLC -42.43	-50.66	-48.01	
	8.64 -35.70	15.56 -10.29	16.53 1.22	16.80 6.45	13.05 2.46	14.89 18.56	19.07 20.41	
39	54.44 .273	80.08 .261	104.57 .106	120.68 .060	114.34 .161	93.90 .292	64.19 .471	
	15.84	-9.80	-34.29	-50.41	-44.07	RSL -23.63	6.09	
	14.84 -27.22	20.91 12.22	11.06 13.14	7.25 13.37	18.35 -0.67	27.38 -24.87	30.22 -23.12	
	81.84 .298	103.09 .127	106.90 .108	121.33 .117	89.25 .323	55.20 .455	43.20 .294	
38	-11.56	LAA -32.82	-36.63	GCK -51.06	-18.97	15.07	27.08	
	24.37 5.70	13.09 7.59	11.52 -5.62	14.22 1.54	28.82 -20.85	25.09 -13.05	12.68 -8.08	
	114.37 .084	106.81 .129	103.20 .170	97.69 .255	41.25 .305	29.00 .236	33.89 .256	
37	-44.09	-36.54	-32.93	-27.41	29.03	41.28	36.39	
	9.65 27.51	13.73 2.73	17.51 5.10	24.88 3.69	12.58 -30.75	6.86 -3.78	8.68 10.68	
	90.93 .208	87.54 .189	68.77 .264	57.39 .295	42.17 .310	25.84 .186	24.42 .237	
	-20.65	-17.26	1.50	12.89	GAG 28.11	44.44	45.85	
36	18.88 39.42	16.51 10.77	18.13 -6.26	16.94 -12.59	13.09 -16.66	4.80 -15.07	5.79 -3.21	
	39.62 .245	36.59 .246	41.16 .374	39.94 .305	33.81 .412	22.65 .158	32.09 .410	
	30.66	33.68	29.12	30.33	36.46	47.62	38.19	
35	9.69 11.08	9.01 -0.34	15.38 8.81	12.17 -1.35	13.94 -3.98	3.57 -5.25	13.15 7.06	

LAT, LONG +
1/16 NWP GRID

1805 Z

TOTAL:
70.27 .515

36.17 -2.63

MEAN	REL. DIS.
	$\bar{B}_T - \bar{B}_{i,j}$
STD. DEV.	$\Delta \bar{B}$

Figure 69

GARDEN CITY, KAN. (GCK) APR. 4, 69 (1855 Z)

	104	103	102	101	100	99	98	97
41	36.31 .652 34.78 23.69 6.25	43.01 .897 28.09 38.60 13.16	64.48 .556 6.62 35.83 28.39	81.56 .385 -10.46 31.40 18.70	97.12 .264 -26.02 25.68 16.99	113.69 .195 -42.59 22.19 14.11	118.54 .208 -47.44 24.72 14.72	
40	41.42 .668 29.68 27.69 3.18	48.93 .561 22.17 27.45 -0.53	78.08 .326 GLD -6.98 25.49 3.54	111.87 .220 -40.77 24.66 12.93	120.76 .233 HLC -49.66 28.16 8.05	103.21 .310 -32.11 32.05 -17.72	99.79 .298 -28.70 29.77 -18.50	
39	50.84 .573 20.26 29.15 -3.60	75.91 .298 -4.81 22.66 -4.17	87.61 .220 -16.51 19.24 -16.96	109.74 .148 -38.64 16.23 -10.94	115.21 .228 -44.11 26.21 0.87	92.42 .451 RSL -21.32 41.64 -1.48	64.14 .538 6.96 34.52 -0.05	
38	96.34 .218 -25.25 21.03 14.50	102.52 .175 LAA -31.43 17.96 -0.57	90.89 .320 -19.80 29.09 -16.01	118.23 .199 GCK 47.13 23.56 -3.10	71.31 .386 -0.21 27.52 -17.94	47.96 .627 23.14 30.09 -7.24	47.67 .477 23.43 22.72 4.47	
37	117.92 .225 -46.82 26.51 3.55	81.59 .287 -10.50 23.44 -25.22	85.31 .291 -14.21 24.83 -17.89	85.53 .354 -14.43 30.31 -12.16	55.77 .389 DDC 15.33 21.69 14.52	42.51 .745 28.59 31.66 13.51	36.14 .783 34.96 28.30 2.25	
36	71.74 .430 -0.64 30.83 -19.19	76.87 .451 -5.77 34.67 -10.67	59.77 .471 11.33 28.14 -9.00	48.57 .757 -22.53 36.77 -8.82	48.42 .674 GAG 22.67 32.63 6.25	29.78 .746 41.32 22.23 3.94	30.89 .787 40.21 24.30 6.47	
35	36.64 .647 34.46 23.69 -2.98	56.08 .610 15.02 34.22 19.49	45.30 .750 25.79 34.00 4.14	41.77 1.011 -29.33 42.23 1.83	35.03 .966 36.07 33.85 1.22	30.04 1.002 41.06 30.11 7.39	43.33 .905 27.76 39.21 11.24	

LAT, LONG +
1/16 NWP GRID

1855 Z

TOTAL:
71.10 .575

40.85 0.83

MEAN	REL. DIS.
	$\bar{B}_T - \bar{B}_{i,j}$
STD. DEV.	$\Delta \bar{B}$

Figure 70

GARDEN CITY, KAN. (GCK) APR. 4, 69 (1948 Z)

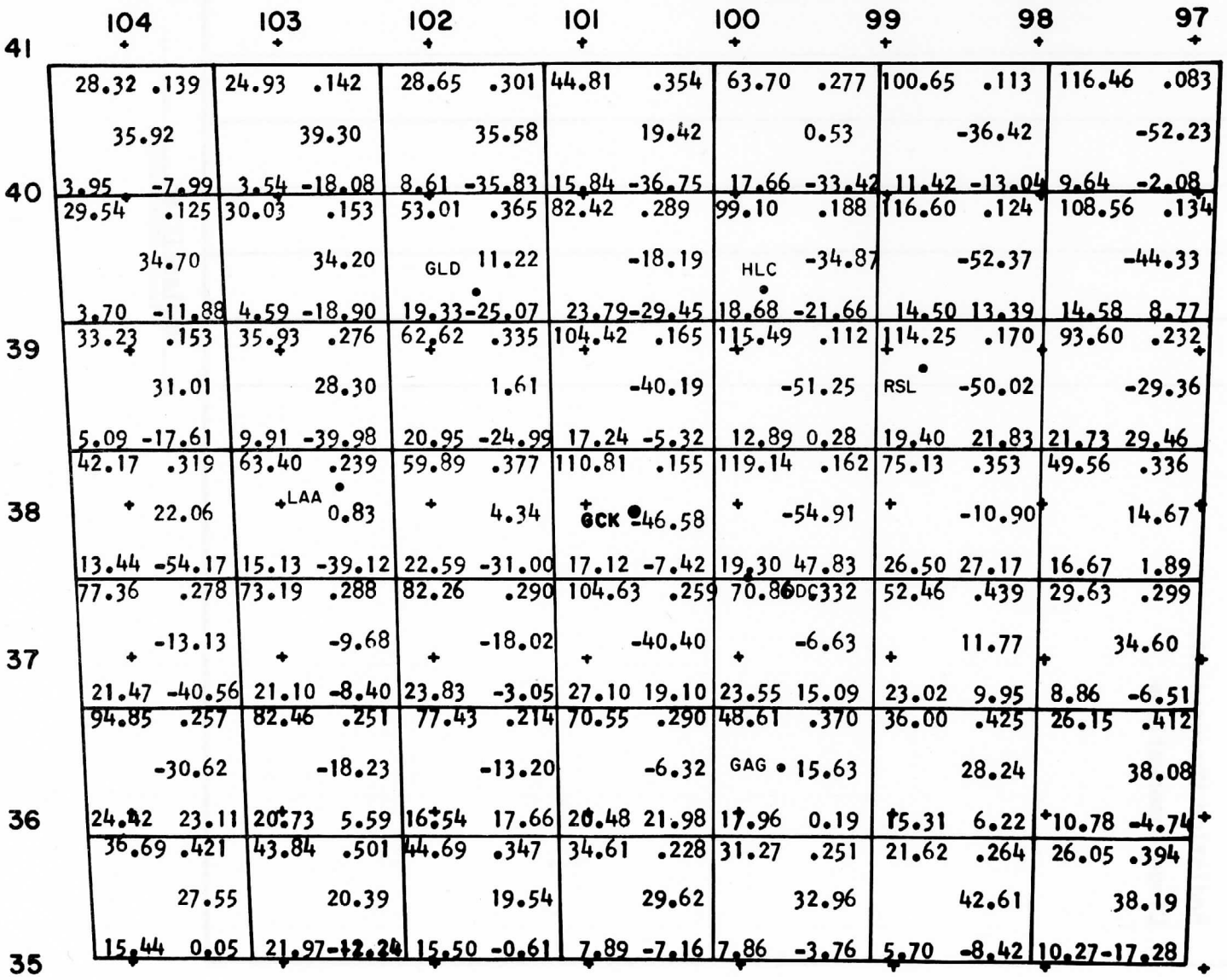

LAT, LONG +
1/16 NWP GRID

1948 Z

TOTAL:
64.23 .548

35.17 6.87

MEAN	REL. DIS.
	$\bar{B}_T - \bar{B}_{I,J}$
STD. DEV.	$\Delta \bar{B}$

Figure 71

Unclassified
Security Classification

14. KEY WORDS	LINK A		LINK B		LINK C	
	ROLE	WT	ROLE	WT	ROLE	WT
Geosynchronous Satellite Data						
Meteorology						
Short Range Forecasting						
Ceiling/Visibility						
Radiation Measurements						
Cloud Observations						

Unclassified
Security Classification

DOCUMENT CONTROL DATA - R & D

(Security classification of title, body of abstract and indexing annotation must be entered when the overall report is classified)

1. ORIGINATING ACTIVITY *(Corporate author)*
The University of Wisconsin
Space Science and Engineering
1225 West Dayton Street, Madison, Wisconsin 53706

2a. REPORT SECURITY CLASSIFICATION
Unclassified

2b. GROUP
NA

3. REPORT TITLE
"A PILOT STUDY ON THE APPLICATION OF GEOSYNCHRONOUS METEOROLOGICAL "SATELLITE DATA TO VERY SHORT RANGE TERMINAL FORECASTING"

4. DESCRIPTIVE NOTES *(Type of report and inclusive dates)*
Scientific. FINAL (1 APRIL 1970 - 31 AUGUST 1970) APPROVED: September 11, 1970

5. AUTHOR(S) *(First name, middle initial, last name)*
Thomas H. Vonder Haar
Richard S. Cram

6. REPORT DATE	7a. TOTAL NO. OF PAGES	7b. NO. OF REFS
30 September, 1970	116	6

8a. CONTRACT OR GRANT NO.	9a. ORIGINATOR'S REPORT NUMBER(S)
F19628-70-C-0207	
b. PROJECT, TASK, AND WORK UNIT NO.	
8628-11-01	NA
c. DOD ELEMENT	9b. OTHER REPORT NO(S) *(Any other numbers that may be assigned this report)*
62101F	
d. DOD SUBELEMENT 681000	AFCRL-70-0493

10. DISTRIBUTION STATEMENT
1 - This document has been approved for public release and sale; its distribution is unlimited.

11. SUPPLEMENTARY NOTES	12. SPONSORING MILITARY ACTIVITY
TECH, OTHER	Air Force Cambridge Research Laboratories (CRH) L.G. Hanscom Field Bedford, Massachusetts 01730

13. ABSTRACT

The study assembles a unified body of data consisting of very high space and time resolution reflected radiance measurements from a geosynchronous satellite (ATS-III) along with concurrent meteorological radar, ceiling, visibility and surface pressure reports at selected air terminals in the central United States. This data set allows familiarization with the meteorological potential of nearly continuous observation of cloud conditions from a geosynchronous platform. It may also serve as initial input to quantitative techniques for evaluating the satellite data and/or for testing its usefulness in very short range weather forecasting. In this regard, a second portion of the study presents arrays of statistical descriptors of the satellite data.

DD FORM 1 NOV 65 1473

Unclassified
Security Classification